Range Corrections in Pionless Three-Particle Systems

A Non-Perturbative Method for Spurious Poles in Infinite and Finite Volume

Zur Erlangung des Grades eines Doktors der Naturwissenschaften (Dr. rer. nat.)
Genehmigte Dissertation von Martin Ebert aus Offenbach am Main
Tag der Einreichung: 27. Juni 2022, Tag der Prüfung: 20. Juli 2022

1. Gutachten: Prof. Dr. Hans-Werner Hammer
2. Gutachten: Prof. Dr. Jens Braun
Darmstadt, Technische Universität Darmstadt

TECHNISCHE UNIVERSITÄT DARMSTADT

Physics Department
Institut für Kernphysik
AG Hammer

Range Corrections in Pionless Three-Particle Systems
A Non-Perturbative Method for Spurious Poles in Infinite and Finite Volume

Accepted doctoral thesis by Martin Ebert

Date of submission: June 27, 2022
Date of thesis defense: July 20, 2022

Darmstadt, Technische Universität Darmstadt

Erklärungen laut Promotionsordnung

§ 8 Abs. 1 lit. c PromO

Ich versichere hiermit, dass die elektronische Version meiner Dissertation mit der schriftlichen Version übereinstimmt.

§ 8 Abs. 1 lit. d PromO

Ich versichere hiermit, dass zu einem vorherigen Zeitpunkt noch keine Promotion versucht wurde. In diesem Fall sind nähere Angaben über Zeitpunkt, Hochschule, Dissertationsthema und Ergebnis dieses Versuchs mitzuteilen.

§ 9 Abs. 1 PromO

Ich versichere hiermit, dass die vorliegende Dissertation selbstständig und nur unter Verwendung der angegebenen Quellen verfasst wurde.

§ 9 Abs. 2 PromO

Die Arbeit hat bisher noch nicht zu Prüfungszwecken gedient.

Darmstadt, 27. Juni 2022

M. Ebert

Abstract

Effective range corrections contribute to pionless effective field theory at next-to-leading order. In a three-particle system described in the particle-dimer picture they enter in the dimer propagator. They can be included perturbatively or non-perturbatively. In a finite volume the perturbative method can lead to singular behavior close to physical bound states. The non-perturbative or resummized method exhibits a spurious pole.
In this thesis, we investigate the problems caused by this spurious pole in infinite volume. We develop a non-perturbative method to avoid these problems. This is accomplished by expanding the contribution of the spurious pole, while treating the contribution of the physical pole exactly. We show that this method leads to a change of the renormalization prescription of the three-body forces. This new method is tested for several model potentials and different observables, including the particle-dimer phase shift and three-body bound states. We observe good convergence and prove that the method preserves the internal consistency of the pionless effective field theory.
In the second part of the thesis, we investigate the effect of the spurious poles on the three-body quantization condition in a finite volume and show that it leads to a spurious series of scattering states and an un-physical merging of energy levels in the energy spectrum. We extend the new non-perturbative method, developed in infinite volume, to finite volume. Finally, we use the method to calculate the energy spectrum and show that we can reproduce the spectrum of a Yamaguchi model very accurately. Moreover, the description of the model improves order by order of the effective filed theory.

Zusammenfassung

Die effektive Reichweite trägt in pionenloser effektiver Feldtheorie in erster Korrektur zur führenden Ordnung bei. Ein Drei-Teilchen System kann im Teilchen-Dimer Bild beschrieben werden. Dabei treten die Korrekturen durch die effektive Reichweite im Dimer-Propagator auf. Sie können störungstheoretisch oder nicht störungstheoretisch betrachtet werden. Bei Rechnungen im endlichen Volumen kann die störungstheoretische Betrachtung zu singulärem Verhalten nahe physikalischer Bindungszustände führen. Die nicht störungstheoretische bzw. resummierte Betrachtung enthält einen unphysikalischen Pol.
In dieser Dissertation werden die Probleme, die dieser unphysikalische Pol im unendlichen Volumen verursacht, untersucht. Es wird eine nicht störungstheoretische Methode entwickelt, um diese Probleme zu umgehen. Dies wird erreicht, indem der Beitrag des unphysikalischen Pols für kleine Energien entwickelt wird. Gleichzeitig betrachten wir den Beitrag des physikalischen Pols exakt. Es wird gezeigt, dass diese Methode zu einer Änderung der Renomierungsvorschriften der Drei-Teilchen Kräfte führt. Die neue Methode wird an verschiedenen Modellen und für verschiedene Observablen getestet. Diese Observablen beinhalten die Partikel-Dimer Phasenverschiebung und gebundene Drei-Teilchen Zustände. Es werden gute Übereinstimmungen erzielt. Außerdem wird gezeigt, dass die Methode die interne Konsistenz der pionlosen effektiven Feldtheorie erhält.
Im zweiten Teil der Dissertation werden die Probleme untersucht, die der unphysikalische Pol in der Quantisierungsbedingung im endlichen Volumen verursacht. Der Pol führt zu einer Reihe von unphysikalischen Streuzuständen im Energiespektrum und unphysikalischen Verschmelzungen zwischen verschiedenen Energieleveln. Die nicht störungstheoretische Methode, die im unendlichen Volumen entwickelt wurde, wird auf das endliche Volumen erweitert. Abschließend wird die Methode verwendet um das Energiespektrum zu berechnen. Es wird gezeigt, dass damit das Spektrum eines Yamaguchi-Modells akkurat reproduziert werden kann. Die Beschreibung des Models verbessert sich Ordnung für Ordnung der effektiven Feldtheorie.

Contents

1 Introduction

Powerful tools in nuclear physics are effective field theories (EFTs). They are based on the observation that low-energy (m_{low}) phenomena in physics are not sensitive to details of the interaction at short distances (or high energies (m_{high})). This separation of scales can be used to construct simple theories that consider only the relevant degrees of freedom. For example, the fundamental theory of the strong interaction, namely quantum chromodynamics (QCD), contains quarks and gluons as degrees of freedom. For low-energy calculations, EFTs, containing hadrons as degrees of freedom, can be used instead. Observables are calculated as expansions in m_{low}/m_{high}. The details of the QCD at short distances are encoded in the interaction strengths of the EFT. These are constants that have to be obtained from experiments or calculated from the more fundamental theory. An early introduction to this concept is given in [71], more recent reviews are for example [7, 24, 31].
An important example of an EFT is pionless effective field theory ($\not\pi$EFT) [15, 43, 44, 68]. It can be used to describe the interaction of nucleons at momenta small compared to the pion mass, $m_{high} \sim m_\pi \approx 140$ MeV. For momenta close or larger than the pion mass, $\not\pi$EFT will break down. The pion exchange can not be treated as a short-range interaction and pions have to be included as a degree of freedom explicitly. This is done in chiral EFT [71, 72]. For even higher momenta additional, more heavy, meson have to be included.
In this thesis, we focus on systems with an unnaturally large scattering length $1/a \sim m_{low} \ll m_\pi$ and a naturally sized effective range $1/r \sim m_{high}$. This means $\not\pi$EFT can be used for typical momenta of $p \sim 1/a$. A prominent example of such a system is neutron-proton scattering in the S-wave triplet ($^3S_1$) or singlet channel ($^1S_0$).

A convenient way to describe a three-particle system with a large scattering length a in $\not\pi$EFT is the particle dimer picture [4, 5, 12, 42]. An auxiliary field, a dimer, is introduced, this consists of two particles. The information of the two-particle system is encoded in the dimer field, which can be used in the three-body system. This results in an effective two-body problem. An important quantity of this picture is the dimer propagator. At leading-order (LO)[1] this can be obtained by a re-summation of an infinite amount of Feynman diagrams with a momentum independent two-body interaction [12]. This interaction can be connected to the two-body scattering length a. The resulting propagator can exhibit a pole with a physical meaning. This physical pole gives the binding energy of a two-body bound state. In the context of neutron-proton scattering, this state is the deuteron. Next-to-leading order (NLO) corrections to this propagator can be obtained by adding a two-body interaction proportional to the kinetic energy of the dimer. This additional interaction can be connected to the two-body effective range r. Therefore, these NLO corrections are also called range corrections. Since $r/a \sim m_{low}/m_{high} \ll 1$, these corrections have to be included perturbatively. This can be accomplished by inserting the energy-dependent interaction

[1] The separation of scales in an EFT allows an expansion in m_{low}/m_{high}. This leads to a power counting, such that corrections at NLO are suppressed compared to LO by $(m_{low}/m_{high})^1$. Correction at N^{2}LO are suppressed by $(m_{low}/m_{high})^2$ and so on.

once between two LO propagators [2, 5]. However, at higher orders, the perturbative range insertion becomes increasingly complicated. It requires the fully off-shell LO propagators. A commonly used method to avoid this is a non-perturbative approach. The corrections are included in the denominator of the propagator and a re-summation, similar to the LO case, is performed [12, 49]. This results in a dimer propagator given by

$$\tau(k^*) = \frac{1}{-1/a - r/2\,(k^*)^2 + k^*}\,,$$

where k^* is the magnitude of the relative momentum of the two particles constituting the dimer in their center-of-mass frame. This is a very appealing form, it can be directly related to the two-particle scattering amplitude in the effective range expansion (ERE) at NLO. In this context, the expansion to higher orders, including for example the shape parameter, is straightforward. However, the re-summarized form comes with a huge downside. As pointed out for example in [6, 28], it exhibits a deep spurious pole. In contrast to the physical pole mentioned above, this pole has no connection to a real physical system. Worse, it can have a negative residue, which leads to violation of unitary, negative spectral densities, and strong numerical instabilities. All of these are serious issues. Without special methods, the propagator above can not be used. An additional way of understanding these problems is that the ERE is used outside its range of applicability and therefore it is not surprising that it leads to non-physical predictions there.
One existing method to avoid these poles is the usage of an ultraviolet cutoff below the position of the pole [6]. This leads to a strong restriction for the cutoff and therefore a restriction of the accuracy of the EFT, which, in general, one likes to avoid. Another method is a perturbative expansion of the propagator for small effective range r, see for example [4, 32, 40] for a NLO expansion and [39, 69] for an expansion at N^{2}LO. While this perturbative method works very well in infinite volume, it has problems with convergence in finite volume [59], see more on the importance and recent developments for finite volume calculations below. Due to the discretized momenta in finite volume, the resummed propagator has to be exchanged by [33, 34]

$$\tau_L(\mathbf{k}, (k^*)^2) = \frac{1}{-1/a - r/2\,(k^*)^2 + S(\mathbf{k}, (k^*)^2)}\,,$$

with the momentum $\mathbf{k}$ of the dimer and the function

$$S(\mathbf{k}, (k^*)^2) = -\frac{4\pi}{L^3}\sum_{\mathbf{p}} \frac{1}{\mathbf{p}^2 + \mathbf{pk} + \mathbf{k}^2/4 + (k^*)^2}, \text{ with } \mathbf{p} \in \frac{2\pi}{L}\mathbb{Z}^3\,.$$

L is the size of the finite volume. This function has a series of singularities above the elastic threshold, $(k^*)^2 < 0$. These singularities are connected to a discrete series of scattering states in finite volume. The problem with the perturbative method is, that these singularities will appear in the expansion in the denominator in higher and higher powers. This will make numerical calculations extremely difficult. Therefore, there is a strong need for a non-perturbative method to solve the issue of spurious poles in the resummed propagator.
The major focus of this thesis is to develop such a non-perturbative method. This will be accomplished by separating the contribution of the physical pole from the contribution of the spurious pole and expanding only the latter. By doing so, we will remove the singularity of the spurious pole, while simultaneously avoiding the higher-order singularities of the function $S(\mathbf{k}, (k^*)^2)$. The seemingly inconsistent treatment of the two contributions will be justified by a change of the renormalization prescription of the three-body forces of the $\not\pi$EFT.

As discussed above, ab-initio calculations are very difficult. One of the most promising methods to do so are calculations on the lattice. The idea of this is, that the space-time will be treated as if it is discretized. Therefore, the considered particles are put on a space-time lattice. This allows for various simplifications of the system, such as allowing the particles to only interact with the next neighboring space-time points. An example of this is lattice QCD [20, 73]. If QCD is put on a lattice, this allows ab-initio access to hadronic processes. However, if numerical calculations are done, the lattice has to end somewhere. An infinite amount of space-time points can not be calculated. Therefore, lattice calculations have to be done in finite volume. An often used finite volume is a cube with periodic boundary conditions[2]. If one wants to connect results from the lattice to an EFT, it is crucial to understand how an EFT behaves in finite volume. Early works addressing this are for example [53, 54]. More recent reviews on the EFTs in finite volume are given by [38, 57]. An important result recently obtained is the quantization condition in finite volume, see [33, 34] for the formalism used in this thesis. An equivalent formulation is given in [35, 36, 56]. This condition allows direct calculations of the volume-dependent three-particle bound and scattering states in $\not\pi$EFT in finite volume. In [21] the quantization condition was simplified by projecting it on the irreducible representations of the cubic group. Since the used finite volume is a cube, the spherical symmetry is reduced to the symmetry of a cube [58, 41]. Therefore, the standard form of a partial-wave expansion can not be used. An additional effect of the finite volume is that only discrete momenta are allowed. This leads to a collapse of momentum integrals to sums. A direct consequence of this is the above form of the dimer propagator in finite volume. To be able to include range corrections to the quantization condition in finite volume, it is necessary to have a non-perturbative method to solve the issues discussed above. After we will have developed such a method in infinite volume, we will extend this method to the finite volume.

This thesis is organized as follows. We start by giving a short overview of the physical concepts that are relevant in the context of the thesis. This includes the elastic scattering of two and three particles, the partial wave expansion, and the parametrization of the scattering amplitude by using the phase shift and the corresponding ERE. We follow this with a summary of the concept of $\not\pi$EFT. Then we give the setup for the main part of the thesis by introducing the particle-dimer picture with a special interest in the inclusion of range corrections. We will show how the range corrections can be included in the dimer propagator in a perturbative [2, 5], as well as in a non-perturbative [12, 49] way. The first chapter is closed by a resume of finite volume physics. We discuss the general motivation for physics in a box with periodic boundary conditions, give a definition, and investigate the direct consequences of this. This includes the discretization of momentum and the reduced cubic symmetry. Finally, we give the three-body quantization condition in finite volume [33, 34] and show how this can be solved for binding energies exploiting the cubic symmetry of the system [21].

In the second part of the thesis, we investigate the issue of spurious poles in infinite volume. As already mentioned the spurious poles are caused by using the ERE outside its range of validity. This and the direct critical consequences of this, namely the negative residue, violation of the unitary relation, and numerical problems, are investigated in detail. We follow this section with a summary of existing methods, which includes the restriction to a low cutoff and a perturbative expansion of the propagator. Here, we especially focus on the problems we see with these methods regarding calculations in finite volume. Thereby, we highlight the need for a non-perturbative method to deal with the issue of the spurious

[2]The boundary conditions are important since they define, how particles close to the end of the volume interact with the edge. Periodic boundary conditions ensure, that the end of the volume is not different to other space-time points.

pole. The remaining part of the chapter is dedicated to the development of such a non-perturbative method. We will introduce the method and carefully show that the method can be justified analytically. In a follow-up step, we will use the method to numerically reproduce the results of selected models. We will show that the non-perturbative method can reproduce the particle-dimer phase shift and bound states of a Yamaguchi model as well as a Gauss model. Additionally, we show that the method conserves the internal consistency of an effective field theory. This will be done by using Lepage plots [51] and a consistency assessment [26, 27].

In the third chapter of the thesis, spurious poles in the finite volume are investigated. We start this by showing how an expected energy spectrum of a Yamaguchi model looks like. It contains bound and scattering states. We will investigate briefly how these states behave with increasing volume size and compare this to the analysis of [21]. Then we follow by showing how the spurious pole expresses itself in finite volume. The pole will cause an additional spurious spectrum of scattering states. It also causes non-physical merging of energy levels, something that will be forbidden in a correct theory by the avoided-level-crossing. In the next section, we will adapt the non-perturbative method to calculations in finite volume. The section will be closed by calculating the energy spectrum using our non-perturbative method and comparing it to the spectrum of the Yamaguchi model. We will show that the method can describe the model accurately and that the description will improve order by order of the $\not\pi$EFT.

In the last part of the thesis, we summarize our findings and give an outlook on closely connected open questions and natural ways to extend the non-perturbative method to further systems.

2 Physical foundation

In this chapter physical concepts, that are relevant in the context of this thesis, are summarized. These include non-relativistic scattering, effective field theories, especially pionless effective field theory in the particle-dimer picture, and physics in a finite volume.

2.1 Scattering theory

In this section general aspects of elastic scattering are summarized, following the introduction given in [77]. We focus on the case of two non-relativistic, spinless particles.
Consider a two-body system, with relative distance $\mathbf{r}$ between the particles and asymptotic relative momentum $\mathbf{p}$. The relative dynamics of the system can be described by a wave function $\Psi_{\mathbf{p}}(\mathbf{r})$. Far away from the center of scattering (where the particles touch each other, $\mathbf{r} = 0$), the wave function can be described as a superposition of an incoming plane wave and a scattered spherical wave.

$$\Psi_{\mathbf{p}}(\mathbf{r}) \overset{r\to\infty}{\longrightarrow} e^{i\mathbf{pr}} + \frac{e^{ipr}}{r} f(\mathbf{p},\mathbf{q})\,. \tag{2.1}$$

The quantity $f(\mathbf{p},\mathbf{q})$ is the scattering amplitude, it depends on the in-going ($\mathbf{p}$) and out-going ($\mathbf{q}$) momenta. The scattering amplitude can be connected to the experimentally measurable differential cross-section by

$$\frac{d\sigma}{d\Omega}(\mathbf{p},\mathbf{q}) = |f(\mathbf{p},\mathbf{q})|^2. \tag{2.2}$$

The scattering amplitude is further related to the on-shell T-Matrix via

$$f(\mathbf{p},\mathbf{q}) = -\frac{m}{4\pi}\langle \mathbf{p}|\; T(E = E_{\mathbf{p}})\; |\mathbf{q}\rangle, \tag{2.3}$$

with $E_{\mathbf{p}} = \mathbf{p}^2/m$. Also note, that $|\mathbf{p}| = |\mathbf{q}|$, due to energy conservation in elastic scattering. In a two-particle system, only the on-shell T-matrix is relevant. However, in the three-particle system it enters off-shell. The full off-shell T-matrix is given by

$$T(\mathbf{p},\mathbf{q},E) = \langle \mathbf{p}|\; T(E)\; |\mathbf{q}\rangle, \tag{2.4}$$

where the momenta $\mathbf{p}$, $\mathbf{q}$, and the energy E are not connected. Due to $|\mathbf{p}| = |\mathbf{q}|$, the scattering amplitude does only depend on $|\mathbf{p}|$ and the angle Θ between $\mathbf{p}$ and $\mathbf{q}$. Therefore a partial-wave expansion can be performed. This yields

$$f(\mathbf{p},\mathbf{q}) = \sum_{l=0}^{\infty}(2l+1) f_l(p) P_l(\cos(\Theta)), \tag{2.5}$$

where $f_l(p)$ are the partial waves, l stands for the different angular momenta, and $P_l(\cos(\Theta))$ are the Legendre polynomials. By investigating the long-distance behavior of the wave function with this expansion, and the expansion of the incoming plane wave in spherical waves, the scattering can be written as

$$\begin{aligned}\Psi_{\mathbf{p}}(\mathbf{r}) &\overset{r\to\infty}{\longrightarrow} \sum_l (2l+1)\left(P_l(\cos(\Theta))\frac{e^{ipr}-e^{-i(pr-l\pi)}}{2ipr} + f_l(p)P_l(\cos(\Theta))\frac{e^{ipr}}{r}\right), \\ &= \sum_l (2l+1)\frac{P_l(\cos(\Theta))}{2ip}\left([1+2ipf_l(p)]\,\frac{e^{ipr}}{r} - \frac{e^{-i(pr-l\pi)}}{r}\right).\end{aligned} \tag{2.6}$$

This allows to further interpret the scattering process. If no scattering takes place, the plane wave can be described by the sum of a spherical in-coming wave $-\exp(-i(pr-l\pi))/r$ and an out-going spherical wave $\exp(ipr)/r$. The scattering modifies the coefficient of the out-going wave. This coefficient is the so-called, S-matrix, or more precisely the l-th diagonal element of the S-matrix.

$$S_l(p) = 1 + 2ipf_l(p). \tag{2.7}$$

The S-matrix fulfills an unitarity relation $|S_l| = 1$. Therefore it can be parameterized by

$$S_l(p) = e^{2i\delta_l(p)}, \tag{2.8}$$

with the l-wave phase shift $\delta_l(p)$. Inserting this parameterization in equation (2.6) allows a physical interpretation of the phase shift. For $\delta_l(p) = 0$ no scattering appears. For $\delta_l(p) \neq 0$ the only change in the wave function at a large distance is a shift in the phase of the out-going wave.
With the phase shift $f_l(p)$ can be written as

$$f_l(p) = \frac{S_l(p)-1}{2ip} = \frac{1}{p\cot(\delta_l(p)) - ip}. \tag{2.9}$$

2.1.1 Phase shift and effective range expansion

For small momenta the phase shift, or more precisely, the quantity in the denominator of equation (2.9) can be expanded. This expansion is called effective rage expansion (ERE) [9, 65]. For the l-th partial wave, it yields

$$p^l \cot\delta_l = -1/a_l + \frac{r_l}{2}p^2 + P_l p^4 + \cdots, \tag{2.10}$$

with the l-wave scattering length a_l, the l-wave effective range r_l, and the l-wave shape parameter P_l. For this thesis, the S-wave ($l = 0$) is the most relevant partial wave. For S-wave interactions the effective range expansion is given by

$$p\cot\delta_S = -1/a_S + \frac{r_S}{2}p^2 + P_S p^4 + \cdots, \tag{2.11}$$

with the S-wave scattering length a_S, the S-wave effective range r_S, and the S-wave shape parameter P_S. For the rest of the thesis, we will always investigate S-waves, therefore we drop the subscribed S. Combining the ERE and equation (2.2) gives a connection between the scattering length and the total cross-section

$$\lim_{E\to 0}\sigma(E) = 4\pi a^2. \tag{2.12}$$

2.1.2 Poles of the scattering amplitude and bound states

Two-body bound states can be identified with poles of the partial-wave scattering amplitude. In the complex momentum plane, they appear on the positive imaginary axis $p = i\gamma$ with $\gamma > 0$. This corresponds to a negative relative energy

$$E = \frac{p^2}{m} < 0. \tag{2.13}$$

For S-waves a condition for bound states due to equation (2.9) yields

$$p \cot \delta_S(p = i\gamma) = ip\,. \tag{2.14}$$

Two-body states with a pole on the negative imaginary axis are called virtual states. States with a pole at negative imaginary part and non-zero positive real part are called resonances. This pole structure is shown in figure 2.1.
Note that the dimer propagator, introduced later, is proportional to the two-body scattering amplitude (compare to figure 2.3). Therefore its poles also are connected to bound states, virtual states, and resonances.

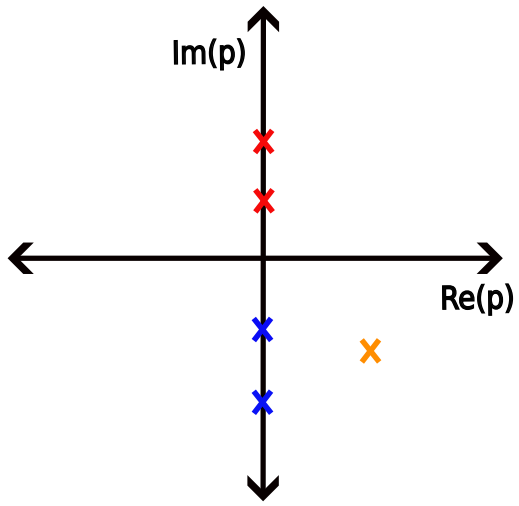

Figure 2.1: The pole structure of the complex momentum plane. The red crosses are bound states, the blue crosses are virtual states, and the orange cross represents a resonance.

2.1.3 Partial wave expansion

A general form of the partial wave expansion is given by [21]

$$\begin{aligned} f(\mathbf{p}) &= \sqrt{4\pi} \sum_{l,m} Y_{l,m}(\hat{\mathbf{p}}) f_{l,m}(p), \\ f_{l,m}(p) &= \frac{1}{\sqrt{4\pi}} \int d\Omega\, Y^*_{l,m}(\hat{\mathbf{p}}) f(\mathbf{p}), \end{aligned} \tag{2.15}$$

where $Y_{l,m}(\hat{\mathbf{p}})$ are spherical harmonics. In the case where $f(\mathbf{p})$ depends only on one angle, this reduces to the expansion in the Legendre polynomials as used in equation (2.5).

2.2 Effective field theory (EFT)

The following introduction to EFTs is inspired by [12] and [80]. Low-energy (m_{low}) phenomena in physics are not sensitive to details of the interaction at short distances (or high energies (m_{high})). This separation of scales can be used to construct simple theories that consider only the relevant degrees of freedom. This is done in EFTs. By the relevant degrees of freedom we mean particle fields, that can be resolved in the investigated energy region. These fields are used to construct the most general Lagrangian. It was shown in [70] that this Lagrangian has to obey all the symmetries of the problem (e.g. Galilean invariance). A Lagrangian which is constructed this way contains an infinite amount of interaction terms in addition to the kinetic terms. By using the separation of scales the relevance of each of these interactions can be obtained. By introducing a power counting it can be shown, that each interaction term scales like $(m_{low}/m_{high})^n$, with different $n \in \mathbb{N}$ for the different interactions. At a chosen accuracy only interactions with corresponding n or lower contribute. Once the relevant terms at a given order n are identified, only a few low-energy constants parametrizing these terms remain. These coupling constants can be determined by matching calculated observables to experimental results, or in the case of this thesis to results of model calculations. This power counting also allows a robust error estimation. The first neglected interaction terms are of order of $(m_{low}/m_{high})^{n+1}$. Therefore an error estimation of an observable O is given by $O\,(m_{low}/m_{high})^{n+1}$.

In this thesis, we investigate a three-particle system in non-relativistic $\not\pi$EFT [15, 43, 44, 68] with a shallow bound two-particle subsystem. This subsystem is often called a dimer. Such a system exhibits an unnaturally large two-body scattering length a. The binding energy of the dimer is approximately $1/(a^2 m)$. Since the dimer is only shallowly bound, the corresponding binding momentum $k_1 = 1/a \sim m_{low}$ scales like the low-energy scale of the theory. On the other hand side, the effective range r of the two-body system is assumed to be of natural size, so it is $1/r \sim m_{high}$. This case can be summarized by $a \gg r$ and the following power counting can be established:

$$\frac{1}{a} \sim p \sim m_{low}; \qquad \frac{1}{r} \sim m_{high}; \qquad \frac{m_{low}}{m_{high}} \ll 1, \tag{2.16}$$

with a typical momentum p of the interaction. A very prominent example of such a system is the neutron-proton scattering in the triplet channel ${}^3S_1$. The corresponding scattering length is $a = 5.42$ fm and the effective range is $r = 1.75$ fm [19]. These values lead to a shallow bound two-body dimer at $E_D = 2.22$ MeV. This state is better known as the deuteron. In this thesis we will investigate a bosonic equivalent of this system, using the same values of a and r. For these values we obtain $r \approx a/3$ and $1/r = 112.35$ MeV $\approx m_{high} = m_\pi = 140$ MeV.

2.3 The three-body system in the particle-dimer picture

The particle dimer picture is a technique to simplify three-particle systems by introducing an auxiliary field, the dimer. A detailed introduction to this picture is for example given in [4, 5, 12, 42]. The idea is that this dimer is a two-particle system in itself. The information of the two-particle system is encoded in the dimer field which can be used in the three-body system resulting in an effective two-body problem. This effective two-particle system contains the dimer and one single particle. If one matches the appearing dimer-related quantities to the two- and three-body forces of the three-particle theory,

the particle dimer picture is mathematically equivalent to the three-body system. Except for terms at higher-order in the EFT expansion, meaning terms suppressed by orders of m_{low}/m_{high}. This matching has been considered in the literature already many times (see, e.g. [3, 4, 12]).
For a system with S-wave interactions the Lagrangian in the particle-dimer formalism takes the following form [6]:

$$\begin{aligned}\mathcal{L}_d =& \psi^\dagger \left(i\partial_0 + \frac{\nabla^2}{2m} \right) \psi + \sigma d^\dagger \left(i\partial_0 + \frac{\nabla^2}{4m} + \Delta \right) d + \frac{f_0}{2} \left(d^\dagger \psi^2 + \text{h.c.} \right) \\ &+ h_0 d^\dagger d \psi^\dagger \psi \; + h_2 d^\dagger d (\psi^\dagger \nabla^2 \psi + (\nabla^2 \psi^\dagger)\psi) + \cdots .\end{aligned} \tag{2.17}$$

d denotes the dimer field and ψ is the single-particle field. m is the mass of the single-particle. The sign of $\sigma = \pm 1$ is linked to the sign of the effective range r. In our case ($r > 0$) this implies $\sigma = -1$. f_0 is the strength of the decay (re-combination) of a dimer into two single particles, which is connected to the two-body scattering length a. The terms proportional to h_0 and h_2 are three-body forces. Note that an EFT for three bosons needs a three-body force even at LO to describe three-body observables correctly [4, 18]. The h_0 term is such a leading order three-body force, the h_2 is a N^{2}LO three-body force. The ellipses in the second line stand for higher-order three-body forces. Higher-order three-body forces come with additional factors of $(\nabla^2)^n$ and are suppressed by $(m_{low}/m_{high})^{2n}$.
Note that the particle dimer picture will work especially well in a system with a physical two-body bound state. This is the case we consider in this thesis. The unnaturally large positive two-body scattering length a leads to a two-body shallow bound state with $E_D \approx 1/a^2 m$. However, the particle dimer picture will also work if such a state is not present in the theory.
The Lagrangian in the particle dimer picture leads to the following one and two-body Feynman rules [6, 5]. For the single-particle propagator one obtains

$$S_1(p_0, \mathbf{p}) = \frac{i}{p_0 - \mathbf{p}^2/(2m) + i\varepsilon}. \tag{2.18}$$

The bare dimer propagator at LO is connected to the term $\sigma d^\dagger \Delta d$ in the Lagrangian. It is given by

$$S_D^{LO} = -\frac{i}{\Delta}. \tag{2.19}$$

The bare dimer propagator at NLO is connected to the full kinetic term shown in equation (2.17). It is given by

$$S_D^{NLO}(p_0, \mathbf{p}) = -\frac{i}{\Delta + p_0 - \mathbf{p}^2/(4m)}. \tag{2.20}$$

Note that these bare propagators cannot describe the propagation of the dimer sufficiently. Due to the dimer being a two-particle system in itself, a dressed propagator has to be used, see next section. Finally, the leading-order dimer-decay (=recombine) vertex is given by

$$V^{(0)}_{d^\dagger \psi^2} = -i f_0. \tag{2.21}$$

2.3.1 The dressed dimer propagator

In this section, we calculate the dressed dimer propagator. We start by obtaining the propagator in leading order, meaning taking only the scattering length a into account. In a second step, we will include corrections due to the effective range r, this will be accomplished by two different methods: non-perturbatively and perturbatively.

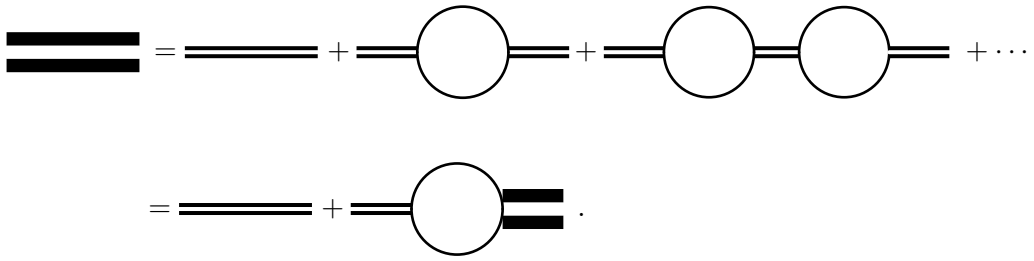

Figure 2.2: Feynman diagrams for the dressed dimer propagator (thick double line). The thin double line stands for the bare propagator at LO, the single lines stand for single-particle propagators. The contact between two single-particle lines and a bare propagator stand for the LO vertex $V^{(0)}_{d^\dagger\psi^2}$. At leading order, all amount of insertion of additional loops contribute. In the second line, the infinite series of diagrams is summed into an integral expression.

The dimer propagator in leading-order

We start, by investigating the dimer propagator at leading order. Since the dimer is a two-particle system the dimer propagator is more complicated than the bare dimer propagator that one obtains from the Lagrangian (equation (2.19)). Due to the term proportional to $d^\dagger\psi^2$ in the Lagrangian the dimer can break up into two single particles and recombine. This can happen multiple times. The corresponding Feynman diagrams can be seen in figure 2.2. This diagrammatic expression is also called the Dyson equation. All these diagrams contribute and therefore the propagator contains infinite many loops. The full dimer propagator is called dressed dimer propagator. For each insertion of a loop, we add a loop, two times the dimer-decay vertex $V^{(0)}_{d^\dagger\psi^2}$ and one bare propagator. The loops[1] count as $p^1 \sim m_{low}$. The vertices together with the bare propagator count as $a \sim 1/m_{low}$ (see below). Therefore each single insertion counts as $ap \sim 1$. In other words, the inclusion of one additional loop does not change the power counting of the diagram. It becomes clear that all infinite parts of figure 2.2 have to be taken into account.
We calculate the contribution of a single loop times one bare propagator. Let the in-going momentum (energy) be $\mathbf{p}$ (p_0) and the loop momentum (energy) $\mathbf{q}$ (q_0) be distributed to one loop-particle having a momentum (energy) of $\mathbf{p}+\mathbf{q}$ (p_0+q_0) and the other loop-particle having $-\mathbf{q}$ ($-q_0$). The contribution

[1]The loops contain two times the single-particle propagator $\sim p^{-1}\,p^{-1}$ and the measure of three-dimensional integral $\sim p^3$.

gives

$$\begin{aligned}
\text{Loop}\cdot S_D^{LO} &= (-if_0)\int^{\Lambda}\frac{d^3\mathbf{q}}{(2\pi)^3}\frac{dq_0}{2\pi}\frac{i}{-q_0-\mathbf{q}^2/(2m)+i\varepsilon}\frac{i}{p_0+q_0-(\mathbf{q}+\mathbf{p})^2/(2m)+i\varepsilon}(-if_0)\frac{-i}{\Delta}\\
&= -\frac{f_0^2}{\Delta}m\int^{\Lambda}\frac{d^3\mathbf{q}'}{(2\pi)^3}\frac{1}{mp_0-p^2/4-\mathbf{q}'^2+i\varepsilon}\\
&= \frac{f_0^2}{\Delta}\frac{m}{4\pi}\left(\frac{2\Lambda}{\pi}+\sqrt{\frac{\mathbf{p}^2}{4}-mp_0-i\varepsilon}\arctan\left(\frac{\sqrt{\frac{\mathbf{p}^2}{4}-mp_0-i\varepsilon}}{\Lambda}\right)-\sqrt{\frac{\mathbf{p}^2}{4}-mp_0-i\varepsilon}\right)\\
&= \frac{f_0^2}{\Delta}\frac{m}{4\pi}\left(\frac{2\Lambda}{\pi}-\sqrt{\frac{\mathbf{p}^2}{4}-mp_0-i\varepsilon}\right)+\cdots .
\end{aligned} \tag{2.22}$$

The integral is ultraviolet divergent, Therefore it has to be regularized. We do this by using a sharp cutoff Λ. In the second step we have shifted $\mathbf{q}' = \mathbf{q} + \mathbf{p}^2/2$, in the third step the Sokhotski–Plemelj theorem (equation (3.31)) was used and in the final step the $\arctan(x)$ was expanded for small arguments[2]. With this expression the dressed propagator can be calculated using the expression for a geometric series.

$$i\tau'^{LO}(\mathbf{p},p_0) = \frac{iS_D}{1-\text{Loop}\cdot S_D} = \frac{1}{\Delta - f_0^2\Lambda m/(2\pi^2)+f_0^2 m/(4\pi)\sqrt{\mathbf{p}^2/4-mp_0-i\varepsilon}}\,. \tag{2.23}$$

Note that this propagator depends on the momentum cutoff Λ. Physical observables cannot depend on it. To remove the Λ-dependence the bare couplings in the Lagrangian f_0 and Δ have to be re-normalized. In the present form of the propagator, this is especially simple. The propagator is directly connected to the two-body scattering amplitude. The on-shell two-body T-matrix can be obtained by adding the dimer-decay vertex on both sides to the propagator, which is shown in figure 2.3. Therefore,

$$\begin{aligned}
T(k) &= (if_0)\tau'^{LO}\left(p_0=\frac{k^2}{m},\mathbf{p}=0\right)(if_0)\\
&= \frac{-f_0^2}{\Delta - f_0^2\Lambda m/(2\pi^2)+f_0^2 m/(4\pi)\sqrt{-k^2-i\varepsilon}} = \frac{4\pi/m}{-4\pi\Delta/(f_0^2 m)+2\Lambda/\pi-ik-i\varepsilon}.
\end{aligned} \tag{2.24}$$

This can be compared to the well known form of the on-shell two-body T-matrix using the effective range expansion:

$$T(k) = \frac{4\pi/m}{k\cot\delta - ik - i\varepsilon} = \frac{4\pi/m}{-1/a+\cdots-ik-i\varepsilon}. \tag{2.25}$$

By comparing the expressions one obtains the re-normalization condition for the two-body coupling constants Δ and f_0.

$$-\frac{1}{a} = -\frac{4\pi\Delta}{f_0^2 m}+\frac{2\Lambda}{\pi}. \tag{2.26}$$

Note that this means $f_0^2 m/\Delta \sim a$. Therefore, the result of equation 2.22 indeed scales like $ap \sim 1$, as anticipated. All insertions of additional loops in figure 2.2 must be taken into account at LO. We conclude this section by giving the dimer propagator at LO as it will be used in the Faddeev equation below (in

[2]This can be done, since $p \sim p_0 \sim m_{low}$ and $\Lambda \sim m_{high}$, so $p/\Lambda \sim m_{low}/m_{high} \ll 1$.

there the multiplicative factors have been absorbed in the normalization of the particle-dimer scattering amplitude):

$$\tau^{LO}(k^*) = \frac{1}{-1/a + k^*}, \tag{2.27}$$

with $(k^*)^2 = 3/4\mathbf{k}^2 - mk_0$.

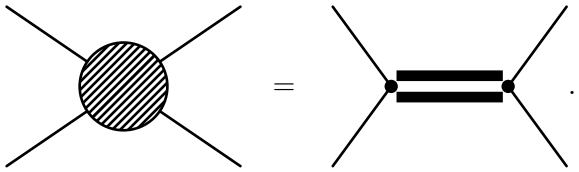

Figure 2.3: The two-body scattering amplitude $T(k)$ in terms of the dimer propagator. The blob with the oblique lines is the two-body scattering amplitude, the thick double line represents the dressed dimer propagator, the small circles stand for the dimer-decay vertices $V^{(0)}_{d^\dagger\psi^2}$.

Non-perturbative range corrections to the propagator

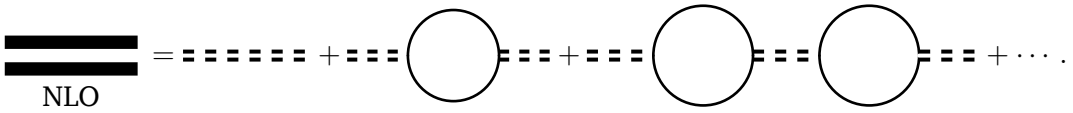

Figure 2.4: Feynman diagrams for the dressed dimer propagator including range corrections. The notation is the same as in figure 2.2, but with the dashed double lines being the bare dimer propagator at NLO. This bare propagator is given by equation (2.20).

There are two ways to include range corrections: perturbatively or non-perturbatively. We briefly summarize both methods and discuss how they are related to each other. For the non-perturbative method we follow the steps discussed in [12], also see [49]. The effective range r in the effective range expansion appears in combination with the momentum squared. Therefore it is natural to include an additional term in the Lagrangian containing derivatives, this can be done[3] by adding additional parts to the kinetic term in the Lagrangian. In equation (2.17) this is already done. The additional terms lead to the changed bare dimer propagator at NLO. This is given by equation (2.20). The dressed propagator has to be modified accordingly. The Dyson series for this can be seen in figure 2.4. The structure of the series is the same as at LO. Therefore we can repeat the steps of the last section, but the LO propagator has to be changed by the NLO version. A easy way of doing so is to exchange Δ by $\Delta + p_0 - \mathbf{p}^2/(4m)$.

[3]Note that this is not unique, alternatively one can add additional decay vertices with derivative terms, this can be seen for example in [34].

For the propagator this yields

$$i\tau'^{NLO}(\mathbf{p}, p_0) = \frac{1}{\Delta - (\mathbf{p}^2/(4m) - p_0) - f_0^2 \Lambda m/(2\pi^2) + f_0^2 m/(4\pi)\sqrt{\mathbf{p}^2/4 - m p_0 - i\varepsilon}}. \tag{2.28}$$

This leads to a two-body scattering amplitude of

$$T(k) = \frac{4\pi/m}{-4\pi\Delta/(f_0^2 m) + 2\Lambda/\pi + 4\pi/(f_0^2 m^2)\, k^2 - ik - i\varepsilon}. \tag{2.29}$$

Comparing this to the NLO version of equation (2.25) directly leads to the effective range expansion in the denominator.

$$T^{NLO}(k) = \frac{4\pi/m}{k\cot\delta - ik - i\varepsilon} = \frac{4\pi/m}{-1/a + r/2k^2 \cdots - ik - i\varepsilon}. \tag{2.30}$$

Therefore the corresponding propagator at NLO as it will appear in the Faddeev equation is

$$\tau^{NLO}(k^*) = \frac{1}{-1/a - r/2(k^*)^2 + k^*}. \tag{2.31}$$

Note that the superscribed NLO can be misleading. In the theory we investigate it is $r \ll a$. If we want to investigate the power-counting of $\tau^{NLO}(k^*)$, it can be expanded for small r. This leads to

$$\tau^{NLO}(k^*) = \tau^{LO}(k^*) + \sum_{n=1}^{\infty} \frac{n!(k^*)^{2n}}{(-1/a + k^*)^{n+1}} \left(\frac{r}{2}\right)^n. \tag{2.32}$$

Therefore the corrections to the LO propagator scale like $p^{2n} p^{-n-1} r^n \sim m_{low}(m_{low}/m_{high})^n$. In other word they are suppressed compared to the LO propagator by $(m_{low}/m_{high})^n$. Strictly speaking only the first term $n = 1$ is a NLO quantity. The propagator $\tau^{NLO}(k^*)$ also contains contributions of higher order. However, it does not contain all possible higher order parts. At N^{3}LO for example corrections due to the shape parameter have to be included. But since higher order contributions can be ignored in an EFT for $m_{low}/m_{high} \ll 1$, $T^{NLO}(k)$ and the following $\tau^{NLO}(k^*)$ can be used as if it are NLO quantities. This method is also called re-summation, since the non-perturbative propagator contains all parts of the sum in equation (2.32).
The benefit of this method is, that the form of equation (2.29) and equation (2.30) are the same. The single terms of the famous effective range expansion can be read off easily. Also, the inclusion of higher-order terms is straightforward. Additional derivative terms in the kinetic part can be directly connected to the higher-order parts (shape parameter, ...) of an ERE. Note, in this case, additional coupling constants are needed. However, it also comes with a downside, equation (2.31) can exhibit spurious poles. In fact, this is the major topic of this thesis and will be discussed below in all detail.

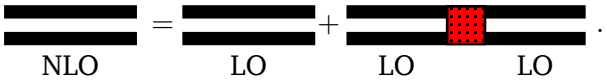

Figure 2.5: The dressed NLO dimer propagator in the perturbative method. The thick double line with the superscribed LO (NLO) is the dressed dimer propagator at LO (NLO) and the red filled square is the momentum dependent vertex $V'^{(2)}_{d^\dagger d}$.

In this section we summarize the method explained in [2, 5]. The perturbative method is based on the natural-sized effective range $r \sim 1/m_{high}$ and the unnaturally large scattering length $a \gg r$. Based on this the bare propagator at NLO can be expanded:

$$S_D^{NLO}(p_0, \mathbf{p}) = -\frac{i}{\Delta + mp_0 - \frac{3}{4}\mathbf{p}^2} = \frac{-i}{\Delta}\left(1 - \left(mp_0 - \frac{3}{4}\mathbf{p}^2\right)^1 + \cdots\right). \tag{2.33}$$

Therefore, the correction to the LO propagator can be understood as an additional possible vertex:

$$V_{d^\dagger d} = i f_2 (k^*)^2. \tag{2.34}$$

With some coupling f_2. If we are interested in the propagator at NLO, meaning a propagator that includes all terms proportional to $(m_{low}/m_{high})^0$ and $(m_{low}/m_{high})^1$, one insertion of this vertex per diagram is sufficient. The NLO correction to the propagator can be obtained by simply adding the LO propagator from both sides to one single NLO vertex. This can be seen in figure 2.5. Therefore the NLO correction to the propagator $\tau(k^*)^{NLO}_{cor}$ is given by

$$\tau^{NLO}_{cor}(k^*) = \tau^{LO}(k^*) V'_{d^\dagger d} \tau^{LO}(k^*) = i f_2 \frac{(k^*)^2}{(-1/a + k^*)^2}. \tag{2.35}$$

This expression can be compared to the perturbative expansion of the two-body scattering amplitude given by equation (2.32). This results in the perturbative dimer propagator:

$$\tau^{NLO}_{pert}(k^*) = \tau^{LO}(k^*) + \tau^{NLO}_{cor}(k^*) = \frac{1}{-1/a + k^*} + \frac{r}{2}\frac{(k^*)^2}{(-1/a + k^*)^2}. \tag{2.36}$$

The relation between the non-perturbative and the perturbative method is clear. By expanding the non-perturbative propagator (equation (2.31)) for small values of the effective range, one obtains the perturbative expression. The higher-order terms can be obtained in the perturbative method by inserting the vertex $V'^{(2)}_{d^\dagger d}$ multiple times. The benefit of the perturbative method is that the propagator $\tau^{NLO}_{pert}(k^*)$ actually is a NLO quantity, it contains all terms suppressed to the LO diagrams by m_{low}/m_{high} and no higher-order terms. However, the sum is slightly more complicated to implement than the single term in the non-perturbative method and the larger exponent of the physical pole in the denominator of the corrections will result in convergence issues in finite volume, compare to section 3.1.4. In this thesis, we use the non-perturbative method, meaning the propagator given by equation (2.31).

2.3.2 The Faddeev equation in the particle-dimer picture

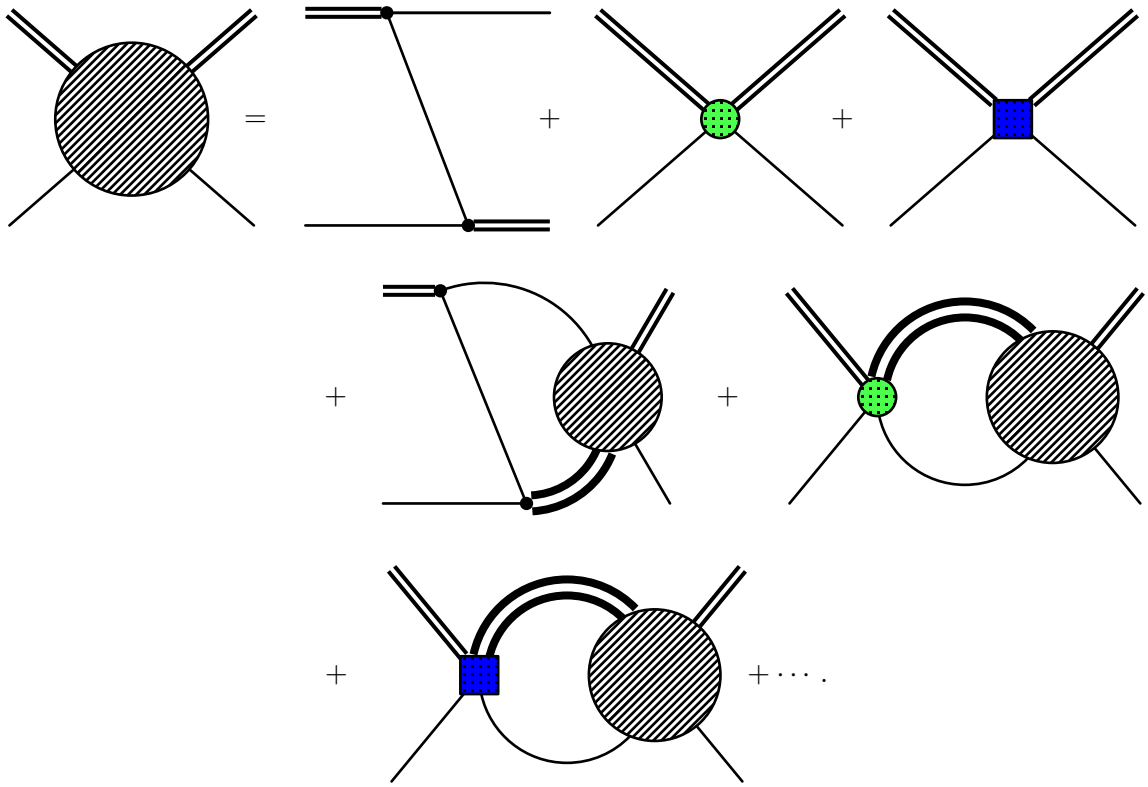

Figure 2.6: The Faddeev equation written in Feynman diagrams. The blob with the oblique lines is the particle dimer scattering amplitude. The thin double line is the bare dimer propagator. The thick double line is the dressed dimer propagator, we use the non-perturbative NLO version of it, which is given by equation (2.31). The single line stands for a single-particle propagator. The green filled circle is a three-body vertex proportional to p^0 and the blue filled square is a three-body vertex proportional to p^2. The second three-body force does not contribute before N^{2}LO. The ellipses stand for even higher-order three-body forces.

Equipped with the dressed dimer propagator, the three-particle system can be described in the particle dimer picture. The particle dimer scattering amplitude $M(\mathbf{p}, \mathbf{q}, E)$ is proportional to the three-particle scattering amplitude. $\mathbf{p}$ ($\mathbf{q}$) denotes the in-going (out-going) relative momentum between the particle and the dimer. E is the transferred energy. The particle dimer scattering amplitude can be calculated by solving the Faddeev equation. A more detailed derivation of the Faddeev equation can be found in [12]. A representation in Feynman diagrams of the Faddeev equation can be seen in figure 2.6. The first diagram on the right-hand side of this stands for the one-particle exchange. The dimer can decay and one of the containing particles can form a new dimer with the single-particle. The second diagram is a LO three-body force. In the particle dimer picture, three-body forces are caused by terms in the Lagrangian containing $d^\dagger d \psi^\dagger \psi$. The third term denotes the first higher-order three-body force, this appears at N^{2}LO. Note that all combinations of LO diagrams also contribute to LO. Therefore all iterations of these diagrams have to be taken into account. This is shown in the second line of figure 2.6. In the

third line, all iterations of the N^{2}LO diagrams are shown. The ellipses stand for higher-order three-body forces.
The Faddeev equation can be written as [12]

$$M(\mathbf{p},\mathbf{q};E) = Z(\mathbf{p},\mathbf{q};E) + 8\pi \int^{\Lambda} \frac{d^3\mathbf{k}}{(2\pi)^3}\, Z(\mathbf{p},\mathbf{k};E)\tau(k^*)M(\mathbf{k},\mathbf{q};E). \tag{2.37}$$

The loop integral diverges for large momenta **k**, therefore it has to be regularized. We choose a sharp ultraviolet cutoff Λ as in the last section. The dimer decay vertices have been absorbed in the normalization of the scattering amplitude. All diagrams of the first line of figure 2.6 have been summarized in the potential Z(**p**,**q**;E), that is given by

$$Z(\mathbf{p},\mathbf{q};E) = \frac{1}{\mathbf{p}^2+\mathbf{q}^2+\mathbf{pq}-mE} + \frac{H_0(\Lambda)}{\Lambda^2} + \frac{H_2(\Lambda)}{\Lambda^4}\frac{3}{8}\left(\mathbf{p}^2+\mathbf{q}^2\right) + \cdots . \tag{2.38}$$

The coefficients $H_0(\Lambda)$ and $H_2(\Lambda)$ are the re-normalized three-body forces. The re-normalization cancels the Λ-dependence of the integral, see below for details. The values of the coefficients H_0 and H_2 have to be fine-tuned to reproduce three-body observables. This will be done for example in section 3.3.2. At N^{2}LO, this includes the term proportional to H_2, this fine-tuning is complicated since H_0 and H_2 cannot be obtained separately. A slightly different potential can be obtained by introducing a trimer auxiliary field[5]:

$$Z(\mathbf{p},\mathbf{q};E) = \frac{1}{\mathbf{p}^2+\mathbf{q}^2+\mathbf{pq}-mE} + \frac{H_0}{\Lambda^2} + \frac{H_2}{\Lambda^4}(mE+\gamma^2) + \cdots , \tag{2.39}$$

with $\gamma = \sqrt{mE_d}$ and the binding energy E_d of the dimer. At N^{2}LO both potentials are equivalent, up to higher orders of the EFT both potentials lead to the same physics. This is proven in [5], in [25] it is assumed that they are also equivalent for higher orders. This potential allows for an independent calculation of H_0 and H_2 and will be used below.
Note that the Faddeev equation (2.37) for $\Lambda \to \infty$ and without three-body forces, meaning $H_0 = 0,\ H_2 = 0, \cdots$, is equivalent to the famous Skorniakov-Ter-Martirosian (STM) equation [67]. Therefore, the version above with three-body forces is also called STM3 equation.
As introduced in the last section, the dimer propagator is given by

$$\tau(\mathbf{k},E) = \tau(k^*) = \frac{1}{k^*\cot\delta(k^*)+k^*}, \tag{2.40}$$

with the two-particle phase shift $\delta(k^*)$. We use the following notation for the loop momentum k^*:

$$k^* = \sqrt{\frac{3}{4}\mathbf{k}^2 - mE}. \tag{2.41}$$

The quantity $k^*\cot\delta(k^*)$ can be expanded by using the ERE (equation (2.11)). Using the LO of this gives the LO propagator (equation (2.27)), using the NLO gives the fully re-summed NLO propagator (equation (2.31).
Following the line of reasoning in [12] the re-normalized LO three-body force can be calculated for a given cutoff by

$$H_0(\Lambda) = \frac{\cos\left[s_0\ln(\Lambda/\Lambda^*)+\arctan(s_0)\right]}{\cos\left[s_0\ln(\Lambda/\Lambda^*)-\arctan(s_0)\right]}, \tag{2.42}$$

where Λ^* is a three-body quantity that has to be obtained by fine-tuning to three-body observables and with s_0 a constant that belongs to the discrete scaling of Efimov states, see below. It is given by $s_0 \approx 1.0062$. If one does all calculations for the same cutoff Λ', the three body force $H_0(\Lambda')$ can be treated as as a constant. This constant can be obtained once, and the Λ-dependence in equation (2.42) can be ignored. Please note that we modify equation (2.42) in the non-perturbative method, developed below, by adding constant and Λ-dependent terms to it. For a fixed Λ' this means changing the constant $H_0(\Lambda')$ by an other constant $H_0'(\Lambda')$.
By performing a partial-wave expansion (compare to section 2.1.3) of the Faddeev equation and projecting to S-waves, meaning $l = 0$, a relation for the S-wave scattering amplitude can be obtained.

$$M_S(p,q,E) = Z_S(p,q,E) + \frac{4}{\pi}\int_0^\Lambda dk\, k^2\, Z_S(p,k,E)\tau(k^*)M_S(k,q,E), \tag{2.43}$$

with the S-wave projection of the potential

$$Z_S(p,q,E) = \frac{1}{2pq}\frac{p^2+q^2+pq-mE}{p^2+q^2-pq-mE} + \frac{H_0}{\Lambda^2} + \frac{H_2}{\Lambda^4}(mE - mE_d) + \cdots . \tag{2.44}$$

The S-wave scattering amplitude is connected to the S-wave particle-dimer phase shift $\delta_S^{(3)}$ by

$$M_S(p,p,E_p) = \frac{N}{p\cot\delta_S^{(3)} - ip}, \tag{2.45}$$

with $E_p = 3/4\, p^2/m - E_d$ and a normalization N. The normalization is calculated in the appendix. For the rest of the thesis we will always consider S-wave quantities, therefore the subscript S will be dropped everywhere in the notation below.

2.4 Efimov states

Efimov [23] discovered that for a three-particle system with an infinite large two-body scattering length $1/a = 0$ an infinite amount of three-body bound states will appear. A more recent revive is given by [13]. These states have a fixed scaling between their binding energy:

$$\frac{E^{(n+1)}}{E^{(n)}} = e^{-2\pi/s_0}. \tag{2.46}$$

While this discrete scaling is only exact in the unitary limit $1/a = 0$, the infinite amount of states will also appear for a finite large value of a. The series of bound states will obviously be cut by the cutoff, however, by increasing the value of Λ, more and more of such states should be found. In section 3.3.5 we will see exactly such behavior in our numerical results.

2.5 Finite volume

In this section we introduce the concepts of physics in a finite volume. We discuss why this is interesting, what we mean by finite volume, what consequences this has to momentum space, and finally we will re-derive the quantization condition in finite volume.

2.5.1 Motivation

Calculations from first principles in physics are often very challenging. The most fundamental theory available for the strong interaction is QCD. It contains quarks and gluons as degrees of freedom. Since ab-initio calculations are very challenging powerful numerical methods have to be used. One of the most promising methods to do so are calculations on the lattice. The idea of this is, that the space-time will be treated as if it is discretized. Therefore the considered particles are put on a space-time lattice. This allows for various simplifications of the system, such as allowing the particles to only interact with the next neighboring space-time points. In the context of the strong interaction, an example of this is lattice QCD [20, 73]. In the low-energy context of this thesis, there is no need to treat the time coordinate in the same manner as the spacial ones. It has not to be discretized. For three space dimensions, a three-dimensional lattice is used. See figure 2.7 for a schematic representation of this. The single space points have a distance of d_{lat} to each other, this is also called lattice spacing. To connect results from the lattice to continuous space, the limit $d_{lat} \to 0$ has to be considered. For example, this can be done by repeating the calculations for multiple values of d_{lat} and extrapolating to zero.
Besides this, an additional restriction has to be made. The discrete space-time in finite volume still contains an infinite amount of points. This is not accessible by numerical calculations. Even a computer can not deal with infinite many terms. Therefore the space has to be restricted, the calculations have to be performed in finite volume. An often-used choice is a finite cubic volume. The benefit of a cubic volume is that all three space dimensions are treated equally. Additionally, the number of space points can be calculated easily. It is given by $(L/d_{lat})^3$ for a cube with edge length L.
Please note that this specification of the volume is not sufficient to perform lattice calculations. A second, needed information is the behavior of the system at the edge of the volume. Therefore, some set of boundary conditions has to be applied. A typical choice is periodic boundary conditions. One does not want to treat space points at the edge of the volume differently than any other space point. After all, in infinite volume, those points are not special in any way. If another set of boundary conditions is used, for example, a hard wall, the space points at the edge have fewer neighbors than every other space point. This could lead to an effective, additionally attractive, or repulsive interaction. By using periodic boundary conditions this can be avoided. The points at the edge 'see' the points at the other edge as their neighbors. Therefore they have the same amount of neighbors as every other space point of the lattice. A schematic representation of periodic boundary conditions is shown in figure 2.8.

2.5.2 Set up

In the context of this thesis finite volume always means a cubic box with edge length L and periodic boundary conditions, compare to figure 2.8. This is a standard choice, that is used in multiple lattice calculations [20, 73]. It is especially elegant to use in position space, since all Cartesian coordinate directions are restricted in the same way. The periodic boundary conditions (that is the behaviour of the wave function $\Psi(\mathbf{r})$ at the surface of the cube) for m particles is defined by

$$\Psi(\mathbf{r}_1 + L\mathbf{n}_1, \cdots, \mathbf{r}_m + L\mathbf{n}_m) = \Psi(\mathbf{r}_1, \cdots, \mathbf{r}_m), \text{ with } \mathbf{n}_i \in \mathbb{Z}^3. \tag{2.47}$$

Here $\mathbf{r}_i$ is the position of the i-th particle. One way of visualizing these conditions is, to connect the surfaces of the box, so particles can leave on one side and enter on the other side. In a 1-D reduction of a box, a line, this would mean, connecting the endpoints of the line and therefore creating a circle. A 2-D analog would be a square. Connecting the edges of this square creates a torus. For a 3-D box, the

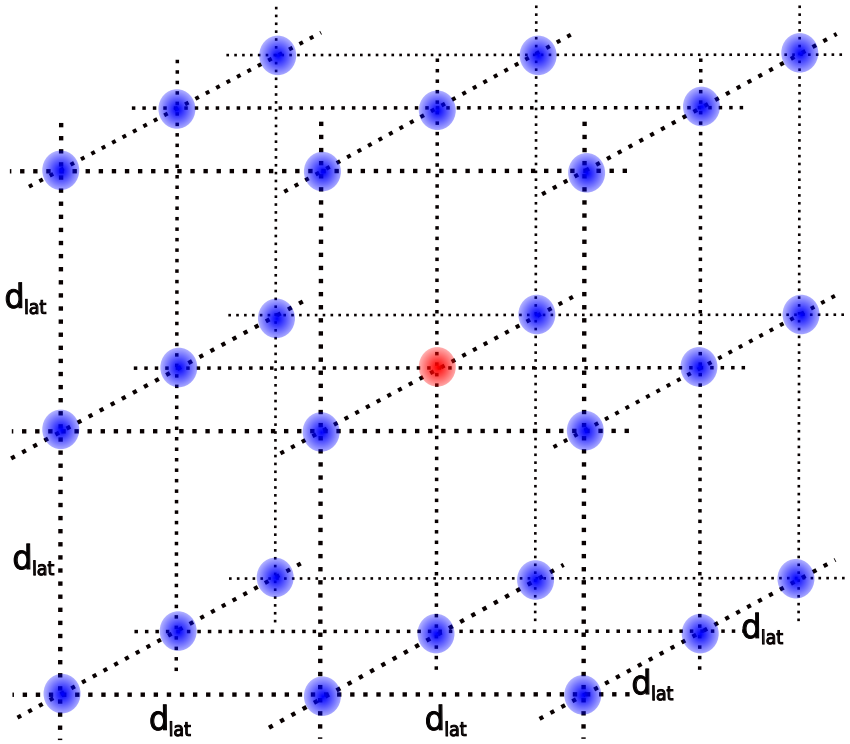

Figure 2.7: A schematic representation of a lattice. The position-space is discrete. Particles can only be on the blue or red dots. The distance between two neighbouring points is given by the lattice spacing d_{lat}. Note that the position-space points at the surface of the finite cubic volume (blue dots) have a different number of neighbours that the points in the inner (red dot). To hinder this special treatment periodic boundary conditions are used.

resulting geometric object is a hyper-torus. Along these lines, an experimental realization of finite volume with periodic boundary conditions can be done. For example, see [16, 17]. However, these realizations are not what is considered here. In this thesis we understand finite volume as a tool to enable lattice calculations. Therefore it is necessary to be able to connect the calculations in finite volume to physics in the infinite volume.
Another way to visualize the boundary conditions is, to fill the whole space with identical copies of the system. In this context, the Lüscher effect can be understood by particles leaving the box and interacting with the **n**-th copy of it.

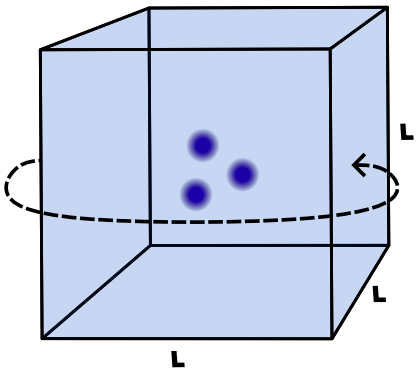

Figure 2.8: Three particles in a finite cubic volume with edge length L (a box) with periodic boundary conditions.

While in this thesis we always consider the boundary conditions given by equation (2.47) other conditions are possible. Different boundary conditions are for example hard walls or twisted periodic boundaries. The latter is important in the context of the topological effect [10]. Note that all choices of boundary conditions influence the results in slightly different ways. It is even possible to exploit these differences to obtain additional information about the physical system [55].
An obvious characteristic of calculations in final volume is that for $L \to \infty$ the volume is infinite again. Thus in this limit, the observables for the 'finite' volume must reproduce observables calculated in infinite volume. This can be used as a simple check of consistency. In the numerical calculations below we will always compare the finite volume results to the infinite volume results to see this convergence.

Finite volume in momentum space

Since we regard the EFT and especially the Faddeev equation (2.37) in momentum space, it is necessary to understand the impact of finite volume (= limited position space) on physics in momentum space. It is well known that the transition between position and momentum space is given by the Fourier transform. Consider a two-particle system with relative distance $\mathbf{r}$, relative momentum $\mathbf{q}$. The Fourier transform yields

$$\Psi(\mathbf{q}) = \int \frac{d^3r}{(2\pi)^3} e^{i\mathbf{qr}} \Psi(\mathbf{r}). \tag{2.48}$$

Shifting the integrand by $\mathbf{n}L$ leads to

$$\Psi(\mathbf{q}) = \int \frac{d^3r}{(2\pi)^3} e^{i\mathbf{qr}+i\mathbf{qn}L} \Psi(\mathbf{r}+\mathbf{n}L) = \int \frac{d^3r}{(2\pi)^3} e^{i\mathbf{qr}+\mathbf{qn}L} \Psi(\mathbf{r}). \tag{2.49}$$

In the last step the boundary condition, equation (2.47), has been used. Equation (2.48) and equation (2.49) can be simultaneously true, if and only if the additional exponential factor equals one, therefore

$$\mathbf{q}\,\mathbf{n}\,L \in 2\pi\,\mathbb{Z}. \tag{2.50}$$

Since $\mathbf{n} \in \mathbf{Z}$, this leads to

$$\mathbf{q} \in \frac{2\pi}{L}\mathbb{Z}^3. \tag{2.51}$$

So in a finite volume with periodic boundary conditions, only discrete momenta are allowed. This discretization of momenta can be understood by phenomenologically comparing it to the well-known result for a particle in an infinite square well potential. Note that this example of a square-well potential does not have a direct connection to the way finite volume is used here, but it should make the connection between limited position space and discrete momenta comprehensible. In this system the special periodic boundary conditions are

$$\Psi(0) = \Psi(L) = 0, \tag{2.52}$$

due to the infinite potential at the borders of the well at $x = 0$ and $x = L$. The results for the wave function are given by (for example [75])

$$\Psi_n(x) = \sqrt{\frac{2}{L}}\sin(xk_n); \text{ with } k_n \in \frac{\pi}{L}\mathbb{Z}. \tag{2.53}$$

Only discrete values of the wavenumber k_n are allowed. Only waves are possible, that fit in the well, This is shown in figure 2.9.

A direct consequence of the discrete momenta, according to equation 2.51, is that appearing momentum integrals collapse to sums over the allowed momenta.

$$\int \frac{d^3\mathbf{q}}{(2\pi)^3} f(\mathbf{q}) \to \frac{1}{L^3} \sum_{\mathbf{q}\in 2\pi/L\cdot\mathbb{Z}^3} f(\mathbf{q}). \tag{2.54}$$

Finally, we note that for $L \to \infty$ the distance between two neighboring momenta vanishes, and the continuum is restored.

2.5.3 Quantization condition in finite volume

We consider the same non-relativistic system in the particle dimer-picture as before. For a relativistic-invariant form see [61]. The Faddeev equation (equation (2.37) in infinite volume) takes a different form in finite volume. As discussed before only discrete momenta are allowed due to the periodic boundary conditions. Therefore, the loop integral collapses to a sum over the discrete momenta. In this section all momenta have to be understood as $\mathbf{k} \in 2\pi/L\,\mathbb{Z}^3$. This reads

$$M_L(\mathbf{p},\mathbf{q},E) = Z(\mathbf{p},\mathbf{q},E) + \frac{1}{L^3}\sum_{\mathbf{k}}^{\Lambda} Z(\mathbf{p},\mathbf{k},E)\tau^L(k^*)M_L(\mathbf{k},\mathbf{q},E). \tag{2.55}$$

Note that the calculation of the dressed dimer propagator $\tau(k^*)$ also contains loop integrals in infinite volume (compare to equation (2.22) for example). The dimer propagator has to be exchanged by a

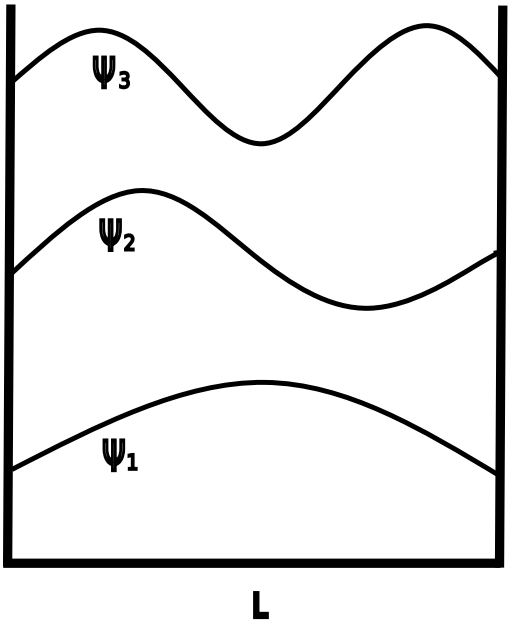

Figure 2.9: Results for the wave function of one particle in a infinite square-well potential, schematic representation. This system shall motivate the connection between finite volume, boundary conditions and discrete momentum space. Only wave functions that fulfill the boundary condition (here $\Psi(0) = \Psi(L) = 0$) are allowed. This leads to waves with discrete wavenumbers. Compare to [75].

finite volume version of it: $\tau(k^*) \to \tau^L(k^*)$. As shown for example in [33, 34] the equivalent of the fully re-summed propagator is given by

$$\tau^L(k^*) = \tau^L(\mathbf{k}, E) = \frac{1}{k^* \cot \delta(k^*) + S_L(\mathbf{k}, E)} = \frac{1}{-1/a - r(k^*)^2/2 + S_L(\mathbf{k}, E)}\,, \tag{2.56}$$

where the ERE has been used up to NLO and

$$S(\mathbf{k}, E) = -\frac{4\pi}{L^3} \sum_{\mathbf{p}} \frac{1}{\mathbf{p}^2 + \mathbf{pk} + \mathbf{k}^2 - mE}. \tag{2.57}$$

This sum is a direct consequence of the discrete momentum in the loops appearing in the dressed dimer propagator. The sum diverges in the ultraviolet and has to be regularized and re-normalized. A simple way to accomplish this is [34] to subtract and add the same sum for some energy $-\mu^2 < 0$.

$$S(\mathbf{k}, E) = \big(S(\mathbf{k}, E) - S(\mathbf{k}, -\mu^2)\big) + S(\mathbf{k}, -\mu^2). \tag{2.58}$$

The term in the brackets is finite and μ-dependent. The second term can be re-written using Poisson's summation formula (equatuion (4.10)), it yields

$$S(\mathbf{k}, -\mu^2) = \mu - \sum_{\mathbf{n}\neq 0} \frac{1}{nL} \exp\left(-\frac{i}{2} L\mathbf{kn} - nL\mu\right), \tag{2.59}$$

with $\mathbf{n} \in \mathbb{Z}^3$ and $n = |\mathbf{n}|$. The μ-dependence of this cancels this of the term in the brackets. A similar approach can be used to write $S(\mathbf{k}, (k^*)^2) = k^* + \Delta(L, k^*)$. In [47, 46, 48] this has be done to derive expressions for the finite volume corrections to two- and three-body bound states. In section 4.1 we use these results to investigate our obtained bound states.
At energies close to the binding energy E_i of a three-body state the scattering amplitude can be written as

$$M_L(\mathbf{p}, \mathbf{q}, E) = \frac{h_i(\mathbf{p}) h_i(\mathbf{q})}{E - E_i} + \text{regular terms}\,. \tag{2.60}$$

This means the in- and out-going momenta decouple. Also note that this expression becomes singular at the binding energy. Therefore the in-homogeneous part of the Faddeev equation can be ignored. Doing so leads to a homogeneous version of equation (2.55).

$$h_i(\mathbf{p}) = \frac{1}{L^3} \sum_{\mathbf{k}}^{\Lambda} Z(\mathbf{p}, \mathbf{k}, E) \tau^L(k^*) h_i(\mathbf{k}). \tag{2.61}$$

Due to the discrete momentum this can be understood as a matrix equation. This has solutions only if

$$\det\left(\tau^L(k^*) - Z(\mathbf{p}, \mathbf{k}, E)\right) = 0\,. \tag{2.62}$$

Therefore the solutions for the energy E of this equation are the binding energies E_i of the three-particle states. Equation (2.62) is also called quantization condition. Also note that it has solutions for $mE = (k^*)^2 < 0$, this solutions correspond to scattering states. While this could be used to determine the finite volume energy spectrum, meaning the bound states and scattering states for different volume sizes L, it is very difficult to solve. The argument of the determinant is a $N^3 \times N^3$ matrix, where N is given by $\max\{n; 2\pi n/L < \Lambda\}$. The number of element of the matrix scale with the inverse volume size by $1/L^6$. For all but very small L this is not practical. A way to reduce this drastically is to perform a partial-wave expansion. However, since the finite volume is a cube, the system is not spherical symmetric. In [21] a projecting of the quantization condition to the irreducible representations of the octahedral group was derived. The octahedral group is the symmetry group of a cube. This qualitatively resembles the partial-wave expansion in the infinite volume. In the next section we will discus the a few aspects of the octahedral group. We follow this, by briefly summarizing the projecting of the quantization condition to the irreducible representations with focus on S-wave interactions.

2.5.4 The octahedral or cubic group

If a cubic volume is used the position-space is no longer spherical symmetric. Instead, the symmetry is reduced to the symmetry of a cube. This symmetry is given by the octahedral group, this is also called the cubic group, crystallographic point group, or angular momentum group of the cubic lattice [41]. We will call it the cubic group G, and the elements of the group g. The cubic group is a finite subgroup of the continuum rotation group SO_3 In this section we introduce the group similar to [8, 21]. An older

more mathematical-oriented introduction is given in [58].
The cubic group consists of 24 rotations R_a and the inversion I of all axes. Combined this are $|G| = 48$ elements. These rotations can be understood as all rotations, that image a cube to itself. If the origin of Cartesian coordinates x, y, z is at the center of the cube with axes parallel to the edges of the cube, the rotations are given by five conjugacy classes [41]:

(I) The identity (1 Rotation).

($3C_2$) Rotations with an angle of π about the three coordinate axes (3 rotations).

($8C_4$) Rotations with an angle of $\pm 2\pi/3$ about the four body diagonals, given by $x = y = z$ ($2 \times 4 = 8$ rotations).

($6C_4$) Rotations with an angle of $\pm\pi/2$ about the three coordinate axes($2 \times 3 = 6$ rotations).

($6C_2'$) Rotations with an angle of π about the axes parallel to six face diagonals, given by e.g. $x = y = 0$ (6 rotations).

A matrix representation R_a of this rotations can be found in [8]. A general element of the cubic group is given by $g = R_a I$, where I is the identity or the inversion of all axes. The cubic group has five irreducible representations [21]:

(A_1) The trivial one-dimensional representation, it is given by 1 for all elements of G.

(A_2) The one-dimensional representation which is -1 for all elements in the classes $6C_4$ and $6C_2'$ and $+1$ else.

(E) The two-dimensional representation. The corresponding matrices are given in [8].

(T_1) The three-dimensional representation. The matrices are given in [8].

(T_2) The three-dimensional representation. The matrices are the same as for T_1, but with an additional -1 for the classes $6C_4$ and $6C_2'$.

Finally, the inversion doubles the number of representations. For each representation we get $X \to X^{\pm}$. This means there are ten irreducible representations: $A_1^{\pm}, A_2^{\pm}, E^{\pm}, T_1^{\pm}, T_2^{\pm}$.

Shells

In this section, we order all the discrete three-dimensional momenta into different shells. These shells are analog to the shells in the partial wave expansion, there they are given by all momenta with the same absolute momentum $|\mathbf{p}|$. Our following definition of the shells is completely equivalent to [21]. All momenta in this section are given in units of $2\pi/L$. We define a shell number s. This number increases with increasing value of $|\mathbf{p}|$. The idea of this shells is, that all momenta in a shell can be created from one reference vector $\mathbf{p}_0$, by acting with the group elements on it $\mathbf{p} = g\mathbf{p}_0$. A way of understanding this is that elements of g can permutate the coefficients of a three-dimensional Cartesian vector. This leads to different types of shells that can not mix. These shells are:

(a) The first type of shell contains only one shell and only one vector, namely $(0, 0, 0)$. We will label it by $s = 1$. All elements of the cubic group leave it invariant.

(b) The second type of shells is given by $\mathbf{p}_0 = (n, 0, 0)$, with $n \in \mathbb{Z}$. This are all momenta on the coordinate axes. In each shell of this type there are $\theta(s) = 6$ elements. For example the shell $s = 2$ with momentum $|\mathbf{p}| = 1$ contains $(1, 0, 0), (-1, 0, 0), (0, 1, 0), (0, -1, 0), (0, 0, 1)$, and $(0, 0, -1)$.

(c) The third type of shells is given by $\mathbf{p}_0 = (n, \pm n, 0)$, with $n \in \mathbb{Z}$. This are all momenta on the diagonals between two axes. In each shell of this type there are $\theta(s) = 12$ elements.

(d) The fourth type of shells is given by $\mathbf{p}_0 = (n, m, 0)$, with $n \neq m$ and $n, m \in \mathbb{Z}$. In each shell of this type there are $\theta(s) = 24$ elements.

(e) The fourth type of shells is given by $\mathbf{p}_0 = (n, \pm n, m)$, with $n \neq m$ and $n, m \in \mathbb{Z}$. In each shell of this type there are $\theta(s) = 24$ elements.

(f) The fifth type of shells is given by $\mathbf{p}_0 = (n, \pm n, \pm n)$, with $n \in \mathbb{Z}$. In each shell of this type there are $\theta(s) = 8$ elements.

(g) The fifth type of shells is given by $\mathbf{p}_0 = (n, m, l)$, with $n \neq m \neq l$ and $n, m, l \in \mathbb{Z}$. In each shell of this type there are $\theta(s) = 48$ elements.

Here $\mathbb{Z}$ does not include the zero. In figure 2.10 a two-dimensional simplification of the shells is shown. An interesting observation is, that for higher absolute momenta, different shells appear, that have the same absolute momentum but are not connected by the cubic group. In three-dimensions this appears first for $|\mathbf{p}| = 9$. This can be created by a type (b) shell by $\mathbf{p}_0 = (3, 0, 0)$. It can also be created by a type (e) shell by $\mathbf{p}_0 = (2, 2, 1)$. We count these as two different shells. For the shown example they are $s = 9$ and $s = 10$. In figure 2.11 a two-dimensional simplification is shown. These different shells with the same absolute momentum can be seen as a leftover of the spherical symmetry in infinite volume. For these values of the absolute momentum, additional rotations leave the system invariant. This is a hint for a larger symmetry. For higher momenta, this will appear more often, compare to figure 4.6. Additionally, it will also appear more often if the volume size is increased. Increasing volume means decreasing the distance between different absolute momenta. The shells begin to overlap by going to the limit $L \to \infty$. In this sense, the spherical symmetry can be restored by sending the cubic volume size to infinite. This is expected since there is no difference between an infinite-sized cube or an infinite-sized sphere mathematically.

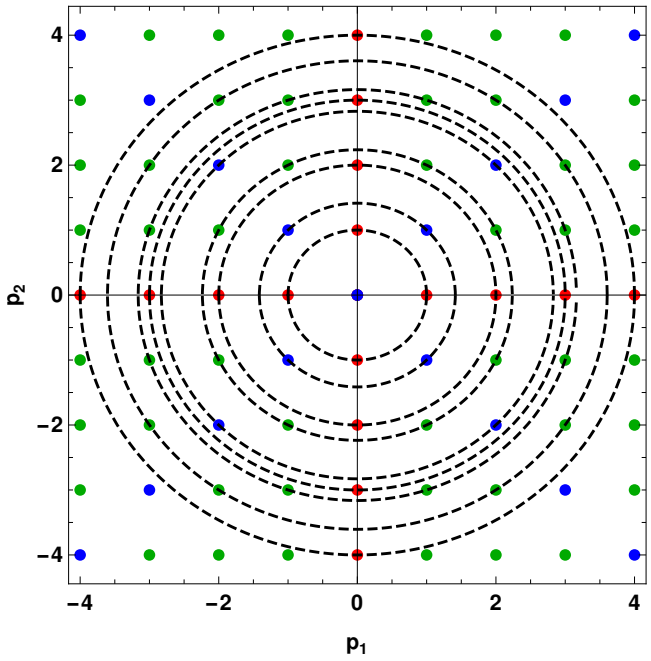

Figure 2.10: Visualization of the shells in 2D. Plotted are the discrete momenta in units of $2\pi/L$. The shells contain all momenta $\{\mathbf{p}\}$ with the same absolute value $|\mathbf{p}|$ that can be transformed to each other by elements g of the cubic group G. The different colors label the different types of shells. In this two-dimensional simplification, only the shells that contain at least one zero appear. The single point in the origin is the shell of type (a), The red dots are shells of type (b), the blue dots are shells of type (c), and the green dots are shells of type (d). The black dashed line circles indicate the same absolute momentum. In two dimensions the cubic group is reduced to the symmetry of a square. This contains mirroring on the coordinate axes and mirroring on the diagonals of the square. The reader can verify that all momenta of the same shell can be transferred into each other by this symmetry operation.

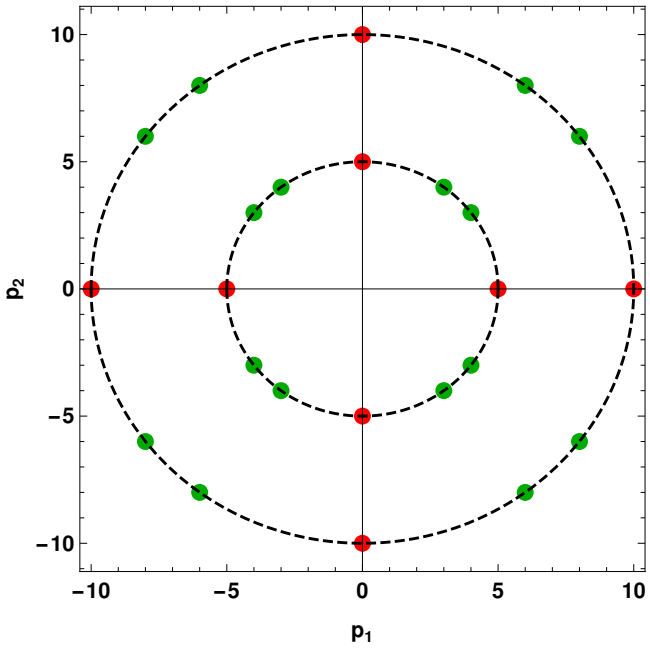

Figure 2.11: Two examples of shells with the same absolute value $|\mathbf{p}|$ (black dashed circles) that are not connected by elements of the cubic group. The green dots indicate a shell of type (d). They can not be mapped to the red dots (a shell of type (b)) and vice versa. They are treated as two separate shells. The first two overlapping shells that are shown, are given by $|\mathbf{p}| = 5$, with $\mathbf{p}_0 = (5, 0)$ for the type (b) and $\mathbf{p}_0 = (4, 3)$ for the type (d) shell. The second two overlapping shells, are given by $|\mathbf{p}| = 10$, with $\mathbf{p}_0 = (10, 0)$ for the type (b) and $\mathbf{p}_0 = (8, 6)$ for the type (d) shell.

Expansion in the irreducible representation

The following section is based on [21]. For the cubic group G a counterpart of the partial-wave expansion (equation (2.15)) can be defined.

$$f(\mathbf{p}) = f(g\mathbf{p}_0) = \sum_{\Gamma} \sum_{\rho,\sigma} T^{\Gamma}_{\sigma,\rho}(g) f^{\Gamma}_{\rho,\sigma}(\mathbf{p}_0), \tag{2.63}$$

where Γ counts all irreducible representations: $\Gamma \in \{A_1^{\pm}, A_2^{\pm}, E^{\pm}, T_1^{\pm}, T_2^{\pm}\}$. The functions $T^{\Gamma}_{\sigma,\rho}$ are the matrix representation of a element $g \in G$ in a given representation Γ. All possible $T^{\Gamma}_{\sigma,\rho}$ are given in [21]. In the context of this thesis, only A_1^+ is relevant, see below. This is also known as the trivial representation and yields for all g

$$T^{A^+}_{\sigma,\rho}(g) = 1. \tag{2.64}$$

This corresponds to the S-wave spherical harmonic $Y_{0,0}(\hat{\mathbf{p}}) = 1$. The Schur orthogonality relations (for example [78]) yields

$$\sum_{g \in G} T^{\Gamma}_{\sigma,\rho}(g) \left(T^{\Gamma'}_{\lambda,\gamma}(g) \right)^* = \frac{|G|}{s_{\Gamma}} \delta_{\Gamma,\Gamma'} \delta_{\sigma,\lambda} \delta_{\rho,\lambda}. \tag{2.65}$$

s_Γ is the dimension of the representation Γ. And $|G| = 48$ is the number of elements in G. With this the quantity $f^\Gamma_{\rho,\sigma}(\mathbf{p}_0)$ can be determined.

$$\sum_{g\in G} \left(T^\Gamma_{\lambda,\delta}(g)\right)^* f(g\mathbf{p}_0) = \frac{|G|}{s_\Gamma} f^\Gamma_{\delta,\lambda}(\mathbf{p}_0). \tag{2.66}$$

This can be seen as the analog of the second part of the equation (2.15).

2.5.5 The quantization condition in the irreducible representation

The following derivation is based on [21]. In the last section an analog of the partial-wave expansion for the cubic group G has been derived. With this the quantization condition (equation (2.61)) can be simplified. First we exchange the sum over the discrete momentum by a sum over all elements g of the group G and a sum over all shells s.

$$\begin{aligned} h(\mathbf{p}) &= \frac{1}{L^3} \sum_{\mathbf{k}}^{\Lambda} Z(\mathbf{p},\mathbf{k},E)\tau^L(k^*)h(\mathbf{k}) \\ &= \frac{1}{L^3} \sum_s \sum_{g\in G} \frac{\theta(s)\tau_L(s)}{|G|} Z(\mathbf{p}, g\mathbf{k}_0)\tau^L(k^*)h(g\mathbf{k}_0(s)). \end{aligned} \tag{2.67}$$

The factor $\theta(s)/|G|$ cancels the fact, that a specific momentum can be constructed form $\mathbf{k}_0$ by different elements g, and therefore appears multiple times in the sum. Also note, $\tau(k^*)$ only depends on the absolute value of $\mathbf{k}$, therefore we write $\tau^L(s)$. We have also dropped the E-dependence to simplify the notation. Multiplying with $\left(T^\Gamma_{\sigma,\lambda}(g')\right)^*$, summarizing over all $g \in G$ and using equation (2.66) yields

$$\frac{|G|}{s_\Gamma} h^\Gamma_{\lambda,\sigma}(r) = \frac{1}{L^3} \sum_s \sum_{\Gamma'} \sum_{\rho,\delta} \frac{\theta(s)\tau_L(s)}{|G|} Z^{\Gamma,\Gamma'}_{\lambda,\sigma;\rho,\delta}(r,s) h^{\Gamma'}_{\rho,\delta}(s), \tag{2.68}$$

with the projection of the potential

$$\begin{aligned} Z^{\Gamma,\Gamma'}_{\lambda,\sigma;\rho,\delta}(r,s) &= \sum_{g,g'\in G} \left(T^\Gamma_{\sigma,\lambda}(g')\right)^* Z(g'\mathbf{p}_0(r), g\mathbf{k}_0(s)) T^{\Gamma'}_{\delta,\rho}(g) \\ &= \sum_{g,g'\in G} \left(T^\Gamma_{\sigma,\lambda}(g')\right)^* Z(g^{-1}g'\mathbf{p}_0(r), \mathbf{k}_0(s)) T^{\Gamma'}_{\delta,\rho}(g). \end{aligned} \tag{2.69}$$

In the last step we used that the potential only depends on the angle between the momenta, meaning $Z(g\mathbf{p}, g\mathbf{k}) = Z(\mathbf{p},\mathbf{k})$. Since the group G is complete, it yields $g^{-1}g' \in G$. Therefore we can define a new

$g'' = g^{-1}g' \in G$ and obtain

$$\begin{aligned} Z^{\Gamma,\Gamma'}_{\lambda,\sigma;\rho,\delta}(r,s) &= \sum_{g,g''\in G} \left(T^{\Gamma}_{\sigma,\lambda}(g\,g'')\right)^* Z(g''\mathbf{p}_0(r),\mathbf{k}_0(s)) T^{\Gamma'}_{\delta,\rho}(g) \\ &= \sum_{g,g''\in G}\sum_{\omega} \left(T^{\Gamma}_{\sigma,\omega}(g)\right)^* \left(T^{\Gamma}_{\omega,\lambda}(g'')\right)^* Z(g''\mathbf{p}_0(r),\mathbf{k}_0(s)) T^{\Gamma'}_{\delta,\rho}(g) \\ &= \sum_{g''\in G}\sum_{\omega} \frac{|G|}{s_\Gamma}\delta_{\Gamma,\Gamma'}\delta_{\sigma,\delta}\delta_{\omega,\rho} \left(T^{\Gamma}_{\omega,\lambda}(g'')\right)^* Z(g''\mathbf{p}_0(r),\mathbf{k}_0(s))) \\ &= \sum_{g\in G} \frac{|G|}{s_\Gamma}\delta_{\Gamma,\Gamma'}\delta_{\sigma,\delta} \left(T^{\Gamma}_{\rho,\lambda}(g)\right)^* Z(g\mathbf{p}_0(r),\mathbf{k}_0(s))) \\ &= \frac{|G|}{s_\Gamma}\delta_{\Gamma,\Gamma'}\delta_{\sigma,\delta} Z^{\Gamma}_{\lambda,\rho}(r,s)\,. \end{aligned} \tag{2.70}$$

In the third step we have used the Schur orthogonality relation (equation (2.65)). We have defined the potential in the irreducible representation by

$$Z^{\Gamma}_{\lambda,\rho}(r,s) = \sum_{g\in\mathcal{G}} \left(T^{\Gamma}_{\rho,\lambda}(g)\right)^* Z(g\mathbf{p}_0(r),\mathbf{k}_0(s)). \tag{2.71}$$

Inserting this into equation (2.68) simplifies it to

$$h^{\Gamma}_{\lambda,\sigma}(r) = \frac{1}{L^3}\sum_s \frac{\theta(s)\tau_L(s)}{|G|}\sum_\rho Z^{\Gamma}_{\lambda,\rho}(r,s) h^{\Gamma}_{\rho,\sigma}(s). \tag{2.72}$$

Analogous to the before this has a solution if

$$\det\left(\tau^L(s)^{-1}\delta_{r,s}\delta_{\lambda,\rho} - \frac{\theta(s)}{GL^3} Z^{\Gamma}_{\lambda,\rho}(r,s)\right) = 0. \tag{2.73}$$

This is the quantization condition in the irreducible representation. Note that this only depends on the shell numbers but not the direction of a single momentum. This reduces the dimension of the matrix drastically. This is a $N \times N$ matrix, however each element contains a sum over all $g \in G$, so this are $48N^2$ terms. Also note that the number of shells that fit under the ultraviolet cutoff does not scale linear with the inverse of L, The density of the shells increase with increasing L, compare this to the discussion around figure 4.6. However, the amount of terms is reduced heavily compared to equation (2.62).
For S-waves only the trivial representation A^+ contributes, therefore for S-waves the quantization qondition simplifies to

$$\det\left(\tau^L(s)^{-1}\delta_{r,s} - \frac{\theta(s)}{GL^3} Z^{A^+}(r,s)\right) = 0, \text{ with } Z^{A^+}(r,s) = \sum_{g\in\mathcal{G}} Z(g\mathbf{p}_0(r),\mathbf{k}_0(s)). \tag{2.74}$$

Note that the case of S-wave interactions is chosen since it is especially simple. Only one representation contributes, for higher partial waves this is not true, different representations will enter for the same partial wave, see for example [49].

3 Spurious poles in infinite volume

The methods, results and discussions presented in this chapter have been partially published in [22]. They are the result of a cooperation with the other authors of this article.

3.1 The problem of spurious poles

As discussed above, the particle-dimer scattering amplitude can be obtained by solving the Faddeev equation:

$$M(\mathbf{p},\mathbf{q};E) = Z(\mathbf{p},\mathbf{q};E) + 8\pi \int^{\Lambda} \frac{d^3\mathbf{k}}{(2\pi)^3} Z(\mathbf{p},\mathbf{k};E)\tau(k^*)M(\mathbf{k},\mathbf{q};E)\,, \tag{3.1}$$

where a sharp ultraviolet cutoff Λ has been used to regularize the loop integral (compare to equation (2.37)). A graphical representation using Feynman diagrams is given in figure 2.6. The dimer propagator is given by

$$\tau(\mathbf{k},E) = \tau(k^*) = \frac{1}{k^* \cot\delta(k^*) + k^*}, \tag{3.2}$$

with the two-particle phase shift $\delta(k^*)$. How this quantity appears can be seen in section 2.3. In this thesis we use the re-summarized propagator at NLO given by equation (2.31). We use the following notation for the loop momentum k^*.

$$k^* = \sqrt{\frac{3}{4}\mathbf{k}^2 - mE}. \tag{3.3}$$

It is chosen such that $k^* \in \mathbb{R}$ below the two-body break-up threshold $4/3mE < \mathbf{k}^2$. Note that this differs by the more commonly used definition by a factor of i. The two-particle phase shift δ is accessible in an EFT by using the effective range expansion (ERE). On a more fundamental level this means the two-body coupling constants in the re-normalized Lagrangian density are fine-tuned to reproduce the parameters of the ERE. More details on this can be found in section 2.2. The ERE for S-waves is given by

$$k^* \cot\delta(k^*) = -\frac{1}{a} - \frac{r}{2}(k^*)^2 + \mathcal{O}\left(r^3(k^*)^4\right), \tag{3.4}$$

where a is the scattering length and r is the effective range, the physical interpretation of this values is discussed in section 2.1.1. As already mentioned in that section, the ERE is an expansion for small momenta k^*.

Keeping only the leading order (LO) term ($\sim (k^*)^0$), results in a pole of $\tau(k^*)$ at $k^* = 1/a$. In a theory with a physical dimer, meaning a bound state of two particles, the binding energy of the state is $E_D^{LO} = 1/(ma^2)$.

For example considering proton-neutron scattering[1] in the S-wave triplet channel ($^3S_1$) the scattering

[1] Of course here we discuss spin-less particles, however the extension does not hinder the argument.

length $a^{LO} = 4.4$ fm results in a pole at $k^* = 45.5$ MeV. Therefore the binding energy of this state is $E_B = (k^*)^2/M = 2.2$ MeV, this is the binding energy of the deuteron, where M is the nucleon mass. Data taken from [19].
However, considering the next-to-leading order (NLO) term ($\sim (k^*)^2$) of the ERE, meaning adding range corrections, this leads to a dimer propagator $\tau(k^*)$ that exhibits two poles:

$$k_1 = \frac{2/a}{1+\sqrt{1-2r/a}} \simeq \frac{1}{a}\,, \qquad k_2 = \frac{1+\sqrt{1-2r/a}}{r} \simeq \frac{2}{r}\,. \tag{3.5}$$

The shown approximations are for case of a naturally large effective range and an unnaturally large scattering length[2], so $r \ll a$. The pole k_1 obviously corresponds to the pole at $1/a$ found before, which is connected to the physical dimer. However the second pole k_2 is suspicious. First, in the case of n-p scattering, there is no deep bound state of the deuteron, so the theory seems to predict a state[3] that is not found in experiments. Second, the range correction in the ERE should not cause additional physical states if considered strictly perturbatively. However, including it in the non-perturbative way introduced in section 2.3.1 causes an additional pole but this pole should not be related to a physical state. Third, the propagator at the additional state k_2 can have a negative residue, this is a crucial problem, since it is connected to negative spectral densities and it contributes to the unitary relation in an un-physical way. Fourth, the presence of the pole makes the numerical standard techniques impossible. The latter two issues will be discussed in more detail in the next section. It becomes clear that the additional pole is un-physical or spurious.
The presence of such pole can be explained by taking a closer look at the ERE. This is an expansion for small values of k^*. Small in this context means that the term test for divergence requires $rk^* < 1$ for the ERE to converge. At the region of the spurious pole k_2 this is not the case $rk_2 \simeq 2$. Strictly speaking, the ERE cannot be used for such high momenta and it is not surprising that it predicts un-physical behaviour in this region. Note that, in general, it is not a problem to use the ERE in the particle-dimer picture outside its range of validity. The propagator appears in the Faddeev equation only in combination with the potential of the interaction $Z(p,k,E)$. By definition, this has to converge to zero for large momenta. This must be the case, since for very high momenta, which means high energy, the particles will not be influenced by an interaction in a meaning full way. So $\tau(k^*) \cdot Z((p,k,E) \to 0$ for $k^* \gg k_1$. For example, the logarithmic decrease in the S-wave projection of the potential (2.44) should fall faster than $\tau(k^*)$. In absence of a spurious pole (for example at LO), this is full-filled. However the singularity at k_2 violates this. The unmodified dimer propagator in ERE at NLO cannot be used around k_2. In the following we discuss the problems caused by the pole in more detail to further highlight the need for an alternative method.

3.1.1 Negative residue, violation of unitarity and un-physical spectral density

The main physical issue with the spurious pole is, that it can exhibit a negative residue. In section 3.15 we will discuss how this appears and for which values of the scattering length a and the effective range r this is the case. In this section, we explain why this negative residue is un-physical and leads to predictions that are not meaningful.

[2] This is the case where pionless EFT is expected to work especially well.
[3] As discussed above, poles of the propagator or the related two-body scattering amplitude have physical meaning, they are bound states, virtual states or resonances. Compare to section 2.1.2.

We start by investigating the presence of the spurious pole to the unitarity relation for the S-matrix. With the S-matrix S, as defined in equation (2.7), the unitarity relation reads:

$$S^\dagger S = I, \tag{3.6}$$

with the identity matrix I. The S-matrix can be parameterized by the phase shift δ. For a system with only one channel, this means S is a one times one matrix, i.e.,

$$S = e^{2i\delta}. \tag{3.7}$$

The unitarity relation directly leads to the condition $\delta \in \mathbb{R}$. Further the unitarity relation is connected to the conservation of the probability current. For a properly normalized in-going (out-going) state $\Psi_{in\,(out)}$ it must hold that

$$1 = \Psi_{out}^\dagger \Psi_{out} = \Psi_{in}^\dagger S^\dagger S \Psi_{in} = \Psi_{in}^\dagger \Psi_{in} = 1. \tag{3.8}$$

The out-going probability must be the same as the in-going. However, if multiple channels are possible, and those additional channels are not treated explicitly, the phase shift can have a positive imaginary part. This leads to

$$\Psi_{out}^\dagger \Psi_{out} = \Psi_{in}^\dagger S^\dagger S \Psi_{in} = \Psi_{in}^\dagger e^{-4\mathrm{Im}[\delta]} \Psi_{in} = e^{-4\mathrm{Im}[\delta]}. \tag{3.9}$$

For $\mathrm{Im}[\delta] = 0$ the one channel result is reproduced. For $\mathrm{Im}[\delta] > 0$ the probability of the out-going state is less than one and a part of the probability current is going to the other channels. In the case of particle-dimer scattering this can be understood as follows. If there is not enough energy in the system to break the dimer (D) into two particles (p) there is only one channel: $pD \to pD$. Consequently, $\mathrm{Im}[\delta_{pD\to pD}] = 0$. If enough energy is present the dimer can split and the channel $pD \to ppp$ opens. A part of the probability current can go into this additional channel, therefore $\mathrm{Im}[\delta_{pD\to pD}] > 0$. This is exactly the case we find in the numerical calculations below for example in figure 3.5. The break-up energy of the dimer is encoded in the Faddeev equation by the physical pole k_1. In section 3.3.2 we show how the presence of the pole k_1 results in an imaginary part of the Faddeev equation and therefore leads to an imaginary part of the phase shift. Now the first problem with the spurious pole is obvious. The additional pole k_2 will contribute to the imaginary part and therefore to the unitary relation as well. An additional channel $pD' \to ppp$ is opened, with a deeply bound dimer D'. In the case of neutron deuteron scattering such a deep deuteron state does not exist, as discussed above. However, the formalism will find the additional un-physical channel and the predictions will be incorrect.
The second problem which regards to the unitarity relation is even more critical. The negative residue of the propagator at the position of the spurious pole will cause a negative imaginary part of the phase shift. To see this, we refer to section 3.3.2. In short, the negative residue will add an overall minus sign, which leads to the opposite sign compared to the physical pole. This results in a negative imaginary part $\mathrm{Im}[\delta] < 0$. With this, the right-hand side of the equation (3.9) becomes larger than one. In other words, the out-going probability is larger than one, which is clearly un-physical. There cannot be a chance of more than one for the channel to happen.

An additional issue, where the influence of the negative residue can be seen more directly, is related to the spectral density $\rho(M^2)$. In [76] it is defined by

$$\rho(E^2) = \sum_\lambda 2\pi Z_\lambda \delta(E^2 - m_\lambda^2) + \text{multi-particle scattering states for } E^2 \gtrsim (2m)^2. \tag{3.10}$$

The index λ stands for single particles with mass $m_\lambda = m$ and possible n-body bound states with a mass of $m_\lambda = (nm - E_B^{(\lambda)})$. $E_B^{(\lambda)}$ is the binding energy of the bound state λ. The quantity Z_λ is the field-strength renormalization of the corresponding state. In this context, the spectral density Z_λ can be understood as the probability to create the corresponding state out of the vacuum. According to [12] the field-strength renormalization of two-body bound states is directly proportional to the residue Z of the two-particle scattering amplitude[4] at the position of the bound-state pole. For the spurious pole k_2 the residue can be negative. Therefore it can have a negative probability for this state to be created from the vacuum. Additionally, in the positive definite spectral density [52] a negative contribution appears. Both is not meaningful, negative probabilities and negative densities are not defined. In figure 3.1 the spectral density for a theory with single-particle mass m, a physical bound state k_1, and the spurious state k_2 with negative residue is sketched.

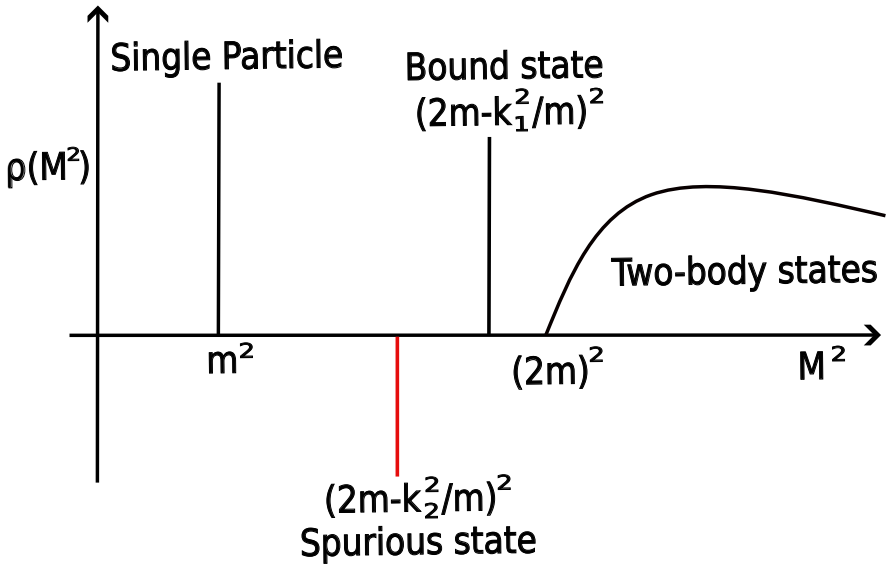

Figure 3.1: Spectral density with a single particle state with mass $M = m$, a physical bound state at $M = 2m - k_1^2/m$ and a spurious state at $M = 2m - k_2^2/m$. The spurious state has a negative residue. This causes a un-physical negative density (red). Also shown is a continuum of two-particle scattering states. The scattering states start at two times the single particle mass. Figure recreated from [76] (with the addition of the spurious state).

3.1.2 Numerical issues caused by the spurious pole

Besides this crucial physical issues, the additional pole has a devastating impact in numerical calculations. In the standard prescription (as described in section 3.3.2) the loop integral is discretized by a Gaussian match. The integral is approximated by a sum with n terms. The limit $n \to \infty$ restores the integral. In other words, for large n the approximation converges to the integral. In actual calculations one can take a large finite value for n and test the convergence. This can be done for example by increasing n slightly, if the integral is converged the results can vary only a little. For example in figure 3.4 this is done. A

[4]Therefore it is also proportional to the pole of the dimer propagator in the particle-dimer picture.

change of n by 10% causes changes in the result of less than 1%. However, if the spurious pole is not treated specially, the value of the propagator at the pole position is, loosely speaking, infinite. For a momentum close to the pole, the propagator is a large number. The term of the sum which is closest to the pole will therefore dominate the entire sum. By slightly varying n the distance to the pole changes slightly but the value of the propagator changes largely. For example the value of the propagator near the pole is $\tau(1.0001\,k_2) \approx -94$ MeV^{-1}. For a tiny change it is $\tau(1.0002\,k_2) \approx -47$ MeV^{-1}. It is clear that this is not converged in the number of steps n at all. In the limit $n \to \infty$ it diverges, the whole approximation of the integral can not be used. Please note, the standard method, meaning a shift of $i\epsilon$ can not be used. Using this would contribute to the unitary relation, and even worse, cause un-physical negative imaginary parts of the phase shift. This is discussed in detail in section 3.3.2.
Please note that this numerical issue only appears if the spurious pole lies on the path of integration. Therefore a sharp cutoff Λ below the pole position removes the problem. However, this reduces the precision of the theory, this is discussed in section 3.1.4 in detail.

3.1.3 Condition for the problems caused by the spurious pole

In this section we investigate in which case the spurious pole k_2 appears and when it will cause the issues discussed above. As explained above, the reason for the unphysical behavior is the negative residue. In the following we investigate when this is the case.
First, we note, $r > 0$ results[5] in $k_1 > 0$ and $k_2 > 0$, therefore k_1 is a shallow pole, while k_2 is a deep pole. In the other case, $r < 0$, it still yields $k_1 > 0$ but $k_2 < 0$. In other words, the second pole is not related to an additional spurious bound state but to a virtual state.
We continue this by investigating the residue of the propagator for the different cases. The residue Z_{k_i} is defined by the propagator expanded around the pole k_i.

$$\tau(k^*) = \frac{Z_{k_i}}{E_{k^*} - E_{k_i}} + \text{regular}, \tag{3.11}$$

with the energy $E_k = k^2/m$. The residue can be calculated using the first term of a Laurent series.

$$\begin{aligned} Z_{k_i}^{-1} &= \frac{d}{dE_{k^*}} \left(\tau(E_{k^*})^{-1}\right)\big|_{E_{k^*}=E_{k_i}} = \frac{d}{dE_{k^*}} \left(-\frac{1}{a} - \frac{r}{2} m E_{k^*} + \sqrt{m E_{k^*}}\right)\Bigg|_{E_{k^*}=E_{k_i}} \\ &= -\frac{rm}{2} + \frac{m}{2}(mE_{k_i})^{-1/2} = \frac{m}{2}\left(k_i^{-1} - r\right). \end{aligned} \tag{3.12}$$

Using $a \gg r$, this results for the shallow pole in

$$Z_{k_1} = \frac{2}{m}\,(a - r)^{-1} > 0, \tag{3.13}$$

which is positive for $r > 0$ as well as for $r < 0$. On the other hand, for the deep pole it reads

$$Z_{k_2} = \frac{2}{m}\left(\frac{r}{2} - r\right)^{-1} = -\frac{4}{mr}. \tag{3.14}$$

This is positive for $r < 0$, which corresponds to a virtual state. For $r > 0$ it is negative, this is exactly the case where the problems discussed in the last section will appear. This is a spurious pole.
Finally, we note that the spurious pole only causes problems if it lies on the path of integration in the

[5] In this thesis, we always assume the scattering length to be positive.

Faddeev equation (equation (3.1)). This goes from $k = 0$ to $k = \Lambda$ with a ultra-violet cutoff Λ. This means as long as $E < 0$ the quantity k^* is always reel and positive. Therefore, the spurious pole is problematic if $k_2 \in \mathbb{R}$ and $k_2 > 0$. In figure 3.3 the inverse propagator $\tau^{-1}(k^*)$ is shown for different r in units of a. It becomes clear that the condition for a problematic spurious pole for $a > 0$ is given by

$$0 < r < \frac{a}{2}. \tag{3.15}$$

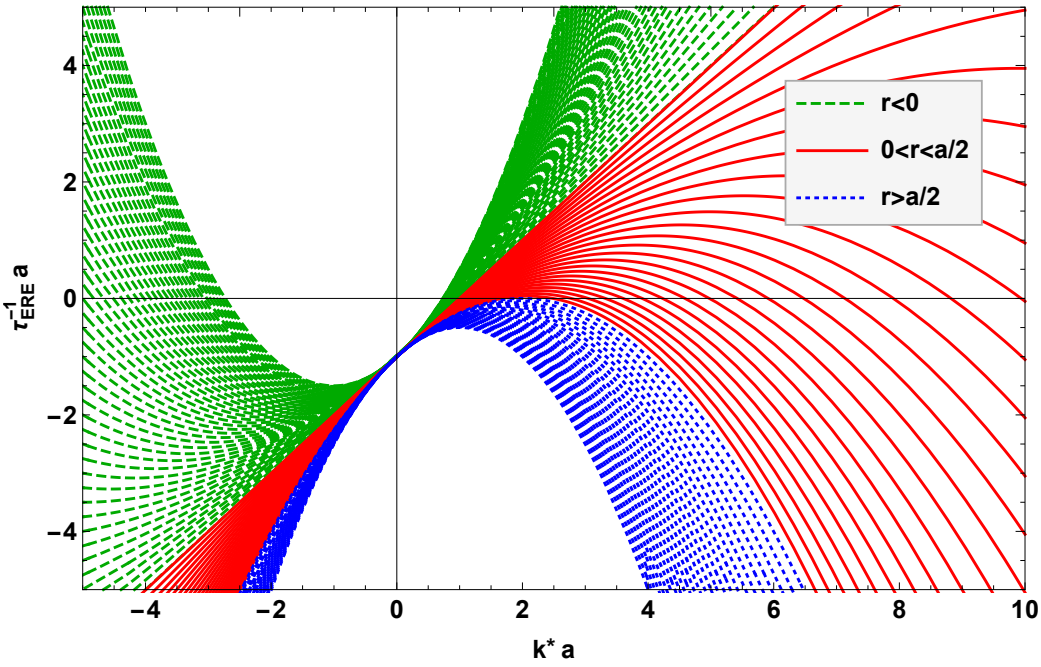

Figure 3.2: The denominator of the dimer propagator $\tau(k^*)$ in units of the scattering length a. Shown is the ERE up to next-to-leading order, this means it includes the range corrections. In green dashed for negative values of the effective range r, in red for values of r with $0 < r < a/2$ and in blue dotted for $r > a/2$. It can be seen, that only for $0 < r < a/2$ the denominator has two roots in $\mathbb{R}^+$. Since the path of integration in the Faddeev equation is real and positive, only in this region the second root can cause problems as a spurious pole.

3.1.4 Existing methods

In this section we discuss methods to solve the issues caused by the spurious pole that already have been proposed before. We especially focus on explaining why and in what situation they can not be used to highlight the need for our new non-perturbative method.

Low cutoff

The most straightforward method to solve the problems discussed above is to regulate the loop integral by a sharp ultra-violet cutoff Λ, as done in equation (3.1), and choose $\Lambda < k_2$. By doing so the spurious pole does not lie in path of integration. The numerical issues are avoided entirely. Recall that it causes

no problems to use the ERE outside its range of applicability as long as it is non singular. This method of cutting away the spurious pole is for example used in [6].
While this is very easy to implement, it comes with a serious downside. Consider a theory with a breakdown scale Λ_b. Besides the correction due to omitted physics starting around Λ_b, errors to the theory are given by regularization artefacts. To ensure that the leading corrections to an EFT is actually given by powers of (p/Λ_b), one has to demand $\Lambda \gtrsim \Lambda_b$. This becomes clear by looking at the re-normalization prescription, equation (2.22). The omitted terms are proportional to

$$ap \arctan\left(\frac{p}{\Lambda}\right) = \frac{ap^2}{\Lambda} + \cdots \sim \frac{p}{\Lambda}, \tag{3.16}$$

for a typical momentum $p \sim 1/a < \Lambda$. If the spurious pole lies below the breakup scale $k_2 < \Lambda_b$ the method therefore requires $\Lambda < \Lambda_b$. So the leading corrections are given by orders of $(p/\Lambda) > (p/\Lambda_b)$. In other words, by using a low cutoff one loses accuracy of the EFT predictions.

Additionally, if the application in lattice calculations is considered, recall, besides the finite volume the lattice is defined by a discretized position space. The particles can only sit on the lattice points (compare to figure **??**). Similar to the case of limited position space that is linked to discrete momentum space, as shown in section 2.5.2, discrete position space is connected to a limited momentum space. Therefore, analogous to equation (2.51), the minimal distance between two lattice points (lattice spacing d_{lat}) is inverse proportional to the cutoff Λ. So restricting the cutoff to be below k_2, forces a lower border to d_{lat}. So the continuum limit $d_{lat} \to 0$ can not be reached. Besides this theoretical limit, the lower border can lower the accuracy of the calculations in this manner.

Fully perturbative method

An often used method, is to fully, perturbatively expand the propagator in the effective range r. This was introduced by [4, 32, 40] in NLO and extended to N^{2}LO in [39, 69]. The expanded propagator $\tau_{pert}(k^*)$ in powers of r up to order N^{m}LO yields[6]

$$\tau^m_{pert}(k^*) = \sum_{n=0}^{m} \frac{n!(k^*)^{2n}}{(-1/a + k^*)^{n+1}} \left(\frac{r}{2}\right)^n. \tag{3.17}$$

This does not exhibit the spurious pole at any given finite order m. This works very well in infinite volume, and is quite straight forward to implement. However in finite volume calculations we expect this to be problematic. As discussed in section 2.5.3, the propagator in a finite volume has to be replaced by a finite volume version of it. This is given by

$$\tau_L(\mathbf{k}, E) = \frac{1}{k^* \cot\delta(k^*) + S((\mathbf{k}, (k^*)^2)}, \tag{3.18}$$

with the function

$$S(\mathbf{k}, (k^*)^2) = -\frac{4\pi}{L^3} \sum_{\mathbf{p}} \frac{1}{\mathbf{p}^2 + \mathbf{pk} + \mathbf{k}^2/4 + (k^*)^2}, \text{ with } \mathbf{p} \in \frac{2\pi}{L}\mathbb{Z}^3. \tag{3.19}$$

[6] Here we reformulate the result of [39] into our notation.

In infinite volume this sum converges to an integral and gives the well known result of equation (3.2). The problem with the expansion (3.17) is, in finite volume the quantity k^* in the denominator has to be replaced by $S(\mathbf{k}, E)$, accordingly. Above the elastic threshold $S(\mathbf{k}, E)$ has an infinite amount of poles, compare to figure 4.1. These poles are directly responsible for the infinite tower of scattering states of the two-particle subsystem. This tower of scattering states can be seen for example in the energy spectrum in figure 4.1. In infinite volume this poles condense to an elastic cut, which is a direct consequence of $S(\mathbf{k}, E) \to k^*$ for $L \to \infty$. In a finite volume, the expansion is producing denominators that become more and more singular with increasing order n. The expansion in r will not work around this additional poles. Compare this argument to [59].

Expansion in the momentum

Another approach for solving the problems of the spurious pole was proposed in [63] and more recently in [64]. They keep the propagator full non-perturbatively, subtract the contribution of the spurious pole and then add an expansion of the contribution for small momenta:

$$\tau(k^*) \to \tau'(k^*) = \tau(k^*) - Z_{k_2} \left(\frac{1}{k^* - k_2} + \frac{1}{k_2} + \frac{k^*}{k_2^2} + \frac{(k^*)^2}{k_2^3} \right), \tag{3.20}$$

with the residue Z_{k_2} of the propagator at the position of the spurious pole k_2. The equation is taken from [64] and rewritten in the notation of this thesis. This method is similar to our non-perturbative method presented in the next section. However, it differs significantly. The expansion added in the method of [64] is an expansion in the momentum k^*, the expansion in our method is an expansion in the energy $E \sim (k^*)^2$. This difference is crucial, since the change in the propagator in the way of [64] will not lead to an additional low-energy polynomial in the effective potential (compare to the next section) but an additional momentum polynomial. The odd powers of this momentum polynomial cannot be absorbed in the renormalization prescription. Therefore we expect this method to produce problems at higher orders of the EFT.

3.2 The non-perturbative method

In this section a non perturbative method to include range corrections that does not exhibit spurious poles is developed. The dimer propagator in NLO of the ERE that exhibits a spurious pole is given by equation (3.2) and (3.4). It has the poles k_1 and k_2 as in equation (3.5). By performing a partial fraction decomposition, it therefore can be written as

$$\tau(k^*) = \frac{2(k_1 + k_2)/r}{(k_2 - k_1)(k^* + k_2)(k^* - k_1)} - \frac{4k_2/r}{(k_2 - k_1)((k^*)^2 - k_2^2)}. \tag{3.21}$$

The first part diverges at the position of the physical pole k_1 and can be treated with standard methods[7]. In this work, the Sokhotski-Plemelj theorem is used, more details are given in section 3.3.2. Therefore, the first part will be taken exactly non perturbatively. This ensures, that the issues with convergence in a finite volume, as discussed above, will not appear. The second part diverges at the position of the spurious

[7] Recall that the $i\epsilon$ is encoded in k^* via $E \to E + i\epsilon$.

pole k_2. A simple $i\epsilon$ would create an additional unphysical imaginary part, which violates unitary and causality. This is similar to the discussion concerning the negative residue in section (3.1). To formulate our new non perturbative method the quantity $f(k^*)$ is introduced:

$$f(k^*) = -\frac{4k_2/r}{(k_2-k_1)((k^*)^2-k_2^2)} - \frac{4k_2/r}{(k_2-k_1)k_2^2}\left[1+\frac{(k^*)^2}{k_2^2}+\frac{(k^*)^4}{k_2^4}+\cdots\right]. \tag{3.22}$$

The first part is the contribution of the spurious pole to $\tau(k^*)$, the second part is a Taylor expansion of this in $(k^*)^2/k_2^2$. Note that $(k^*)^2/k_2^2 < 1$ in the region of unnatural momenta $k \sim 1/a \sim M_{low}$, since $k_2 \sim 2/r \sim M_{high}$. Using this, the Faddeev equation (3.1) can be reformulated as

$$\begin{aligned} M(\mathbf{p},\mathbf{q};E) &= W(\mathbf{p},\mathbf{q};E) + 8\pi\int^{\Lambda}\frac{d^3\mathbf{k}}{(2\pi)^3}\,W(\mathbf{p},\mathbf{k};E)(\tau(k^*)-f(k^*))M(\mathbf{k},\mathbf{q};E)\,, \\ W(\mathbf{p},\mathbf{q};E) &= Z(\mathbf{p},\mathbf{q};E) + 8\pi\int^{\Lambda}\frac{d^3\mathbf{k}}{(2\pi)^3}\,Z(\mathbf{p},\mathbf{k};E)f(k^*)W(\mathbf{k},\mathbf{q};E)\,. \end{aligned} \tag{3.23}$$

with an effective potential $W(\mathbf{p},\mathbf{q};E)$. Note that the quantity $(\tau(k^*)-f(k^*))$ is nothing else than the propagator $\tau(k^*)$, with the contribution of the spurious pole replaced by its Taylor expansion. Most important, it is regular at the position of the spurious pole as long as only a finite number of terms in the expansion in $f(k^*)$ are considered. In other words, the singularity at k_2 is shifted from the propagator $\tau(k^*)$ to the effective potential $W(\mathbf{p},\mathbf{q};E)$. In section 3.2.1 it will be shown, that the integral in the determining equation of W is given by a low-energy polynomial. In this case, the integral part can be absorbed in the low-energy polynomial (the three-body forces) of the original potential $Z(\mathbf{p},\mathbf{q};E)$ (given by equation 2.39). By doing so, the effective potential can be written as

$$W(\mathbf{p},\mathbf{q};E) = \frac{1}{\mathbf{p}^2+\mathbf{q}^2+\mathbf{pq}-mE} + \frac{H_0'}{\Lambda^2} + \frac{H_2'}{\Lambda^4}(mE-\gamma^2) + \cdots. \tag{3.24}$$

So the difference between $W(\mathbf{p},\mathbf{q};E)$ and $Z(\mathbf{p},\mathbf{q};E)$ can be absorbed by a change of the renormalization prescription. In other words $W = Z$, if different values of the three-body forces $H_0, H_2, \cdots$ are used, different than the values one would calculate from the Lagrangian
It is clear that only a finite number of terms in the expansion in $f(k^*)$ can be taken into account. It is also obvious that the ideal number of terms one should consider is directly connected to the number of three-body forces in the potential $Z(\mathbf{p},\mathbf{q};E)$ and therefore to the considered order of the EFT. A detailed discussion and predictions for the ideal number is given in section 3.2.2 as well as a numerical analysis in section 3.3.5. To clarify, we introduce the notation $\tau_i(k^*) = \tau(k^*) - f_i(k^*)$, where $f_i(k^*)$ is the expansion in equation (3.22) up to the i-th order. It yields

$$\begin{aligned} \tau_1(k^*) &= \frac{2(k_1+k_2)/r}{(k_2-k_1)(k^*+k_2)(k^*-k_1)} + \frac{4k_2/r}{(k_2-k_1)k_2^2}, \\ \tau_2(k^*) &= \frac{2(k_1+k_2)/r}{(k_2-k_1)(k^*+k_2)(k^*-k_1)} + \frac{4k_2/r}{(k_2-k_1)k_2^2}\left(1+\frac{(k^*)^2}{k_2^2}\right), \\ \tau_3(k^*) &= \frac{2(k_1+k_2)/r}{(k_2-k_1)(k^*+k_2)(k^*-k_1)} + \frac{4k_2/r}{(k_2-k_1)k_2^2}\left(1+\frac{(k^*)^2}{k_2^2}+\frac{(k^*)^4}{k_2^4}\right). \end{aligned} \tag{3.25}$$

In figure 3.3 this three orders of $\tau_i(k^*)$ compared to the original propagator in the effective range expansion can be seen. As expected they all describe the original propagator very precise at the position of the physical pole k_1. They do not exhibit the spurious pole. And they differ to the original propagator

for large momenta by a polynomial. The resulting change in physical observables can be removed by changing the renormalization prescription as proved in the next section.
To conclude, to avoid the problems caused by the spurious state the following modified version of the Faddeev equation (2.37) can be solved:

$$M(\mathbf{p},\mathbf{q};E) = Z(\mathbf{p},\mathbf{q};E) + 8\pi \int^{\Lambda} \frac{d^3\mathbf{k}}{(2\pi)^3}\, Z(\mathbf{p},\mathbf{k};E)\tau_i(k^*)M(\mathbf{k},\mathbf{q};E). \tag{3.26}$$

Here and everywhere below the differences between $W(\mathbf{p},\mathbf{k};E)$ and $Z(\mathbf{p},\mathbf{k};E)$ or more precise between the three-body forces $H_0, H_2, \cdots$ and $H_0', H_2', \cdots$ have been dropped. Since the three-body forces are fine-tuned to reproduce three-body observables of a model or experiments, there are no real differences from a users point of view.

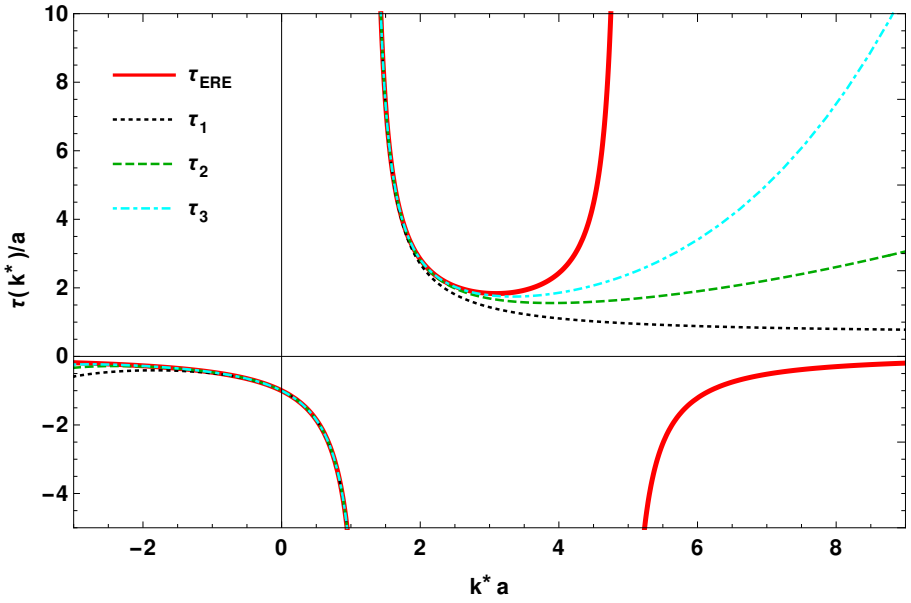

Figure 3.3: The dimer propagator $\tau(k^*)$ in units of the scattering length a. For demonstration purposes we choose $r \simeq a/3$. Shown is the propagator $\tau_{ERE}(k^*)$ in the effective range expansion up to NLO in red and the propagator in the different orders of the subtraction scheme as described by equation (3.25), the constant leading order subtraction $\tau_1(k^*)$ in black dotted, the next-to-leading order $\tau_2(k^*)$ proportional to $(k^*)^2$ in green dashed and the next-to-next-to-leading order $\tau_3(k^*)$ proportional to $(k^*)^4$ in cyan dot-dashed. It can be seen that all orders describe the ERE very precise around the physical pole $k_1\, a \simeq 1$. By construction none of them, except the ERE, exhibits the spurious pole k_2. For $k^* < k_2$ the description becomes better order by order of the subtraction scheme. For large values of k^* the differ from $\tau_{ERE}(k^*)$. However they differ only by a polynomial in $(k^*)^2$. The resulting difference in observables can be removed by changing the renormalization prescription of the EFT.

3.2.1 The effective potential *W*

In this section it is shown that the difference between the potential $Z(\mathbf{p},\mathbf{q};E)$ and the effective potential $W(\mathbf{p},\mathbf{q};E)$ can be absorbed by a redefinition of the three-boy forces $H_0, H_2, \cdots$. To proof this, we show the difference is given by a low-energy polynomial. By this we mean two cases,

(a) The difference is given by a polynomial in the energy E or a polynomial the momenta squared, $\mathbf{p}^2$ or $\mathbf{q}^2$. In this case the polynomial can be absorbed by redefining the constants $H_0, H_2, \cdots$ of the three-body forces, as given by equation (2.38) or (2.39).

(b) The difference is given by a polynomial of the cut-off Λ. In this case it can also be absorbed by the three-body forces. The Λ-dependence of $H_0(\Lambda), H_2(\Lambda)$ has to be changed accordingly. This can be done by changing equation (2.42).

Before we show this, we anticipate that the coefficients of the polynomials are, in general, complex numbers. This is actually the case, for example a non-vanishing imaginary part will be shown explicitly in equation (3.32). If one likes to absorb this into the three-body forces, they also would need to be complex. Complex three-body forces are not an unknown concept. Physical deep bound two-body states, states above the break-up scale of the EFT $\sqrt{|mE_B|} > \Lambda_b$, can be included by complex three-body couplings [11]. This is exclusive for states with a clear physical meaning. An additional imaginary part contributes to the unitary relation. The spurious pole k_2 however is an artefact, as stated above. It must not have a physical equivalent in the imaginary part of $H_0, H_2, \cdots$. Since the exact theory has no spurious poles, it is save to remove this, by dropping the imaginary part in the corrections in the effective potential W entirely. By doing so, we ensure that the unitary relation is not modified by the artefact. Also compare this to the discussion around equation (3.85). As will be stated there, an additional imaginary part in W gives an additional contribution to the imaginary part of the particle-dimer phase shift. Due to the negative residue of the spurious pole, this can be negative. This is un-physical, therefore the imaginary part should be dropped.
The potential $Z(\mathbf{p}, \mathbf{q}; E)$ describes a one particle exchange and three-body contact interactions[8], it is given by equation (2.39). The effective potential $W(\mathbf{p}, \mathbf{q}; E)$ is used to carry the singularity of the propagator, it is defined in equation (3.23) in the last section. By iteration of this equation we obtain a Born series

$$W = Z + ZfZ + ZfZfZ + \cdots = Z + W^{(1)} + W^{(2)} + \cdots . \tag{3.27}$$

We focus on showing $W^{(1)}$ is a low-energy polynomial, the other parts will be analogous.

$$\begin{aligned} W^{(1)} &= 8\pi \int^{\Lambda} \frac{d^3\mathbf{k}}{(2\pi)^3} Z(\mathbf{p}, \mathbf{k}; E) f(k^*) Z(\mathbf{k}, \mathbf{q}; E) \\ &= W^{(1)}_{ee} + W^{(1)}_{e0} + W^{(1)}_{0e} + W^{(1)}_{00} + W^{(1)}_{02} + W^{(1)}_{20} + W^{(1)}_{22} + \cdots . \end{aligned} \tag{3.28}$$

Here we split the contribution from the original potential $Z(\mathbf{p}, \mathbf{k}; E)$ into the component of the one particle exchange, denoted by a subscript e, and the components of the three-body forces, denoted by subscript $0, 2, \ldots$. The number counts the power of k^* of the three-body force.

[8] Compare this to the Feynman diagrams in figure 2.6.

The contribution of two leading order three-body forces $W_{00}^{(1)}$

We start with the most simple contribution $W_{00}^{(1)}$. This describes the pairing of the leading order three-body forces H_0/Λ^2 of both potentials $Z(\mathbf{p},\mathbf{k};E)$ and $Z(\mathbf{k},\mathbf{q};E)$.

$$\begin{aligned} W_{00}^{(1)} &= 8\pi \int^{\Lambda} \frac{d^3\mathbf{k}}{(2\pi)^3} \frac{H_0}{\Lambda^2} f(k^*) \frac{H_0}{\Lambda^2} = -\frac{32\pi k_2/r}{k_2-k_1} \left(\frac{H_0}{\Lambda^2}\right)^2 I_{00}\,, \text{ with} \\ I_{00} &= \int^{\Lambda} \frac{d^3\mathbf{k}}{(2\pi)^3} \left\{ \frac{1}{k^{*2}-k_2^2-i\varepsilon} + \frac{1}{k_2^2}\left(1+\frac{k^{*2}}{k_2^2}+\cdots\right)\right\} = I_{00}^{pole} + I_{00}^{expand}. \end{aligned} \tag{3.29}$$

The negative sign of $-i\varepsilon$ is equivalent to the prescription $E \to E + i\varepsilon$. In the last step the integral I_{00} is divided in the part containing the spurious pole I_{00}^{pole} and a part from the expansion I_{00}^{expand}. The first part can be rewritten as

$$\begin{aligned} I_{00}^{pole} &= \int^{\Lambda} \frac{dk}{2\pi^2} \frac{k^2}{3/4k^2-(mE+k_2^2)-i\varepsilon} \\ &= \int^{\Lambda} \frac{dk}{2\pi^2} \frac{4/3k^2}{(k-\sqrt{4/3}\sqrt{mE+k_2^2}-i\varepsilon)(k+\sqrt{4/3}\sqrt{mE+k_2^2}+i\varepsilon)}. \end{aligned} \tag{3.30}$$

It is use-full to use the Sokhotski–Plemelj theorem:

$$\lim_{\epsilon\to 0} \int_a^b dx \frac{f(x)}{x-c\pm i\epsilon} = \mathcal{P}\int_a^b dx \frac{f(x)}{x-c} \mp i\pi f(c), \tag{3.31}$$

if $c \in [a,b]$ and $\mathcal{P}$ denotes the principal value integral. With this the imaginary part of the integral I_{00} is given by

$$\text{Im}\, I_{00} = \text{Im}\, I_{00}^{pole} = \frac{2}{3\sqrt{3}\pi}\sqrt{k_2^2+mE} = \frac{2k_2}{3\sqrt{3}\pi}\left\{1+\frac{mE}{k_2^2}+\cdots\right\}. \tag{3.32}$$

In the last step the root is expanded for small mE/k_2^2. The result is a polynomial in the energy E. Therefore $W_{00}^{(1)}$ has a non-vanishing imaginary part. In principle, it can be absorbed in the three-body forces, since it is a polynomial. To perform this one would need complex three-body couplings with the consequences discussed above. Imaginary three-body forces can only be caused by deep physical states, in the original system there are no such states, and therefore the new method is not allowed to have them. Consequently, we drop all imaginary parts. The real part of I_{00}^{pole} is

$$\begin{aligned} \text{Re} I_{00}^{pole} &= \mathcal{P}\int_0^{\Lambda} \frac{dk}{2\pi^2} \frac{k^2}{3/4k^2-(mE+k_2^2)} \\ &= \frac{2}{3\pi^2}\left(\Lambda - \sqrt{\frac{4}{3}}\sqrt{mE+k_2^2}\arctan\left[\frac{\sqrt{4/3}\sqrt{mE+k_2^2}}{\Lambda}\right]\right) = \frac{2}{3\pi^2}\Lambda + \cdots. \end{aligned} \tag{3.33}$$

Finally the total real part of I_{00} is given by

$$\text{Re}\, I_{00} = \text{Re}\, I_{00}^{pole} + I_{00}^{expand} = \frac{2}{3\pi^2}\,\Lambda + \frac{1}{2\pi^2 k_2^2}\left(\frac{1}{3}\,\Lambda^3 + \frac{1}{k_2^2}\left(\frac{3}{20}\Lambda^5 - \frac{1}{3}\,\Lambda^3 mE\right)+\cdots\right). \tag{3.34}$$

This is a polynomial in the sharp cut-off Λ and the energy E. This can be adsorbed by a redefinition of the three-body forces as discussed above in case (b).

The contribution of the mixing of a one-particle exchange and a leading order three-body force $W_{e0}^{(1)}$

In the second part, we consider $W_{e0}^{(1)}$, meaning the combination of a one-particle exchange from one $Z(\mathbf{p},\mathbf{k};E)$ and the leading order three-body force H_0/Λ^2 from the other $Z(\mathbf{k},\mathbf{q};E)$.[9]

$$W_{e0}^{(1)} = 8\pi \int^{\Lambda} \frac{d^3\mathbf{k}}{(2\pi)^3} \frac{1}{\mathbf{p}^2+\mathbf{pk}+\mathbf{k}^2-mE-i\epsilon} f(k^*) \frac{H_0}{\Lambda^2} = -\frac{32\pi k_2/r}{k_2-k_1}\frac{H_0}{\Lambda^2} I_{e0}\,. \tag{3.35}$$

Similar to above the integral I_{e0} can be divided into the part of the spurious pole and the expansion in $f(k^*)$.

$$\begin{aligned} I_{e0} &= \int^{\Lambda} \frac{d^3\mathbf{k}}{(2\pi)^3} \frac{1}{(\mathbf{p}^2+\mathbf{pk}+\mathbf{k}^2-mE-i\epsilon)} \left\{ \frac{1}{k^{*2}-k_2^2-i\varepsilon} + \frac{1}{k_2^2}\left(1+\frac{k^{*2}}{k_2^2}+\cdots\right)\right\} \\ &= I_{e0}^{pole} + I_{e0}^{expand}. \end{aligned} \tag{3.36}$$

The pole contribution is given by

$$I_{e0}^{pole} = \int^{\Lambda} \frac{d^3\mathbf{k}}{(2\pi)^3} \frac{4}{3} \frac{1}{(\mathbf{p}^2+\mathbf{pk}+\mathbf{k}^2-mE-i\epsilon)(\mathbf{k}^2-\rho^2-i\epsilon)}, \tag{3.37}$$

with $\rho^2 = 4/3(k_2^2+mE)$. Extending the upper border from this integral from Λ to infinity is equivalent to adding a low-energy polynomial.[10]

$$I_{e0}^{pole,\infty} = I_{e0}^{pole} - \text{polynomial}. \tag{3.38}$$

Using this and the 'Feynman-trick' [76]

$$\frac{1}{A^a B^b} = \frac{\Gamma(a+b)}{\Gamma(a)\Gamma(b)} \int_0^1 \frac{dx\, x^{a-1}}{[xA+(1-x)B]^{a+b}}, \tag{3.39}$$

the integral $I_{e0}^{pole,\infty}$ can be written as

$$\begin{aligned} I_{e0}^{pole,\infty} &= \frac{4}{3}\int_0^1 dx \int^{\infty} \frac{d^3\mathbf{k}}{(2\pi)^3} \frac{1}{\left[\mathbf{k}^2+x\mathbf{p}^2+x\mathbf{pk}-xmE-(1-x)\rho^2-i\epsilon\right]^2} \\ &= \frac{4}{3}\int_0^1 dx \int^{\infty} \frac{d^3\mathbf{k}}{(2\pi)^3} \frac{1}{\left[\mathbf{k}^2+x(1-x/4)\mathbf{p}^2-xmE-(1-x)\rho^2-i\epsilon\right]^2}. \end{aligned} \tag{3.40}$$

In the second step the loop momentum $\mathbf{k}$ is shifted to $\mathbf{k}-x/2\,\mathbf{p}$. Since the integration goes to infinity in all directions, this does not change the integral. Now the integrand does only depend on k^2, and can be calculated using for example [76]:

$$\int \frac{d^Dx}{(2\pi)^D} \frac{1}{(x^2+\Delta)^n} = \frac{1}{(4\pi)^{D/2}} \frac{D}{2} \frac{\Gamma(n-D/2)}{\Gamma(n)} \left(\frac{1}{\Delta}\right)^{n-D/2}, \tag{3.41}$$

[9] The other similar contribution, namely $W_{0e}^{(1)}$ will be completely equivalent.
[10] Since $\Lambda > \rho$, there is no additional pole in $1/(\mathbf{k}^2-\rho^2)$ if $k > \Lambda$.

which is known from dimensional regularization. Therefore

$$\begin{aligned} I_{e0}^{pole,\infty} &= \frac{4}{3}\frac{1}{8\pi}\int_0^1 dx \frac{1}{[x(1-x/4)\mathbf{p}^2 - xmE - (1-x)\rho^2 - i\epsilon]^{1/2}} \\ &= \frac{1}{6\pi}\int_0^1 dx \frac{1}{[A^2 - 1/4\mathbf{p}^2(x-x_0)^2 - i\epsilon]^{1/2}}, \end{aligned} \tag{3.42}$$

where

$$x_0 = \frac{2(\mathbf{p}^2 - mE + \rho^2)}{\mathbf{p}^2}; \text{ and } A^2 = \frac{(\mathbf{p}^2 - mE + \rho^2)^2}{\mathbf{p}^2} - \rho^2. \tag{3.43}$$

It yields with $p = \sqrt{\mathbf{p}^2}$

$$\begin{aligned} I_{e0}^{pole,\infty} &= \frac{-1}{3\pi i p} \ln\left[(x-x_0) + i\sqrt{\frac{4A^2}{p^2} - (x-x_0)^2 - i\epsilon}\right]\Bigg|_0^1 \\ &= \frac{1}{4\pi}\frac{1}{k_2^2}\sqrt{-mE + \frac{3}{4}p^2 - i\epsilon} + \cdots + \text{polynomial}. \end{aligned} \tag{3.44}$$

The calculation for the last step can be found in appendix 6.1 in more detail. The first part is not a polynomial in the energy E. However we continue by calculating the part from the expansion. Firstly we consider only the leading order in k^*/k_2 of the expansion of the quantity $f(k^*)$.

$$\begin{aligned} I_{e0,LO}^{expand} =& \int^\Lambda \frac{d^3\mathbf{k}}{(2\pi)^3}\frac{1}{k_2^2}\frac{1}{(\mathbf{p}^2 + \mathbf{pk} + \mathbf{k}^2 - mE - i\epsilon)} \\ =& \frac{1}{k_2^2}\int^\Lambda \frac{d^3\mathbf{k}}{(2\pi)^3}\left(\frac{1}{(\mathbf{p}^2 + \mathbf{pk} + \mathbf{k}^2 - mE - i\epsilon)} - \frac{1}{\mathbf{k}^2 - \mu^2}\right) + \frac{1}{k_2^2}\int^\Lambda \frac{d^3\mathbf{k}}{(2\pi)^3}\frac{1}{\mathbf{k}^2 - \mu^2} \\ =& \frac{1}{k_2^2}\int^\infty \frac{d^3\mathbf{k}}{(2\pi)^3}\left(\frac{1}{(\mathbf{p}^2 + \mathbf{pk} + \mathbf{k}^2 - mE - i\epsilon)} - \frac{1}{\mathbf{k}^2 - \mu^2}\right) + \frac{1}{k_2^2}\int^\Lambda \frac{d^3\mathbf{k}}{(2\pi)^3}\frac{1}{\mathbf{k}^2 - \mu^2} \\ & - \frac{1}{k_2^2}\int_\Lambda^\infty \frac{d^3\mathbf{k}}{(2\pi)^3}\left(\frac{1}{(\mathbf{p}^2 + \mathbf{pk} + \mathbf{k}^2 - mE - i\epsilon)} - \frac{1}{\mathbf{k}^2 - \mu^2}\right) \\ =& \frac{1}{k_2^2}\int^\infty \frac{d^3\mathbf{k}}{(2\pi)^3}\left(\frac{1}{(\mathbf{p}^2 + \mathbf{pk} + \mathbf{k}^2 - mE - i\epsilon)} - \frac{1}{\mathbf{k}^2 - \mu^2}\right) + \text{polynomial}, \end{aligned} \tag{3.45}$$

where we introduce a arbitrary scale μ, to ensure the integral is finite.[11] Now the finite integral can be solved using dimensional regularization and a shift $\mathbf{k} \to \mathbf{k} - \mathbf{p}/2$ similar to above.

$$I_{e0,LO}^{expand} = -\frac{1}{4\pi}\frac{1}{k_2^2}\sqrt{-mE + \frac{3}{4}p^2 - i\epsilon} + \text{polynomial}. \tag{3.46}$$

The non-polynomial part of $I_{e0,LO}^{expand}$ cancels exactly the leading order non-polynomial part of equation (3.44). It becomes clear that higher orders in the expansion of $f(k^*)$ will cancel the higher orders of I_{e0}^{pole} in a similar pattern. To conclude, this contribution to $W^{(1)}$ is also a low-energy polynomial in the meaning of case (a) above.

[11] The divergent parts $\sim \Lambda, \mu$ are absorbed in the polynomial.

The contribution of two one-particle exchanges $W_{ee}^{(1)}$

Finally we show that the contribution of the one-particle exchange for both potentials Z is also given by a low-energy polynomial. Again the integral can be divided in a part with the spurious pole and the expansion:

$$\begin{aligned} W_{ee}^{(2)} &= -\frac{32\pi k_2/r}{k_2-k_1}\left(I_{ee}^{pole}-I_{ee}^{subtr}\right), \\ I_{ee}^{pole} &= \frac{4}{3}\int^{\Lambda}\frac{d^3\mathbf{k}}{(2\pi)^3}\,\frac{1}{\mathbf{p}^2+\mathbf{pk}+\mathbf{k}^2-mE-i\varepsilon}\,\frac{1}{\mathbf{k}^2-\rho^2-i\varepsilon}\,\frac{1}{\mathbf{k}^2+\mathbf{kq}+\mathbf{q}^2-mE-i\varepsilon}, \\ I_{ee}^{expand} &= -\frac{1}{k_2^2}\int^{\Lambda}\frac{d^3\mathbf{k}}{(2\pi)^3}\,\frac{1}{\mathbf{p}^2+\mathbf{pk}+\mathbf{k}^2-mE-i\varepsilon}\left(1+\frac{k^{*2}}{k_2^2}+\cdots\right)\frac{1}{\mathbf{k}^2+\mathbf{kq}+\mathbf{q}^2-mE-i\varepsilon}. \end{aligned} \tag{3.47}$$

The pole-integral I_{ee}^{pole} is ultraviolet-finite, which can be seen by simple power-counting arguments. Therefore the limit $\Lambda\to\infty$ can be taken. This integral can be rewritten by using the 'Feynman-trick', equation (3.39), twice.

$$\begin{aligned} I_{ee}^{pole} &= \frac{4}{3}\int_0^1 dx\int^{\infty}\frac{d^3\mathbf{k}}{(2\pi)^3}\,\frac{1}{\left[\mathbf{k}^2-mE+x\mathbf{p}^2+(1-x)\mathbf{q}^2+x\mathbf{pk}+(1-x)\mathbf{qk}\right]^2}\,\frac{1}{\mathbf{k}^2-\rho^2-i\varepsilon} \\ &= \frac{4\Gamma(3)}{3}\int_0^1 dx\int_0^1 dy\, I_{ee}^{pole,k}, \end{aligned} \tag{3.48}$$

with the momentum integral

$$I_{ee}^{pole,k} = \int^{\infty}\frac{d^3\mathbf{k}}{(2\pi)^3}\,\frac{y}{\left[\mathbf{k}^2-ymE+y(x\mathbf{p}^2+(1-x)\mathbf{q}^2+x\mathbf{pk}+(1-x)\mathbf{qk})-(1-y)\rho^2-i\epsilon\right]^3}. \tag{3.49}$$

Analog to equation (3.44) this can be shifted by $\mathbf{k}\to\mathbf{k}-y/2(x\mathbf{p}+(1-x)\mathbf{q})$.

$$\begin{aligned} I_{ee}^{pole,k} &= \int^{\infty}\frac{d^3\mathbf{k}}{(2\pi)^3}\,\frac{y}{\left[\mathbf{k}^2-ymE-1/4y^2((x\mathbf{p}+(1-x)\mathbf{q})^2+y(x\mathbf{p}^2+(1-x)\mathbf{q}^2)-(1-y)\rho^2-i\epsilon\right]^3} \\ &= \frac{1}{32\pi}\,\frac{y}{\left[-ymE-1/4y^2((x\mathbf{p}+(1-x)\mathbf{q})^2+y(x\mathbf{p}^2+(1-x)\mathbf{q}^2)-(1-y)\rho^2-i\epsilon\right]^{3/2}}. \end{aligned} \tag{3.50}$$

In the last step equation (3.41) was used. Therefore

$$I_{ee}^{pole} = \frac{1}{12\pi}\int_0^1 dx\int_0^1 dy\frac{y}{(A+By+Cy^2-i\varepsilon)^{3/2}}, \tag{3.51}$$

with the short notation

$$A=-\rho^2,\quad B=-mE+\rho^2+x\mathbf{p}^2+(1-x)\mathbf{q}^2,\quad C=-\frac{1}{4}(x\mathbf{p}+(1-x)\mathbf{q})^2. \tag{3.52}$$

The integral over the variable y can be performed, yielding:

$$\begin{aligned} I_{ee}^{pole} =& \frac{1}{6\pi}\int_0^1 dx \frac{1}{4AC-B^2}\left(\frac{2A}{(A-i\varepsilon)^{1/2}} - \frac{2A+B}{(A+B+C-i\varepsilon)^{1/2}}\right) \\ =& \frac{1}{6\pi}\int_0^1 dx \frac{1}{4AC-B^2}\left(\frac{2A}{(-\beta^2-i\varepsilon)^{1/2}}\right. \\ & \left. - \frac{2A+B}{(-mE+x\mathbf{p}^2+(1-x)\mathbf{q}^2-\frac{1}{4}(x\mathbf{p}+(1-x)\mathbf{q})^2-i\varepsilon)^{1/2}}\right). \end{aligned} \tag{3.53}$$

The first part is a low-energy polynomial, for the second part we expand the fraction for large values of $\rho \sim k_2 \sim M_{high}$.

$$-\frac{2A+B}{4AC-B^2} = -\frac{3}{4k_2^2} - \frac{3}{16k_2^2}\left(5mE - 9(x\mathbf{p}^2+(1-x)\mathbf{q}^2+3(x\mathbf{p}+(1-x)\mathbf{q})^2)\right) + \cdots . \tag{3.54}$$

We pause the calculation of the x-integral and turn our attention to the integral I_{ee}^{expand} depending to the expansion in $f(k^*)$. We consider the leading order of this expansion.

$$\begin{aligned} I_{ee,LO}^{expand} &= \frac{1}{k_2^2}\int_0^\infty \frac{d^3\mathbf{k}}{(2\pi)^3}\frac{1}{\mathbf{p}^2+\mathbf{pk}+\mathbf{k}^2-mE-i\varepsilon}\frac{1}{\mathbf{k}^2+\mathbf{kq}+\mathbf{q}^2-mE-i\varepsilon} \\ &= \frac{1}{k_2^2}\int_0^1 dx \int_0^\infty \frac{d^3\mathbf{k}}{(2\pi)^3}\frac{1}{\left[\mathbf{k}^2-mE-i\varepsilon+x\mathbf{pk}+x\mathbf{p}^2+(1-x)\mathbf{kq}+(1-x)\mathbf{q}^2\right]^2} \\ &= \frac{1}{k_2^2}\frac{1}{8\pi}\int_0^1 dx \frac{1}{(-mE+x\mathbf{p}^2+(1-x)\mathbf{q}^2-\frac{1}{4}(x\mathbf{p}+(1-x)\mathbf{q})^2-i\varepsilon)^{1/2}}. \end{aligned} \tag{3.55}$$

Here the 'Feynman-trick', a shift $\mathbf{k} \to \mathbf{k} - 1/2(x\mathbf{p}+(1-x)\mathbf{q})$ and the dimensional regularization integral are used once more. The result is exactly the same integral as in the first part in the expansion (3.54) of the non-polynomial part of I_{ee}^{pole}, except a relative minus sign. So they cancel in equation (3.47). Higher orders in the expansion in I_{ee}^{expand} will cancel higher orders of equation (3.54) similarly. Therefore the correction to the potential given by $W_{ee}^{(1)}$ is indeed a low-energy polynomial as in case (a), discussed above.

Other contributions to $W^{(1)}$ and higher orders of the effective potential W

In the last section, it was shown that all considered contributions to the effective potential W at leading-order $W^{(1)}$ are low-energy polynomials. This was shown explicitly for $W_{ee}^{(1)}$, $W_{e0}^{(1)}$ and $W_{00}^{(1)}$. However the leading-order $W^{(1)}$ contains, in principle, an infinite amount of additional terms like $W_{e2}^{(1)}$, $W_{e4}^{(1)}, \cdots$. Those terms correspond to additional three-body forces proportional to $(k^*/\Lambda)^2$, $(k^*/\Lambda)^4, \cdots$. In other words the number of terms is only limited by the order of the EFT. Without showing the calculations for the additional terms in detail we argue that they are also low-energy polynomials.
On a mathematical level the correction $W_{e2}^{(1)}$ differs from $W_{e0}^{(1)}$ by an additional factor of $(k^*)^2 = 3/4k^2 - mE$ in the integrand and constants.

$$W_{e2}^{(1)} = 8\pi\int^\Lambda \frac{d^3\mathbf{k}}{(2\pi)^3}\frac{3/4\mathbf{k}^2-mE}{\mathbf{p}^2+\mathbf{pk}+\mathbf{k}^2-mE-i\epsilon}f(k^*)\frac{H_2}{\Lambda^4} = -\frac{32\pi k_2/r}{k_2-k_1}\frac{H_2}{\Lambda^4}\left(\frac{3}{4}\cdot I_{e2} - mE\cdot I_{e0}\right). \tag{3.56}$$

The 'new' integral I_{e2} is the same as the 'old' one I_{e0} except an additional factor k^2.

$$I_{e2} = \int^{\Lambda} \frac{d^3\mathbf{k}}{(2\pi)^3} \frac{\mathbf{k}^2}{(\mathbf{p}^2 + \mathbf{pk} + \mathbf{k}^2 - mE - i\epsilon)} \left\{ \frac{1}{k^{*2} - k_2^2 - i\varepsilon} + \frac{1}{k_2^2}\left(1 + \frac{k^{*2}}{k_2^2} + \cdots\right)\right\}. \tag{3.57}$$

While this additional factor indeed makes the calculations more difficult, the general pattern is unchanged. The non-polynomial part of the pole $1/(k^{*2} - k_2^2 - i\epsilon)$ will be canceled exactly by the non-polynomial part of the expansion, so $W_{e2}^{(1)}$ is also a low-energy polynomial. This argument holds for all additional three-body forces, the appearing integrals can be reduced to already known integrals with additional factors of k^2. Similar contributions like $W_{02}^{(1)}$ or $W_{22}^{(1)}$ can be reduced to integrals known from $W_{00}^{(1)}$ modulo additional factors of k^2. To summarize all contributions to the leading order correction to the potential are low-energy polynomials. Therefore the entire leading order correction is a low-energy polynomial.

Finally, we discuss higher order corrections in the Born series shown in equation (3.27). The second order is given by

$$W^{(2)} = 16\pi^2 \int^{\Lambda} \frac{d^3\mathbf{k}}{(2\pi)^3} Z(\mathbf{p}, \mathbf{k}; E) f(k^*) \int^{\Lambda} \frac{d^3\mathbf{k}'}{(2\pi)^3} Z(\mathbf{k}, \mathbf{k}'; E) f(k'^*) Z(\mathbf{k}', \mathbf{q}; E). \tag{3.58}$$

It is obvious that the integral over k' is the same as for $W^{(1)}$, which is, as we showed, a low-energy polynomial in k^2, q^2 and E. This leads to the integral over k containing only parts like $W_{e0}^{(1)}$ or $W_{00}^{(1)}$, which are also low-energy polynomials. This argument can be extended to an arbitrary number of iterations in the Born series. So it holds for all orders, $W^{(n)}$ is a low-energy polynomial.

To summarize the last sections, we showed that all corrections to the effective potential are low-energy polynomials, so

$$W(\mathbf{p}, \mathbf{q}; E) = Z(\mathbf{p}, \mathbf{q}; E) + \text{polynomial}. \tag{3.59}$$

Therefore the difference between the effective potential W and the physical potential Z can be absorbed by a change of the renormalization prescription. This can be achieved by simply changing the values of the three-body forces $H_0(\Lambda), H_2(\Lambda), \cdots$ for a given cut-off Λ.

3.2.2 Order of the subtracted polynomial

The core of the method we present here is the changed propagator $\tau_i(k^*) = \tau(k^*) - f_i(k^*)$, where the index i counts the number of terms in the expansion of the contribution of the spurious pole in $(k^*/k_2)^2$. The expressions for $i = 1, 2, 3$ are given by equation (3.25). At first thought one could assume, that accuracy of the method can be increased by adding more terms. Indeed, the propagator around the physical pole $k_1 \sim 1/a$ is reproduced more precisely by adding more terms, this can be seen in figure 3.3. But $f_i(k^*)$ is also part of the effective potential W, given by equation (3.23). In the last section we have carefully demonstrated, that the correction due to $f_i(k^*)$ is given by a low energy polynomial and therefore can be absorbed in the three-body forces of the original potential $Z(p, k, E)$. Obviously, this is only true if for a given order of the polynomial there is a three-body force with the same momentum dependence. Higher order terms cannot be absorbed, and therefore will not improve the accuracy of the EFT. So what is the optimal number of subtractions i for a given order of the EFT.
Note that this is a highly non-perturbative problem, so a perturbative power-counting argument can only

give a hint of the optimal choice. A numerical check is highly needed, this will be performed in section 3.3.5. The usage of numerical results in this manner was also used for example in [4], to show the need for a three-body force at LO in pionless EFT for three bosons. Being aware of this shortfalls the power-counting can be established as the following. The corrections to W are given by $W^{(1)}, W^{(2)}, \cdots$, defined in equation (3.27). The single parts that contribute to this are the potential $Z(p,q,E)$, the subtraction $f_i(k^*)$ and the integration measure. For small momenta Z counts as $\mathcal{O}(p^{-2})$ and the integration measure d^3k counts as $\mathcal{O}(p^3)$. Note that $f_i(k^*)$ is given by the entire pole contribution minus the expansion up to order $2(i-1)$. Therefore $f_i(k^*)$ counts as the first not subtracted term. So the quantities $f_1(k^*)$, $f_2(k^*)$, $f_3(k^*)$ count as $\mathcal{O}(p^2)$, $\mathcal{O}(p^4)$ and $\mathcal{O}(p^6)$ respectively. Each iteration of the Born series for W contains an additional factor of Z, f and d^3k, therefore the counting increases by at least $\mathcal{O}(p^{-2+2+3}) = \mathcal{O}(p^3)$. So the leading correction to W is given by $W^{(1)}$.
For the subtraction $f_1(k^*)$ it follows, $W^{(1),f_1}$ counts as $\mathcal{O}(p^{3-2+2-2}) = \mathcal{O}(p^1)$. For $f_2(k^*)$ the quantity $W^{(1),f_2}$ counts as $\mathcal{O}(p^{3-2+4-2}) = \mathcal{O}(p^3)$. And for $f_3(k^*)$ it is $W^{(1),f_3} = \mathcal{O}(p^{3-2+6-2}) = \mathcal{O}(p^5)$. If the theory contains only one three-body interaction H_0 (this is the case at LO and NLO) this counts as $\mathcal{O}(p^0)$. Therefore the first neglected corrections to the potential $Z(p,k,E)$ are at order $\Delta Z^{NLO} = \mathcal{O}(p^2)$. Following this power-counting rules, the leading order corrections to the effective potential $W_{f_i}^{NLO}$ at NLO of the EFT with i subtractions are given by

$$\begin{aligned}
\Delta W_{f_1}^{NLO} &= \Delta Z^{NLO} + W^{(1),f_1} = \mathcal{O}(p^2) + \mathcal{O}(p^1) = \mathcal{O}(p^1), \\
\Delta W_{f_2}^{NLO} &= \Delta Z^{NLO} + W^{(1),f_2} = \mathcal{O}(p^2) + \mathcal{O}(p^3) = \mathcal{O}(p^2), \\
\Delta W_{f_3}^{NLO} &= \Delta Z^{NLO} + W^{(1),f_3} = \mathcal{O}(p^2) + \mathcal{O}(p^5) = \mathcal{O}(p^2).
\end{aligned} \tag{3.60}$$

In other words using f_2 instead of f_1 increases the accuracy by a power of one. But using f_3 instead of f_2 does not increase it at all. Therefore, the ideal choice for the number of subtractions at NLO is given by f_2, and one should use the modified propagator $\tau_2(k^*)$ in the Faddeev equation. At N^{2}LO the situation changes, we have an additional three-body force proportional to p^2, so the corrections to the potential are $\Delta Z^{N^2LO} = \mathcal{O}(p^4)$. For the corrections to the effective potential this leads to

$$\begin{aligned}
\Delta W_{f_1}^{N^2LO} &= \Delta Z^{N^2LO} + W^{(1),f_1} = \mathcal{O}(p^4) + \mathcal{O}(p^1) = \mathcal{O}(p^1), \\
\Delta W_{f_2}^{N^2LO} &= \Delta Z^{N^2LO} + W^{(1),f_2} = \mathcal{O}(p^4) + \mathcal{O}(p^3) = \mathcal{O}(p^3), \\
\Delta W_{f_3}^{N^2LO} &= \Delta Z^{N^2LO} + W^{(1),f_3} = \mathcal{O}(p^4) + \mathcal{O}(p^5) = \mathcal{O}(p^4).
\end{aligned} \tag{3.61}$$

The accuracy increases by using f_2 instead of f_1 by a power of two but it further increases by one, if one uses f_3 instead of f_2. At this point the accuracy of the potential $Z(p,k,E)$ is reached and it cannot be improved by adding subtractions in f_i. So the optimal choice for the propagator at N^{2}LO is $\tau_3(k^*)$. In table 3.2.2 these findings are collected.
The arguments in this section can easily be extended to higher orders of the EFT, each time when a additional three-body force is added, the power of the neglected corrections in the potential $Z(p,k,E)$ increases by two. A additional subtraction in $f_i(k^*)$ increases the order of $W^{(1),f_i}$ by, again, two. It becomes clear, that for every additional three-body force an additional subtraction should be used. Note that, at this point, this extension cannot be tested easily. At N^{3}LO of the EFT the shape parameter P is included in the ERE, and therefore additional spurious poles can appear. To be able to deal with them the non-perturbative method has to be extended to higher orders of the EFT. In the outlook of this thesis, this is sketched.
We close the section by reminding, that perturbative power-counting arguments can only give an estimation of the optimal number of subtractions. In section 3.3.5, more robust conclusions based on numerical results are given.

Table 3.1: Appearance of 2- and 3-body parameters per order of the EFT power counting and the prediction of the optimal choice for the propagator.

Order	2-body parameters	3-body parameters	Predicted optimal propagator
LO	a	H_0	-
NLO	$a,\, r$	H_0	$\tau_2(k^*)$
N^{2}LO	$a,\, r$	$H_0,\, H_2$	$\tau_3(k^*)$

3.3 Numerical test

In this section we test the method developed above numerically. To accomplish this, an EFT using the method is used to predict or describe different model potentials. These models act as an underlying exact theory. Therefore they do not exhibit spurious poles. We investigate three identical bosons. The bosons interact pairwise via a separable S-wave potential and are described in the particle-dimer picture. The first model uses the Yamaguchi potential [74] as interaction, the second uses a Gaussian potential [**?**]. We will fine-tune the two-body parameters a and r of the EFT fitting the parameters of the pairwise interaction of the two models. The three-body interaction strengths $H_0, H_2, \cdots$ are given to reproduce three-body results of the models at chosen values of momentum. Finally, we investigate how well our predictions of the EFT describe the models. Observables we look at are the real and imaginary part of the particle-dimer phase shift $\delta^{(3)}$, the combination $p \cot \delta^{(3)}$ which is closely related to the particle-dimer scattering amplitude and three-body bound states.

3.3.1 Yamaguchi model

The first model we use to test our method is the Yamaguchi model [74]. The pairwise two-body interaction in the model is given by the Yamaguchi potential $V_Y(p,q)$. This is a separable potential, with the regulator $\chi(p)$. In this section we follow the well known procedure for separable potentials, as described in detail for example in [79].

$$V_Y(p,q) = \lambda \chi(p)\chi(q) \text{ , where } \chi(p) = \frac{\beta^2}{\beta^2 + p^2}. \tag{3.62}$$

The value λ gives the strength of the potential, β is connected to the range. Those two-body parameters can be connected to the scattering length a and the effective range r of an EFT. To do this we calculate the two-body scattering amplitude for the Yamaguchi potential.

$$t_Y(p,q,z) = \chi(p) d_Y(z) \chi(q), \tag{3.63}$$

with

$$d_Y(z) = \left[\frac{1}{\lambda} - \int_0^\infty \frac{d^3q}{(2\pi)^3} \frac{\chi^2(q)}{z - E_q - i\epsilon} \right]^{-1}, \tag{3.64}$$

where $E_q = q^2/m$. The integral can be solved analytically. With this the on-shell two-body scattering amplitude t_Y yields

$$\begin{aligned} t_y(p,p,E_p) &= \chi^2(p)\left[\frac{1}{\lambda} - \frac{m\beta^3}{8\pi(p+i\beta)^2}\right]^{-1} \\ &= \left[\left(\frac{m\beta}{8\pi}+\frac{1}{\lambda}\right) + \left(\frac{2}{\beta 2\lambda} - \frac{m}{8\pi\beta}\right)p^2 + \frac{1}{\beta^4\lambda}p^4 + \frac{m}{4\pi}ip\right]^{-1} \\ &= -\frac{4\pi}{m}\left[\left(-\frac{\beta}{2}-\frac{4\pi}{m\lambda}\right) + \left(\frac{1}{2\beta} - \frac{8\pi}{m\beta^2\lambda}\right)p^2 - \frac{4\pi}{m\beta^4\lambda}p^4 - ip\right]^{-1}. \end{aligned} \tag{3.65}$$

Here the amplitude is expanded in the momentum p. Note that this is exact, for the Yamaguchi potential there are no contributions beyond p^4. The requirement $t_{EFT}(p,p,E_p) = \#t_Y(p,p,E_p)$, leads to rules that connects the EFT two-body parameters to the Yamaguchi parameters. The constant of proportionally is chosen, such that the imaginary part of the denominator in $t_{EFT}(p,p,E_p)$ and $t_Y(p,p,E_p)$ is $-p$ in both cases. This results in rules for the scattering length a, the effective range r and the shape parameter P_4:

$$-\frac{1}{a} = -\frac{\beta}{2} - \frac{4\pi}{m\lambda},\ r = \frac{1}{\beta} - \frac{16\pi}{m\beta^2\lambda} \text{ and } P_4 = -\frac{4\pi}{m\beta^4\lambda}. \tag{3.66}$$

In the numerical calculations in the next sections we choose a and r equal[12] to the np-triplet scattering parameters $a = 5.4164$ fm and $r = 1.7536$ fm [19]. Using the neutron mass $m = 939.565$ MeV gives the Yamaguchi parameters as

$$\lambda = -0.00013 \text{ MeV}^{-2},\ \beta = 278.796 \text{ MeV}. \tag{3.67}$$

These values give a shape parameter $P_4 = 0.131$ fm^3. This does not appear in the EFT power counting before N^{3}LO. Since the value is small compared to a and r the results at N^{2}LO can be slightly better than one would expect. The chosen values result in a two-body bound state (in the Yamaguchi model and in the EFT) with mass $M_d = 2m - E_d$ and a binding energy $E_d = 2.22$ MeV. In the case of np scattering this would be the deuteron. This means a physical pole in the two-body scattering amplitude at $k_1 = \sqrt{mE_d} = 45.69$ MeV. The unmodified EFT gives an additional spurious pole at $k_2 = 179.37$ MeV.

The model we consider does not contain additional three-body forces[13]. The particle-dimer scattering amplitude $M_Y(k,p,E)$ in the Yamaguchi model in S-wave can be calculated by solving the Faddeev equation:

$$M_Y(k,p,E) = 2Z_Y(k,p,E) + \frac{1}{\pi^2}\int_0^\infty dqq^2 Z_Y(k,q,E)\tau_Y(q,E)M_Y(q,p,E), \tag{3.68}$$

with the dimer propagator $\tau_Y(q,E)$, given by

$$\tau_Y(q,E) = d_Y(z)\big|_{z=3q^2/(4m)-E-i\epsilon} = \frac{8\pi}{m\beta^3}\frac{(\beta+\gamma)^2(\beta+\sqrt{3q^2/4-mE})^2}{2\beta+\gamma+\sqrt{3q^2/4-mE}}\frac{1}{\gamma-\sqrt{3q^2/4-mE}}, \tag{3.69}$$

[12] In this thesis we study three bosons, so those parameters are not directly linked to any real physical problem. However with the chosen values direct calculations are possible and they allow a intuition for the appearing values. For example the physical pole k_1 of this values is given by $\approxeq 46$ MeV, which gives a binding energy of the corresponding dimer of $k_1^2/m \approxeq 2.2$ MeV. Obviously this is the binding energy of the deuteron in the fermionic case. The generalisation of our method to particles with spin is straightforward.

[13] However the EFT does. A pionless EFT for three bosons needs three-body forces starting at leading order to describe three-body systems correctly [4].

where we used the notation $\gamma = \sqrt{-m\lambda\beta^3/(8\pi)} - \beta = \sqrt{mE_d}$ and $E \to E + i\epsilon$ is implicit. As mentioned above only a one-particle exchange and no three-body forces are considered as possible interactions. For a separable potential in S-wave this yields

$$\begin{aligned} Z_Y(p,q,E) &= \frac{1}{2}\int_{-1}^{1} d\cos\theta_{p,q} \frac{\chi(\mathbf{q}+1/2\mathbf{p})\chi(-\mathbf{p}-1/2\mathbf{q})}{E-\mathbf{p}^2/(2m)-\mathbf{q}^2/(2m)-(\mathbf{q}+\mathbf{q})^2/(2m)} \\ &= \frac{m}{2}\int_{-1}^{1} du \frac{\beta^2}{\beta^2+p^2/4+q^2+pqu} \frac{\beta^2}{\beta^2+p^2+q^2/4+pqu} \frac{1}{mE-p^2-q^2-pqu}. \end{aligned} \tag{3.70}$$

Before we discuss the numerical treatment of the model we introduce the particle-dimer phase shift $\delta_Y^{(3)}$ in the Yamaguchi model by

$$M_Y(p,p,E_p) = -\frac{3m\beta^3}{8\gamma(\beta+\gamma)^3} \frac{1}{p\cot\delta_Y^{(3)} - ip}. \tag{3.71}$$

Note that the normalization is different to the normalization in case of the EFT. This does not cause problems, since only observables like $\delta^{(3)}$ or the bound states are compared, which are obviously independent of this normalization. The normalization is calculated in appendix 6.2.2.

The EFT at LO

The relations to connect the EFT to the model (equation (3.66)) are given with respect to the EFT in NLO (and higher). In principle, it is possible to also use them for LO by calculating the scattering length a, as stated, and setting the effective range to zero, $r = 0$. However, this would give the physical pole k_1, therefore the binding energy of the dimer and the break-up incorrect or unprecise. Alternative one could use the binding energy of the dimer as an input directly. Since there is only one parameter at LO they can be connected uniquely. In the following we use this. The scattering length at LO is given by

$$a^{LO} = \left(\sqrt{|ME_d|}\right)^{-1} = 4.3193 \text{ fm}. \tag{3.72}$$

The propagator at LO also leads to a different kernel $K(p,q,E_q)$ in the treatment of the physical pole. The kernel $K_i(p,q,k)$ for NLO and N^{2}LO will be introduced in equation (3.75). For the LO calculations this kernel is exchanged by the following LO version.

$$K(p,q,k) = Z(p,k,E_q)\frac{4k^2}{\pi} \frac{1/a^{LO} + \sqrt{3/4(k^2-q^2)+(1/a^{LO})^2}}{3/4(q+k)}. \tag{3.73}$$

The remaining treatment of the physical pole and the discretization are completely analogous to below. But the normalization is also slightly different than in NLO (and N^{2}LO), it is given by

$$M^{LO}(p,p,E_p) = \frac{3a^{LO}}{16} \frac{1}{p\cot\delta_{LO}^{(3)} - ip}. \tag{3.74}$$

This is shown in appendix around equation (6.15).

Equation (3.68) can be solved for the scattering amplitude using numerical standard procedures. We approximate the integral by a sum with Gaussian weights, and take care of the physical pole k_1 with a method based on the Sokhotski–Plemelj theorem (equation (3.31)). The same method is also used for the numerical EFT calculations. The method is explained in detail in section 3.3.2. Further we use a cutoff $\Lambda = 1500$ MeV to regulate the integral. Contrary to the integrals in the EFT the integral in equation (3.68) is ultraviolet finite, due to the regulator $\chi(p)$. So this cutoff has no connection to regularization and really is an approximation. To ensure this and estimate the error caused by this approximation we repeat the calculations for slightly varied values of Λ and calculated the relative difference for chosen values of momentum. The resulting error is less than 1% for all momenta considered.
The second origin of numerical errors for the Yamaguchi model are the number of steps in the Gaussian approximation of the integral. We use $n = 1000$ steps. In figure 3.4 this is investigated. Similar to above we slightly vary the number of steps, and compare the results to each other. A variation of 10% causes deviations of less than 0.07%.
Also note that we do not use contour rotation or similar techniques to deal with the branch cut above the two-body break-up. We use a brute force approach, this means simply choosing a lot of steps of discretization to integrate over it. This can be done, since the singularities of the branch cut are removable singularities. This method was used for similar systems for example in [49]. While this very simple to implement, it creates slightly larger numerical errors above the break-up. If fact it can be seen in figure 3.4, the numerical errors increase heavily above the break-up. However, in the context of this thesis the accomplished numerical accuracy is sufficient compared to the EFT error.

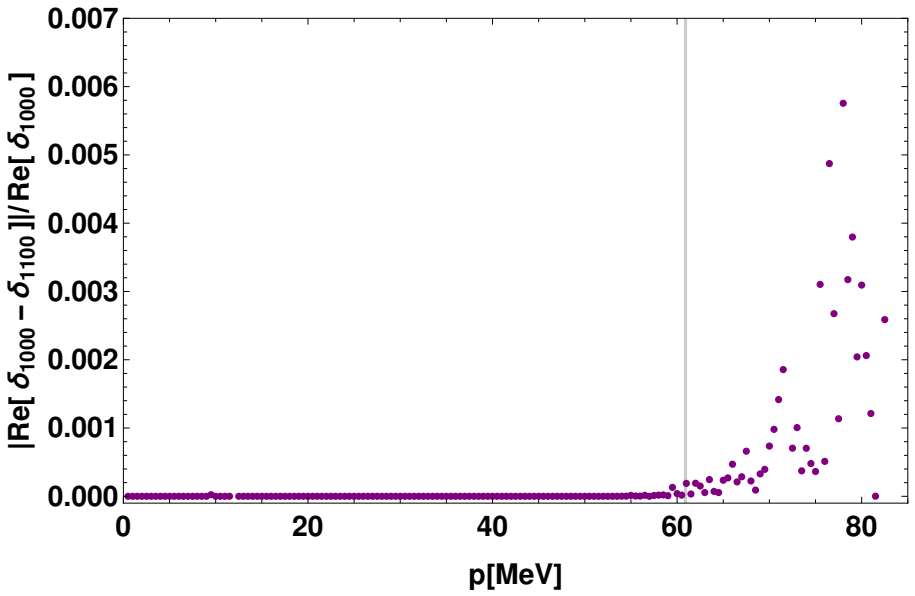

Figure 3.4: Relative difference between the results for numerical calculations with $n = 1000$ and $n = 1100$ discretization steps. The difference of 10% in the number of steps causes deviations of less than 0.7%. Below the break-up (gray line) the difference is even smaller.

3.3.2 Numerical treatment of Faddeev equations

In this section we discuss the numerical treatment of Faddeev equations. The principal method is the same for the EFT, the Yamaguchi and Gauss model. To obtain the particle-dimer scattering amplitude for the three cases the following Faddeev equations have to be solved. For the EFT using the method for the spurious pole use equation (3.26) and for the Yamaguchi model use equation (3.68). In this section we we show the numerical method for the EFT. The other cases are similar, additional remarks are given in the corresponding sections. The numerical treatment contains two steps. The treatment of the physical pole k_1 and the discretization of the loop integral. In absence of a physical pole the first step can be skipped.

Treatment of the physical pole

In this section the Sokhotski-Plemelj theorem (equation (3.31)) is used to avoid numerical problems caused by the physical pole k_1. The particle-dimer S-wave phase shift can be obtained by setting the S-wave projection of the Faddeev equation (3.26) on-shell, $mE_q = 3q^2/4 - mE_D = 3q^2/4 - k_1^2$. By factoring out the pole explicitly, this can be written as

$$\begin{aligned} M(p,q,E_q) &= Z(p,q,E_q) + \frac{4}{\pi}\int_0^\Lambda dk\, k^2\, Z(p,k,E_q)\tau_i(k^*)M(k,q,E_q) \\ &= Z(p,q,E_q) + \int_0^\Lambda dk \frac{K_i(p,q,k)}{k-q-i\varepsilon} M(k,q,E_q), \end{aligned} \tag{3.75}$$

with the potential in S-wave projection (given by equation 2.44) and a kernel $K_i(p,q,k)$. The kernel is given by

$$K_i(p,q,k) = \frac{4}{\pi}k^2 Z(p,k,E_q)\tau_i(k^*)(k-q-i\varepsilon) = \frac{4}{\pi}k^2 Z(p,k,E_q)\tau_i^{rest}(k^*). \tag{3.76}$$

The quantity $\tau_i^{rest}(k^*)$ is the modified propagator without the part that diverges at the position of the physical pole $(k-q)$. This can be calculated by using the first part of a Laurent series:

$$\tau_i^{rest}(k^*) = \left(\frac{d}{dq}\tau_i^{-1}(q^*)\right)^{-1}\Bigg|_{q\to k}. \tag{3.77}$$

Alternatively at the position of the physical pole [14] in the kernel $K(p,q,q)$ one can re-substitute $\tau_i(k^*) \to \tau(k^*)$. This allows an easy analytic calculation of the kernel:

$$\tau_i^{rest}(k^*)|_{k=q} \to \tau^{rest}(k^*) = \frac{-2/r\sqrt{3/4(k^2-q^2)+k_1^2}+k_1}{3/4(k+q)(\sqrt{3/4(k^2-q^2)+k_1^2}-k_2)}. \tag{3.78}$$

Due to the different propagator at LO of the EFT, for the calculations in LO the kernel has to be exchanged by the LO version of it. This can be seen in equation (3.73). Using the Sokhotski-Plemelj theorem the Faddeev equation reads

$$M(p,q,E_q) = Z(p,q,E_q) + \mathcal{P}\int_0^\Lambda dk \frac{K_i(p,q,k)}{k-q} M(k,q,E_q) + i\pi K_i(p,q,q)M(p,q,E_q). \tag{3.79}$$

[14] This means $k = q$. Here the modified propagator $\tau_i(k^*)$ is the same as the unmodified version $\tau(k^*)$ by construction.

By adding and subtracting the kernel at $q = k$ it yields

$$\begin{aligned} M(p,q,E_q) = Z(p,q,E_q) + \mathcal{P}\int_0^\Lambda dk \frac{K_i(p,q,k)M(k,q,E_q) - K_i(p,q,q)M(q,q,E_q)}{k-q} \\ + \mathcal{P}\int_0^\Lambda dk \frac{K_i(p,q,q)M(q,q,E_q)}{k-q} + i\pi K_i(p,q,q)M(p,q,E_q). \end{aligned} \tag{3.80}$$

The first integral is finite at the position of the pole. Therefore the principal value integral is the same as a standard integral. The second integral can be solved exactly.

$$\begin{aligned} M(p,q,E_q) &= Z(p,q,E_q) + \int_0^\Lambda dk \frac{K_i(p,q,k)M(k,q,E_q) - K_i(p,q,q)M(q,q,E_q)}{k-q} \\ &\quad + \ln\left[\frac{\Lambda-q}{q}\right] K_i(p,q,q)M(q,q,E_q) + i\pi K_i(p,q,q)M(p,q,E_q) \\ &= Z(p,q,E_q) + \int_0^\Lambda dk \frac{K_i(p,q,k)M(k,q,E_q)}{k-q} + w(q)K_i(p,q,q)M(p,q,E_q), \end{aligned} \tag{3.81}$$

with the weight of the pole contribution

$$w(q) = -\int_0^\Lambda dk \frac{1}{k-q} + \ln\left[\frac{\Lambda-q}{q}\right] + i\pi. \tag{3.82}$$

If the discretization of the integrals is done properly the divergence of the first part is canceled by the divergence in $w(q)$ exactly.

For the Yamaguchi model the numerical approach is the same. Except the kernel for the EFT $K_i(p,q,k)$ is exchanged by a kernel for the Yamaguchi model. The kernel for the model is given by

$$K_Y(p,q,k) = \frac{1}{\pi^2} k^2 Z_Y(p,k,E_q)\tau_Y^{rest}(k^*), \tag{3.83}$$

with the remaining propagator at the position of the physical pole $k = q$:

$$\tau_Y^{rest}(k^*)|_{k=q} = \frac{16\pi}{3m}\frac{\gamma}{\beta^3}\frac{(\beta+\gamma)^3}{k}. \tag{3.84}$$

Before we show the discretization, we discuss why this method can not be used for the spurious pole k_2. At a purely mathematical level a shift of $-i\epsilon$ would solve the numerical problem of diverging integrals. However, using this and the Sokhotski-Plemelj theorem gives rise to an additional imaginary part as can be seen above. This is unphysical since a change in the imaginary part of $M(p,p,E_p)$ would also change the imaginary part of the particle-dimer phase shift $\delta^{(3)}$. A non-vanishing imaginary part of the particle-dimer phase shift $\delta^{(3)}$ is directly connected to additional channels of the investigated system. For example the physical pole, which is connected to a bound dimer state, results in a positive imaginary part above $4/3E_D$. This can be seen for example in figure 3.5 (below). This shows an additional possible interaction, namely the break-up of the dimer into two single particles. This can be understood easily by remembering the connection of the S-wave phase shift to the S-matrix

$$S_0(p) = e^{2i\delta_0}. \tag{3.85}$$

A positive imaginary part of the phase shift gives an exponential function with a negative real exponent, so a damping. In other words the amplitude of the outgoing current is lower than amplitude of the incoming current. The missing part goes to the additional channel, which is not included in the theory explicitly.
So, an imaginary part caused by the spurious pole would mean an additional channel, and therefore a possible additional physical particle. As we discussed above this is not the case, the pole is an artefact of the ERE and does not represent additional physics. A closer inspection of the kernel in this case further highlights the problem. $K_i(p,q,k)$ can be interpreted by the '-1' part of a Laurent series, this is given the residuum at $k = k_2$. As we discussed above this is negative for the spurious pole. So it can result in a negative imaginary part of the phase shift.[15] This means for the S-matrix an exponential function with a positive real exponent. So, the amplitude of the outgoing current can be larger than the incoming current. This violates causality and clearly is unphysical. So, treating the spurious pole as a physical one does not work. It is necessary to use specific methods like the method presented in this thesis.

Discretization

In this section it is described how the Faddeev equations can be solved numerically. We assume that the physical pole is already treated as shown in the last section. So, we solve equation (3.81) instead of equation (3.26). For the Yamaguchi model use the corresponding Faddeev equation with the kernel given by equation (3.83). The loop integral is approximated by a discretized version, which is given by

$$\int_0^\Lambda dk \to \sum_{j=1}^{N} \omega_j k_j, \tag{3.86}$$

with the Gaussian weights ω_j. For the integral in the pole contribution $w(q)$ (equation (3.82)) the same discretization is used. Therefore the discrete version of the Faddeev equation yields

$$M(p,q,E_q) = Z(p,q,E_q) + \sum_{j=1}^{N} \omega_j \frac{K_i(p,q,k_j)}{k_j - q} M(k_j,q,E_q) + w(q) K_i(p,q,k_{N+1}) M(q,q,E_q), \tag{3.87}$$

where the discretized version of the weight of the pole is

$$w(q) = \ln\left((\Lambda - q)/q\right) - \sum_{j=1}^{N} w_j/(q_j - q) + i\pi. \tag{3.88}$$

To obtain a solvable system, also the in-going momenta p are discretized, $p \to k_i$. To get a quadratic matrix this follows the same prescription as k, especially the number of steps N are the same,

$$M(k_i,q,E_q) = Z(k_i,q,E_q) + \sum_{j=1}^{N} \omega_j \frac{K_i(k_i,q,k_j)}{k_j - q} M(k_j,q,E_q) + w(q) K_i(k_i,q,q) M(q,q,E_q). \tag{3.89}$$

The final trick is to add an additional step in the discretization of $p \to k_i$ as

$$k_{N+1} = q. \tag{3.90}$$

[15] The relation between the sign of the kernel and the sign of Im$[\delta^{(3)}]$ is not obvious. A short motivation is that the sign for the physical pole is positive, which causes a positive imaginary part. The spurious pole has a negative sign, so one expects a negative imaginary part.

We can identify the same q in the pole contribution and write

$$M(k_i,q,E_q) = Z(k_i,q,E_q) + \sum_{j=1}^{N} \omega_j \frac{K_i(k_i,q,k_j)}{k_j - q} M(k_j,q,E_q) + w(q) K_i(k_i,q,k_{N+1}) M(k_{N+1},q,E_q). \tag{3.91}$$

Note that, in this sense, the index i goes from 1 to $N+1$ and if the pole contribution is added to the sum the index j also goes up to $N+1$. Therefore we can write the $N+1$ equations for k_i all as a matrix equation.

$$\vec{M}(q) = \vec{Z}(q) + K(q)\vec{M}(q), \tag{3.92}$$

with the vectors

$$\vec{M}(q) = \begin{pmatrix} M(k_1,q,E_q) \\ \vdots \\ M(k_N,q,E_q) \\ M(k_{N+1},q,E_q) \end{pmatrix} \quad \text{and} \quad \vec{Z}(q) = \begin{pmatrix} Z(k_1,q,E_q) \\ \vdots \\ Z(k_N,q,E_q) \\ Z(k_{N+1},q,E_q) \end{pmatrix}. \tag{3.93}$$

The $(n+1)\times(n+1)$ matrix $K(q)$ is given by the elements

$$K_{ij}(q) = \begin{cases} \omega_j \, K(k_i,q,k_j)/(k_j - q), & \text{if } j \in [1,\cdots,N] \\ w(q) \, K(k_i,q,k_N+1), & \text{if } j = N+1. \end{cases} \tag{3.94}$$

The linear system (3.92) can be solved by using standard numerical methods. For the results shown in the next chapters we us the command 'LinearSolve' in Mathematica by Wolfram Research. In a last step the result for the scattering amplitude is solved for the particle-dimer phaseshift δ. The relation between these quantities is

$$M_Y(p,p,E_p) = \frac{3}{32}\frac{r}{k_1}(k_2 - k_1)\frac{1}{p\cot\delta_Y^{(3)} - ip}. \tag{3.95}$$

The normalization is calculated in the appendix.

Three-body forces for the EFT

Above we discussed how the two-body parameters a and r of the EFT can be adjusted to reproduce the Yamaguchi parameters λ and β. Although the Yamaguchi model has no additional three-body forces, pionless EFT needs three-body forces to correctly reproduce three-body observables of the model, even at leading order [4]. In table 3.2.2 it is shown at which order of the EFT expansion how many three-body forces are considered. Since regularization of the divergent loop integrals in the Faddeev equation the three-body forces have to be renormalized. In this thesis a sharp ultraviolet cut-off Λ is used to regularize the integrals, therefore all three-body forces are Λ-dependent quantities $H_0(\Lambda)$, $H_2(\Lambda)$, $\cdots$. As discussed in section 2.2 there are, in general, two methods to obtain the values of the three-body forces.

(a) If the more fundamental theory or (as here) the exact model is known, they can be calculated as Λ-dependent functions. Unfortunately, this is not possible easily, if the method presented in this thesis is used. This is due to the change of the renormalization prescription described in section

3.2.1. There it is shown in detail, that the effective potential W is the original potential Z plus a low energy polynomial. This additional polynomial is than absorbed into the three-body forces. Consequently the values of $H_0(\Lambda)$, $H_2(\Lambda)$, $\cdots$ change. To be able to calculate this new values to the exact model, the polynomial has to be calculated. This is not done here, however is possible along the analytic calculations shown in section 3.2.1.

(b) If three-body observables of the model (or experimental three-body observables) are known, the three-body forces can be fine-tuned to reproduce these values. This highlights the EFT concept, that the details of short range physics are not relevant for the system at low energies. For each three-body force one additional input parameter is needed.

Here the second method is used. The Yamaguchi model mimics the 'real physics' we want to describe. So we calculate three-body observables in the model and use them as input to the EFT. Then the three-body forces are fine-tuned to reproduce them. For the first three-body force H_0 we calculate the quantity $p\cot(\delta_Y^{(3)}(p))$ in the model at $p = 0.001$ MeV. This is approximately[16] given by the negative inverse of three-body scattering length $a^{(3)}$. The fine-tuning is done by performing the following prescription.
We choose an arbitrary value for H_0, do the calculations for the EFT and compare the result to the result of the model, $\Delta\mathcal{O}(H_0) = p\cot(\delta_Y^{(3)}) - p\cot(\delta_{EFT}^{(3)})|_{p=0}$. Then the value of H_0 is varied $H_0' = H_0 + \Delta H_0$ and the new result is compared to the model again. If the result is closer than before, $|\Delta\mathcal{O}(H_0')| < |\Delta\mathcal{O}(H_0)|$, we keep the new H_0' and repeat this. If the result is worse, the direction of the shift is changed $H_0' = H_0 - \Delta H_0$. If the sign of the difference changes, $\text{sgn}\,[\Delta\mathcal{O}(H_0')] \neq \text{sgn}\,[\Delta\mathcal{O}(H_0)]$, the last step is repeated with $H_0' = H_0 + \Delta/2$. This is repeated until $\Delta\mathcal{O}(H_0')/(p\cot(\delta_Y^{(3)})) < 5 \cdot 10^{-4}$.
At LO and NLO of the EFT there is only this single three-body force. At N^{2}LO an additional three-body force proportional to H_2 appears. Analogous to above it would be convenient to fine-tune this to the effective range $r^{(3)}$. This can be done for example by calculating the second derivative of $p\cot(\delta_Y^{(3)})$ at threshold. However, to obtain the derivatives, multiple points near threshold have to be calculated. Therefore we save calculation time and fine-tune H_2 to a single point, namely to $p\cot(\delta_Y^{(3)}(p))$ at $p = 10$ MeV. The matching to this single result is performed equivalent to the prescription for H_0. Please note, in the momentum scheme (equation (2.38)) the result at threshold depends on both three-body forces H_0 and H_2. The calculations would be slightly more complicated, so we use the energy scheme (equation (2.39)). In this scheme the quantity $p\cot(\delta^{(3)})|_{p=0}$ is independent of H_2, such that H_0 can be obtained and fixed. Afterwards H_2 can be obtained separately.
As discussed above the results for the three-body forces are cut-off dependent, in the following we choose $\Lambda = 250$ MeV or $\Lambda = 600$ MeV. Also note, since the absorbed polynomial depends of the number of subtractions in the propagator (equation (3.25)), the values of H_0 and H_2 also dependent on this number. The final results we obtain for the three-body forces are given in table 3.2.

[16] The effective range expansion yields $p\cot(\delta^{(3)})|_{p=0} = -1/a^{(3)}$. For technical reasons the calculations at the threshold $p = 0$ MeV are challenging. So, we approximate $a^{(3)}$ by being very close to the threshold.

Table 3.2: The three-body couplings H_0 and H_2 for the different values of the cutoff Λ, and different number of subtractions in the propagator $\tau(k)$ (no subtraction is needed at LO). All quantities are given in MeV units. The values of H_0 are the same at NLO and N^{2}LO, whereas $H_2 = 0$ at NLO.

	τ_i	$H_0(\Lambda = 250)$	$H_2(\Lambda = 250)$	$H_0(\Lambda = 600)$	$H_2(\Lambda = 600)$
LO		-2.65		0.20	
NLO & N^{2}LO	τ_1	-0.41	0.13	0.43	-4.10
	τ_2	-0.59	0.32	-0.55	1.01
	τ_3	-0.66	0.42	3.71	1111.5

3.3.3 Particle-dimer phase shift

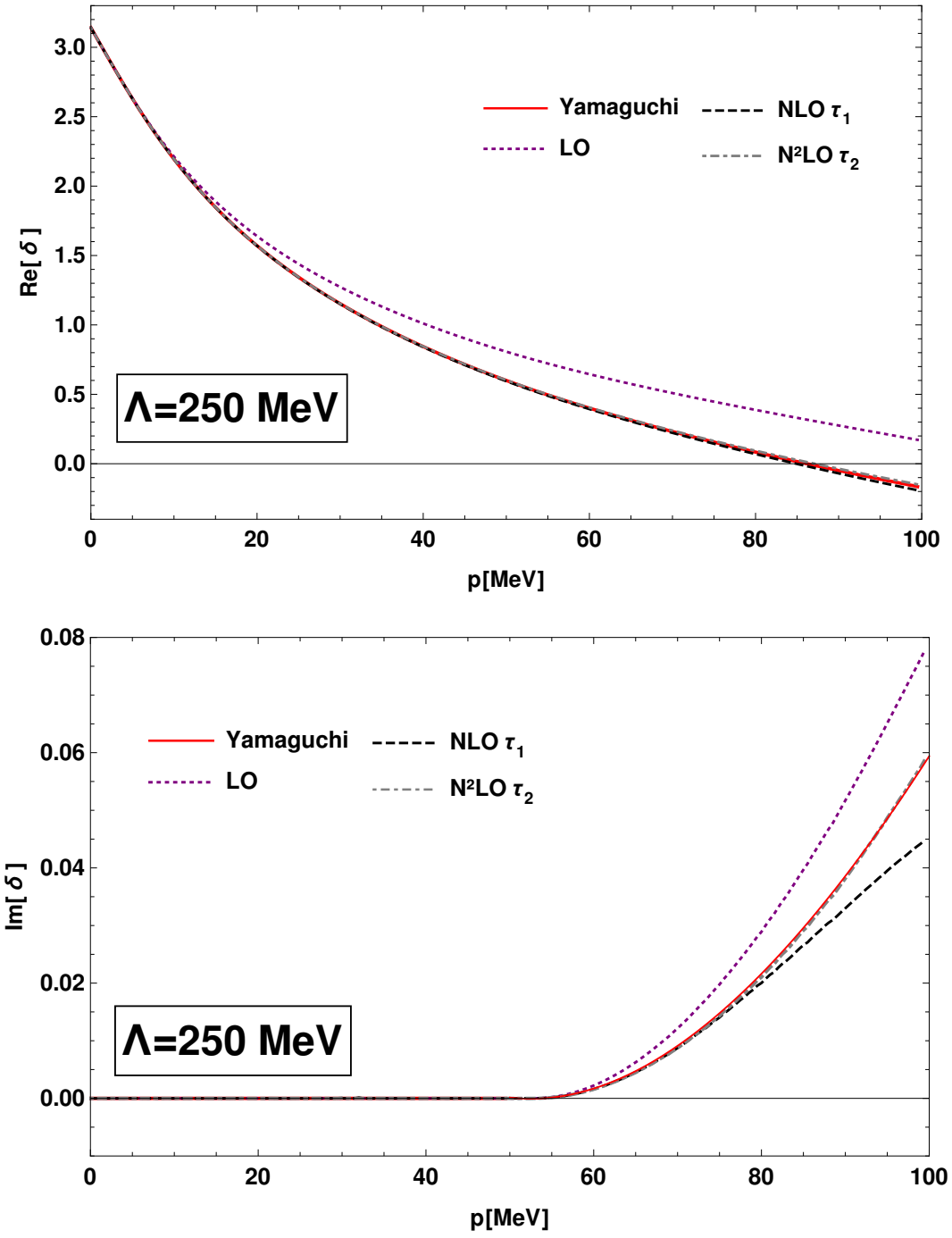

Figure 3.5: Numerical results for real (above) and imaginary (below) part of the particle-dimer phase shift δ for the Yamaguchi model. Red solid line: the result obtained in the Yamaguchi model; in purple dotted: the LO result; in black dashed: the NLO result for τ_1; in gray dot-dashed: the N^{2}LO result for τ_2. For the real part the NLO and N^{2}LO results are on top of the Yamaguchi model. For the imaginary part the N^{2}LO results are on top of the model. The cutoff was set to the value $\Lambda = 250$ MeV.

In this section the results for the particle-dimer phase shift $\delta^{(3)}$ are shown[17]. The parameters of the EFT are fine-tuned to reproduce the Yamaguchi model. This is described in detail above. The Yamaguchi and the two-body parameters of the EFT are given by equation (3.67), the three-body forces of the EFT by table 3.2. We investigate how precise the description is.
The EFT using the method presented in this thesis contains two different expansions:

(a) The EFT expansion (i.e., including more derivative terms in the Lagrangian that are accompanied with the independent couplings). This expansion is labeled by LO, NLO, and N^{2}LO. The amount of two- and three-body parameters per order is given by table 3.2.2.

(b) The Taylor-expansion of the spurious pole given by the different orders of $\tau_i(k^*)$, defined by equation (3.25).

The convergence of these expansions needs to be investigated separately. In this section we focus on the first expansion and choose the subtracted propagators $\tau_1(k^*)$ and $\tau_2(k^*)$ in the calculations at NLO and N^{2}LO, respectively[18]. This differs to the expectation given in section 3.2.2 by one. We will motivate this choice by numerical results discussed in section 3.3.5.
In the upper part of figure 3.5 the results for the real part of the particle-dimer phase shift are shown. In the EFT a sharp cut-off of $\Lambda = 250$ MeV is chosen. It can be seen that LO is precise only at small momenta, whereas NLO can describe data at much higher values of the relative momentum p. The situation further improves at N^{2}LO. However this improvement is very small (practically not visible at this scale). In the lower part of figure 3.5 the imaginary part of δ is shown. It can be seen that the NLO and N^{2}LO results describe the model better than the LO results, while the N^{2}LO results are clearly improved compared to NLO. To summarize the results, the EFT at different orders behaves as expected. It can predict the Yamaguchi model, and it improves order by order. However, if this improvement follows the systematic improvement that defines EFT, a more elaborate study of the problem is necessary. This is performed in the next section, using the so-called Lepage plots and a constancy assessment.
The errors of the EFT calculation for $p > 1/a$ can be estimated as $(p/\Lambda)^{n+1}$ at N^{n}LO. A more detailed evaluation of the EFT errors is presented in the discussion of possible choices for $\tau_i(k^*)$ below.

Further, we discuss physical interpretations of the results of the particle-dimer phase shift. Remember that the investigated model describes three identical bosons interacting pairwise by the Yamagchi potential, such that this are observations for the model and not directly connected to a real physical system. (Compare to the discussion in section 3.3.1.)
It can be noted, that the imaginary part is zero for $p \lesssim 55$ MeV and positive above. This is consistent with the expectations. The positive imaginary part indicates an additional channel, so a additional possible interaction, namely the dimer break-up. Compare this to the discussion around equation (3.85). The expected value for the dimer break-up is $4/3ME_D \to p \approx 53$ MeV.
We close this section by repeating the numerical calculations for a different choice of the cut-off, $\Lambda = 600$ MeV. The results for the phase shift can be seen in Fig. 3.6. It can be seen that all observations discussed above also holds here. The description of the EFT improves order by order for the real part as well as for the imaginary part. This fulfils the requirement of an EFT, more precise of the renormalization, that all observables are cut-off independent, except corrections of order $(p/\Lambda)^{n+1}$.

[17] To simplify the notation the superscribed (3) is dropped here and in the sections below.
[18] At LO there are no range corrections. Therefore there is no spurious pole and the method is not used.

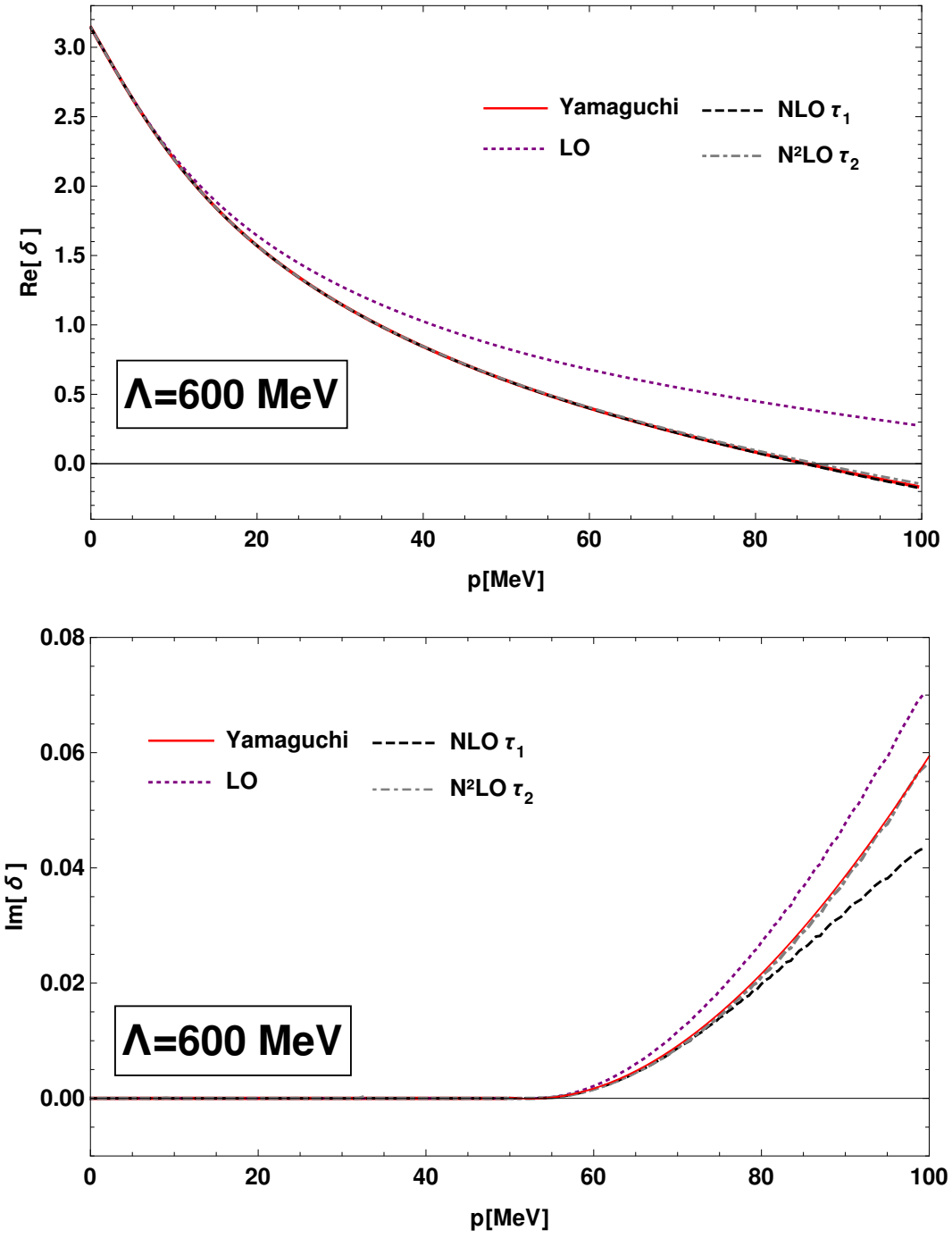

Figure 3.6: Numerical results for real (above) and imaginary (below) part of the particle-dimer phase shift δ for the Yamaguchi model. Red solid line: the result obtained in the Yamaguchi model; in purple dotted: the LO result; in black dashed: the NLO result for τ_1; in gray dot-dashed: the N^{2}LO result for τ_2. For the real part the NLO and N^{2}LO results are on top of the Yamaguchi model. For the imaginary part the N^{2}LO results are on top of the model. The cutoff was set to the value $\Lambda = 600$ MeV.

3.3.4 Lepage plots and consistency assessment

In the last section we have shown that our non-perturbative method can reproduce the results of a Yamaguchi model. Notwithstanding this, in the context of EFT the systematic improvement of the description order by order is equally important. Let $p \sim M_{low}$ be the momentum of the system[19], and the break-down scale $\Lambda_b \sim M_{high}$ is the limit, where neglected low-distance physics become important. In this case, the EFT claims to describe a physical system exact up to corrections of order $(p/\Lambda_b)^n$. The power n of this corrections increases order by order of the EFT. For the pionless EFT considered here, the correction to the results at LO is $(p/\Lambda_b)^1$, at NLO $(p/\Lambda_b)^2$ and at N^{n}LO $(p/\Lambda_b)^{n+1}$. This systematic improvement can be used as an error estimation of the theory. This is done for example in figure 3.9 and figure 3.10. This can also be exploited as a check for the consistency of the EFT. The re-normalization (and every change to it, as performed using our method) has to preserve this systematic improvement. A well established method was proposed by Lepage [51]. If results of the fundamental theory (or experimental data) are available, double-logarithmic plots, so called Lepage plots, allow one to directly determine n and therefore test the systematic increase of n. A similar test was suggested by Grießhammer [27, 26] recently, where the EFT is compared to the same EFT for a different cut-off Λ. This can test the consistency of the EFT without needing known models (or data). In the following, we will describe these tests in more detail and perform them for the EFT using our non-perturbative method.

We start with the Lepage plots. We want to use our EFT to describe an observable, say the particle-dimer phaseshift δ. The EFT of order N^{n}LO claims to be exact up to corrections of $(p/\Lambda_b)^{n+1}$. Therefore

$$\left|\frac{\delta_Y - \delta_{EFT}}{\delta_Y}\right| = c(k_{typ}, p, \Lambda_b, \Lambda)\left(\frac{(k_{typ}, p)}{\Lambda_b}\right)^{n+1-\eta} + \cdots , \tag{3.96}$$

where δ_Y is the phase shift for the Yamaguchi model, δ_{EFT} is the phase shift calculated with the EFT. $c(k_{typ}, p, \Lambda_b, \Lambda)$ is the proportionality constant of the correction. The constant can depend on the momenta, but it can be assumed to be slowly varying compared to $(p/\Lambda)^n$, compare to [27]. The quantity η describes the corrections due to the denominator and its p-dependence. In general, this can not be predicted. The momentum $k_{typ} \sim M_{low}$ is a typical momentum of the system. This causes additional corrections to the corrections described above. These corrections follow the same pattern as the corrections proportional to p. Equation (3.96) is meant in the way that the leading contributions to the corrections are given by (p/Λ_b) if $p > k_{typ}$ and by (k_{typ}/Λ_b) if $p < k_{typ}$. In the following we assume $p \gg k_{typ}$. This will be discussed below. Therefore, taking the logarithm on both sides yields

$$\ln\left[\left|\frac{\delta_Y - \delta_{EFT}}{\delta_Y}\right|\right] \approx c' + (n+1-\eta)\,\ln\left[\frac{p}{\Lambda_b}\right] = c'' + (n+1-\eta)\,\ln[p]\ . \tag{3.97}$$

Here, c' and c'' stand for some constants in which the different momentum independent parts are absorbed. Hence, the slope in a double-logarithmic plot gives the order n of the neglected terms. To determine this slope, a linear function can be fitted to the numerical results. The fit for the LO results of the EFT can be used to determine η. Since $n \in \mathbb{N}_0$, the slope has to increase from order to order by exactly[20] one. This can be used as a criterium to evaluate the consistency of the description of the model by the EFT.

[19] This is the momentum for which the EFT is designed to work.

[20] An increase of exactly one is the theoretical prediction. Obviously, the actual increase of the fitted slopes can deviate due to numerical uncertainty. This will be discussed below.

Additionally, the internal consistency of an EFT can be investigated following the same lines. In [26] and more elaborated in [27], Griesshammer suggested a consistency assessment, that does not depend on a model or data at all. Analogous to above, an EFT claims to be exact to some order of $(p/\Lambda_b)^n$. If one compares the same EFT at the same order, but for different cut-offs, say $\Lambda_1 < \Lambda_2$, they can only differ in terms proportional to the next order $(p/\Lambda_b)^{n+1}$. Therefore, for an observable, e.g. the particle-dimer phase shift, it yields

$$\left| \frac{\delta_{EFT(\Lambda_2)} - \delta_{EFT(\Lambda_1)}}{\delta_{EFT(\Lambda_2)}} \right| = c(\Lambda_1, \Lambda_2, k_{typ}, p, \Lambda_b) \left(\frac{(k_{typ}, p, \Lambda_1, \Lambda_2)}{\Lambda_b} \right)^{n+1-\eta} + \cdots . \tag{3.98}$$

Here the slowly varying function $c(\Lambda_1, \Lambda_2, k_{typ}, p, \Lambda_b)$ can obviously depend on both cut-offs Λ_1 and Λ_2. Effectively, the more precise EFT (the EFT with the higher cut-off) takes the role of the model. The quantity η describes the LO p-dependence of $\delta_{EFT(\Lambda_2)}$, and will be determined from the fit at the LO. Note that the η for the consistency assessment does not have to be the same as for the Lepage plots. Similarly to above, the slope of the linear fit to a double-logarithmic plot gives the exponent of equation (3.98). The exponent has to increase by exactly one, order by order of the EFT.

As mentioned above, the dependence of equation (3.96) and equation (3.98) on the typical momentum k_{typ} complicates the determination of the slopes. This can be circumvented by restricting the analysis to the region defined by $k_{typ} \ll p$. An additional restriction is given by the break-down scale Λ_b of the EFT. At $p \sim \Lambda_b$ the EFT is not expected to work at all. This gives the "window of opportunity", where the slopes can be determined:

$$k_{typ} \ll p \ll \Lambda_b \sim \Lambda \, . \tag{3.99}$$

The typical momentum for the system given by equation (3.67) is $k_{typ} \sim 1/a \approx 37$ MeV. The situation becomes slightly more complex due to the value of the model $\delta_Y = 0$ MeV for $p \approx 80$ MeV. (Compare to figure 3.5.) This is part of the denominator in equation (3.96) and expresses itself via a spike in the Lepage plots. This spike makes the determination of the order n through the slopes impossible. The same problem appears in the consistency assessment, since NLO and N^2LO predict $\delta_{EFT} = 0$ MeV, correctly. To avoid this, we restrict our-self to a lower upper border of the "window of opportunity". We choose the window to be between 42 MeV and 55 MeV. The major source of uncertainty for the slopes is caused by the choice of the window. By slightly varying the borders we estimate the error of the obtained slopes by around 10%.

In figure 3.7 (above) the Lepage plots are shown for the real part of the particle-dimer phase shift $Re[\delta]$. Figure 3.7 (below) shows the consistency assessment. We show the results for LO, NLO and N^{2}LO for the EFT for a cut-off of $\Lambda = 250$ MeV. The number of subtractions i in τ_i is chosen according to the results of the next chapter. We choose τ_1 for NLO and τ_2 for N^{2}LO . The slopes are obtained in the highlighted "window of opportunity". They are given in table 3.3 (left). In the table we also give the additional results for the different choices of i. The corresponding Lepage plots and consistency assessments can be seen in figure 6.1 in the appendix. First, we note that all slopes increase order by order as expected. Second, the obtained increase agrees with the expected increase of approximately one, if the 10% error is considered. Third, the difference between the slopes for one order but different τ_i is not significant. Besides the arguments given in the next chapter, this motivates to take the most simple case, namely τ_1, for NLO. For N^{2}LO there is an additional three-body force H_2, so one more subtraction has to be be used. Note that the slope for N^{2}LO and τ_2 in the consistency assessment is unnaturally large. This is due to an accidental zero around $p \approx 30$ MeV. This is caused by a change of the sign of $\delta_{EFT(\Lambda_2)} - \delta_{EFT(\Lambda_1)}$ and

has no direct physical implication. The corresponding values for τ_1 and τ_3 are close to the expected value of 5, their plots do not exhibit accidental zeros, see figure 6.1 in the appendix.

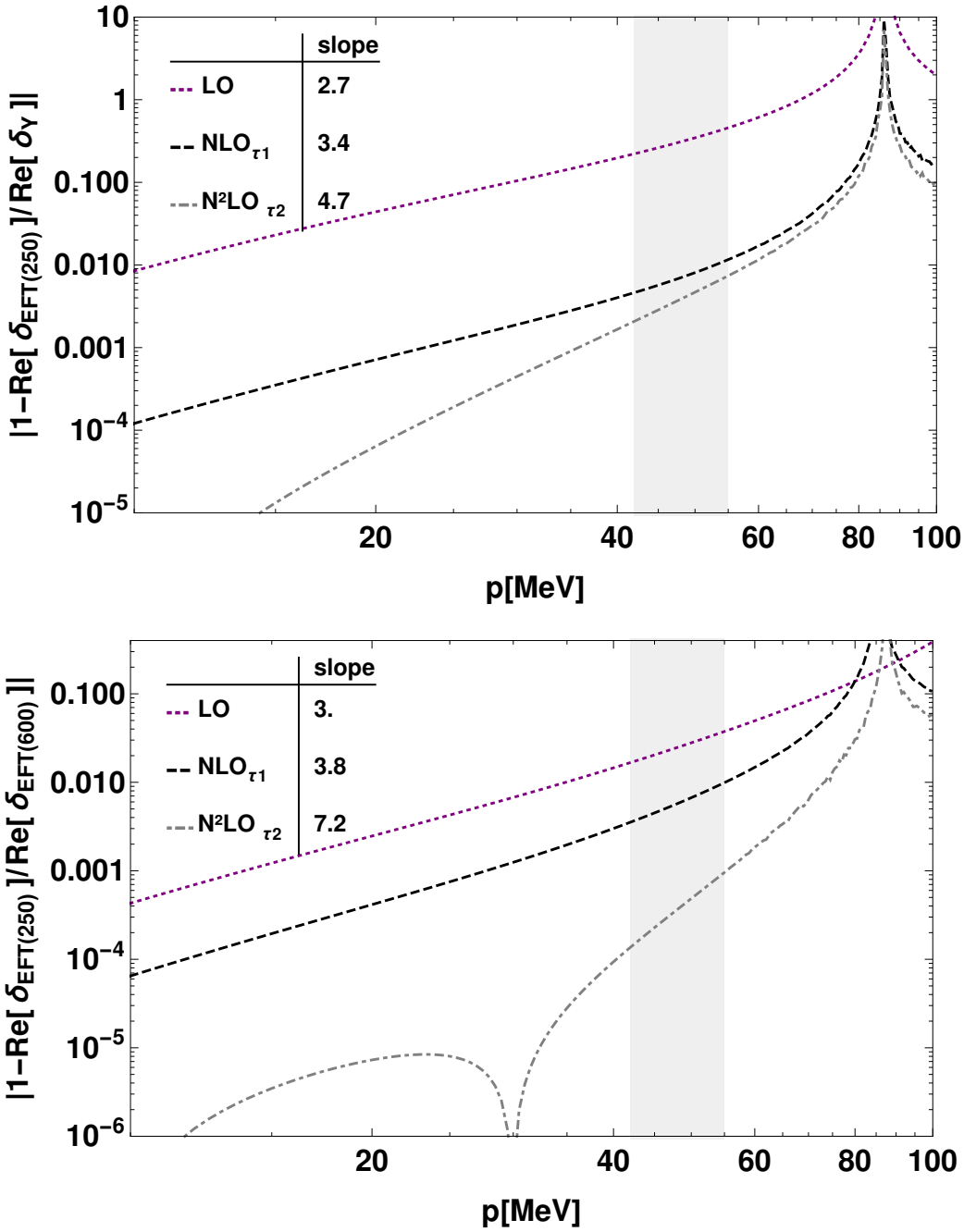

Figure 3.7: Lepage plot (above) and consistency assessment (below) for the particle-dimer phase shift in the Yamaguchi model. The “window of opportunity” is chosen to be between 42 MeV and 55 MeV for all orders (gray shaded region). The spike (zero of δ (figure 3.5)) around 80 MeV limits us to low energy regions. Note that the LO result does not predict this zero, therefore the spike is not visible in the consistency assessment at LO. For the Lepage plot the results are divided by the Yamaguchi results. Therefore, the spike can be seen at all orders. As expected, the slope is increasing by approximately one, order by order. The deviant value for N^{2}LO τ_2 is due to the accidental zero around 30 MeV (change in the sign), compare to [27].

Table 3.3: Results for the slopes for the particle-dimer phase shifts δ fitted in the "window of opportunity" for the Yamaguchi model. The uncertainty in the slopes is about 10%. Left for the Lepage plot, right for the consistency assessment. The value with the asterisk * is unnaturally large due to an accidental zero, compare to figure 3.7 (below).

slope fit	LO	NLO	N^{2}LO
no sub.	2.7		
τ_1		3.4	4.4
τ_2		3.6	4.7
τ_3		3.6	5.0

slope fit	LO	NLO	N^{2}LO
no sub.	3.0		
τ_1		3.8	5.3
τ_2		4.0	7.2*
τ_3		4.0	4.9

To further investigate the systematics of the EFT using our method, we repeat this analysis for the quantity $Re[p\cot\delta]$ (the observable considered in [27]). This follows the exact same lines as above, replace δ_x by $p\cot\delta_x$ in equation (3.98). Obviously, the values of c and more important η change, besides the p-dependence is unchanged. The consistency assessment is shown in figure 3.8, the obtained slopes are given in table 3.4. It can be seen that the general pattern is unchanged. The slope increases order by order, and the increase is approximately one. We also compare our results to the results in [27]. Although the investigated system is not exactly identical to the three bosons here, the obtained results are very close for LO and NLO. For N^{2}LO τ_1 gives a comparable slope, our result for τ_2 is unexpected large, again due to the accidental zero. However, the result for τ_3 is significant smaller, this further motivates our choice to recommend not using three subtractions at N^{2}LO.

Table 3.4: Slope fits for $k\cot\delta$ in the consistency assessment for the Yamaguchi model. The "window of opportunity" was chosen between 42 MeV and 55 MeV. The uncertainty in the slopes is about 10%. Shown are the fits to the results for $Re[p\cot\delta]$. The value with the asterisk * is unnaturally large due to an accidental zero.

slope	LO	NLO	N^{2}LO
fit in [27]	1.9	2.9	4.8
our fit, no sub.	1.8		
our fit, τ_1		2.8	4.6
our fit, τ_2		2.9	6.1*
our fit, τ_3		2.8	3.6

To summarize the results of the last sections, using an EFT, while treating the spurious pole non-perturbatively as proposed above, we have explicitly demonstrated that the numerical solution converges to the exact result, obtained in the Yamaguchi model. Additional, we have shown that this convergence follows the systematic improvement postulated by the definition of an EFT.

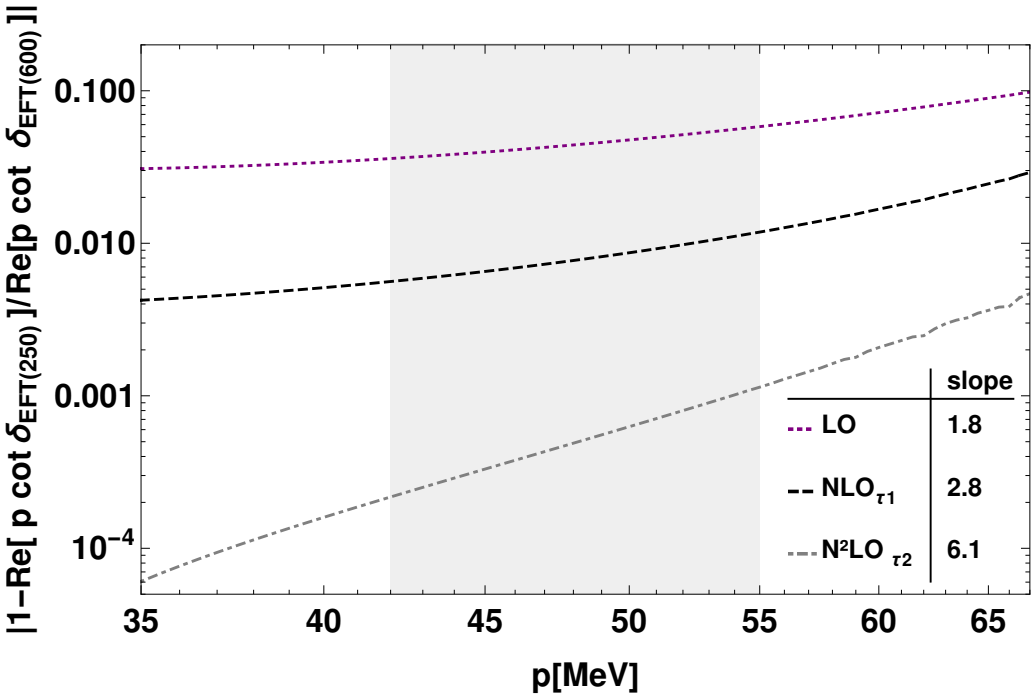

Figure 3.8: The consistency assessment for the quantity $Re[p\cot\delta]$, zoomed to the "window of opportunity" (shaded in gray), which is chosen to be between 42 MeV and 55 MeV. Note that all orders can be described in the window by linear functions very precisely. The slope shown in the inset describes the order of the EFT. The increase from LO to NLO is one as expected. The increase from NLO to N^{2}LO is larger than expected, due to the accidental zero around 30 MeV, compare to figure 3.7.

3.3.5 Order of the subtracted polynomial

In section 3.2.2 we predicted the optimal number of terms i of the modified propagator $\tau_i(k^*)$. The predictions for the EFT are $\tau_2(k^*)$ at NLO and $\tau_3(k^*)$ at N^{2}LO, compare to table 3.2.2. As already mentioned, these predictions are based on perturbative power-counting arguments, which can only give a hint for a highly non-perturbative problem. In this section we revisit the question of the preferred choice for i, but confront it with numerical results. We consider three observables: the particle-dimer phaseshift (real and imaginary part), the slopes of the Lepage and consistency assessment plots, and the three-body bound states.

(a) The particle-dimer phaseshift. The results for the real/imaginary part of the phaseshift can be seen in figure 3.9 (above/below) at NLO of the EFT. The results for the first three values of i are shown. We zoomed into the region above 50 MeV, since below this value there is no difference visible between the different i. For the real part, the results for $\tau_1(k^*)$ describe the Yamaguchi model best. $\tau_2(k^*)$ gives slightly worse results, and it gets worse for $\tau_3(k^*)$. This is especially true for the

position of the predicted zero[21]. For the imaginary part a tiny improvement from $\tau_1(k^*)$ to $\tau_2(k^*)$ is visible. However, this only holds for very large values of the momentum p and the improvement is well below the expected EFT accuracy. The results for $\tau_1(k^*)$ agree with the model everywhere within the EFT uncertainty, except for the largest considered values of momentum. There is no further improvement from $\tau_2(k^*)$ to $\tau_3(k^*)$. This indicates that at NLO the propagator $\tau_1(k^*)$ is the best choice.
For N^{2}LO (compare to figure 3.10) the real part of the phaseshift is again described best by $\tau_1(k^*)$. However the difference between $\tau_1(k^*)$ and $\tau_2(k^*)$ is smaller than the error bands. On the other hand, the imaginary part is described best by $\tau_2(k^*)$ and the improvement is significant. There is no improvement form $\tau_2(k^*)$ to $\tau_3(k^*)$, neither in the real nor in the imaginary part. We conclude, $\tau_2(k^*)$ is the optimal choice at N^{2}LO.

(b) The slopes of the Lepage plots and the consistency assessment. In table 3.3 the results are given for the different orders of the EFT and the different values of i. All obtained slopes[22] of the same order of the EFT agree within the estimated error of 10%. No improvement between the different choices of i can be noted at all. Therefore it is reasonable to choose the smallest value for i available at NLO, this means $\tau_1(k^*)$. If one considers only the slopes, there is no specific reason not to choose $\tau_1(k^*)$ also at N^{2}LO. However, this also is not an argument against $\tau_2(k^*)$.

(c) The three-body bound states. The bound states, and how they can be calculated, will be discussed in the next section. At this point we state that the Yamaguchi model exhibits two bound states, one shallow bound state at $E_B^{shallow} = -2.356$ MeV and a deep bound state at $E_B^{deep} = -24.797$ MeV. In table 3.3.5 the predictions of the EFT for the different orders and $\tau_i(k^*)$ can be seen. The shallow state can be described by all orders and all choices of i with high accuracy, there is no significant difference between the choices of i. In case of the deep bound state there are differences. For NLO the state is described the best by $\tau_1(k^*)$. $\tau_2(k^*)$ gives a worse result and $\tau_3(k^*)$ is even worse. For N^{2}LO the best prediction is given by $\tau_2(k^*)$, while the difference between $\tau_1(k^*)$ and $\tau_2(k^*)$ is very small. $\tau_3(k^*)$ is, again, the worst.

To conclude these observations, for the EFT at NLO the best choice is $\tau_1(k^*)$. All three benchmarks agree on this. At N^{2}LO (a) and (c) indicate that one is advised to choose $\tau_2(k^*)$, while (b) gives no clear statement, but also does not disagree with $\tau_2(k^*)$. Therefore we advice to choose $\tau_2(k^*)$. While this disagrees with the predictions based on perturbative arguments given before, we highlight that the general pattern of higher i at higher EFT orders holds. Increasing the order of the EFT, therefore including an additional three-body force, allows us to absorb an additional term in the expansion in $\tau_i(k^*)$. The optimal choice for i increases with the number of three-body forces. In table 3.3.5 we summarize the results of this section. Finally note, these observations also hold for the different choices of the effective range and the Gauss model as will be discussed below.

[21] Note that the shown error bands at a predicted value of zero are not meaning full. This is due to the fact that the error is estimated as a relative error of $(p/\Lambda)^2$. While this is appropriate else, for a value of zero this creates an absolute error of zero.

[22] Except the diverging value for N^{2}LO and $\tau_2(k^*)$, due to the accidental zero. Compare to the discussion under figure 3.8

Table 3.5: The optimal choice for the propagator at different orders of the EFT based on numerical calculations.

Order	2-body parameters	3-body parameters	Obtained optimal propagator
LO	a	H_0	-
NLO	$a,\ r$	H_0	$\tau_1(k^*)$
N^{2}LO	$a,\ r$	$H_0,\ H_2$	$\tau_2(k^*)$

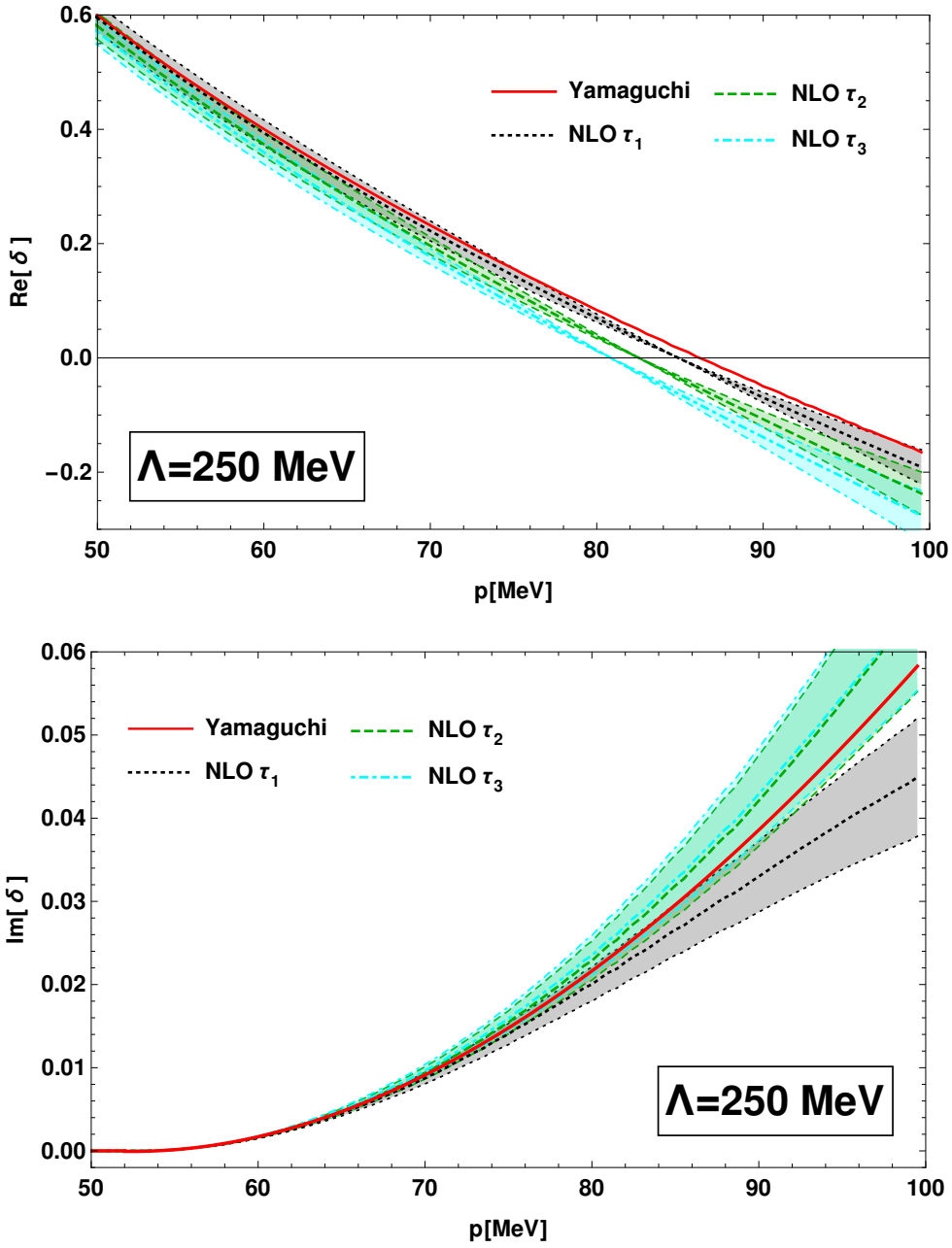

Figure 3.9: Real (above) and imaginary (below) part of the particle-dimer phase shift δ calculated for the Yamaguchi model and the EFT at NLO for different choices of the number of subtractions in the propagator $\tau_i(k^*)$. The uncertainty bands are estimated using a naive power-counting of the EFT error, given by $Re[\delta]\ (p/\Lambda)^2$ and $Im[\delta]\ (p/\Lambda)^2$.

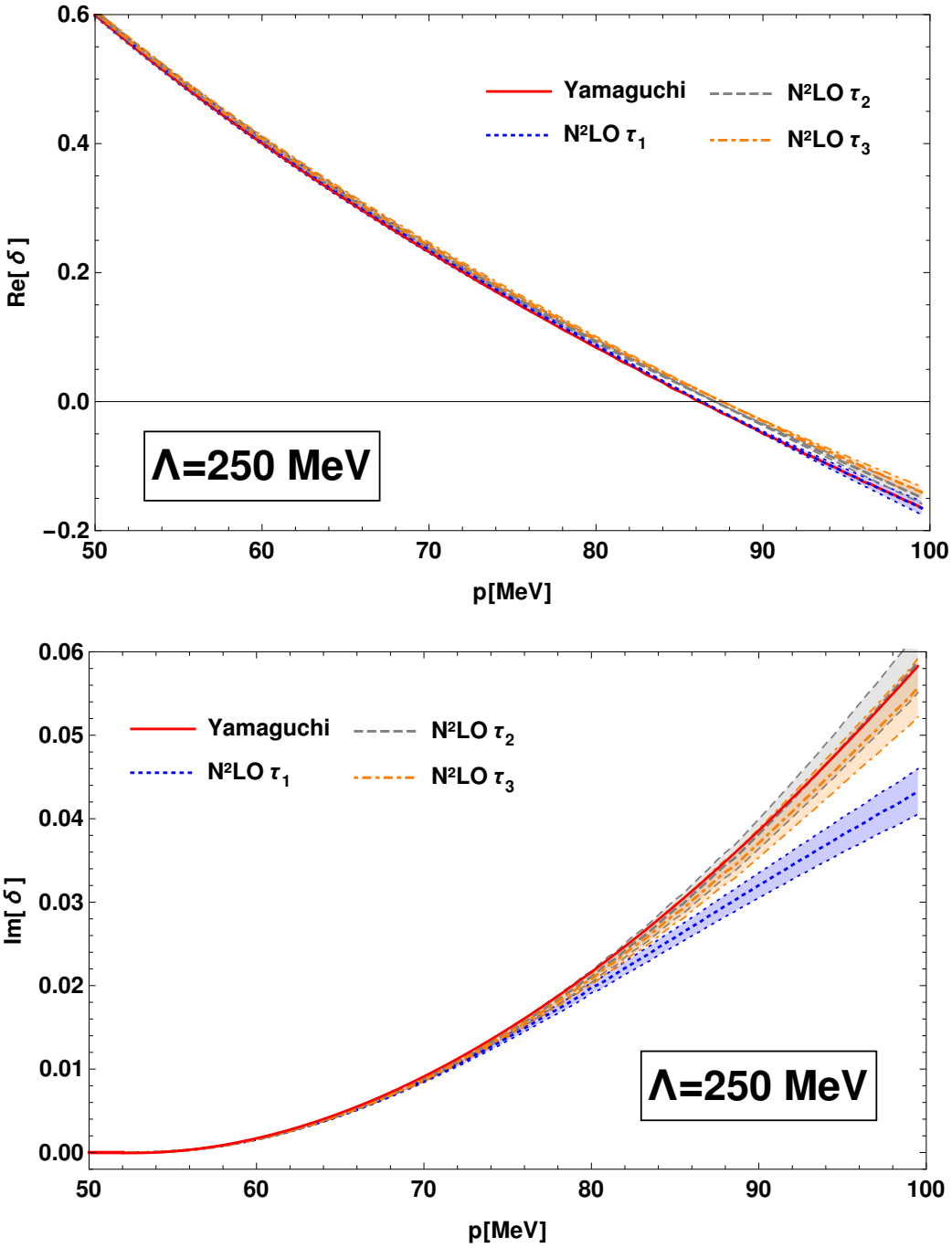

Figure 3.10: Real (above) and imaginary (below) part of the particle-dimer phase shift δ calculated for the Yamaguchi model and the EFT at N^{2}LO for different choices of the number of subtractions in the propagator $\tau_i(k^*)$. The uncertainty bands are estimated by a naive power-counting of the EFT error, given by $Re[\delta]\ (p/\Lambda)^3$ and $Im[\delta]\ (p/\Lambda)^3$.

Bound states

As an additional test of the non-perturbative method, we search for three-body bound states in the EFT and compare them to the bound states of the Yamaguchi model. As described before, at the energy of a bound state E_B the scattering amplitude becomes singular. Since the inhomogeneous part of the Faddeev equation (3.26) will not become singular, therefore it is sufficient to consider only the homogenus part of it

$$M(p,q,E) = \frac{4}{\pi}\int_0^\Lambda dk\, k^2 Z(p,k,E)\tau_i(k^*)M(k,q,E). \tag{3.100}$$

Furthermore, at the position of the bound state E_B the momentum dependence decouples and the scattering amplitude can be parameterized as

$$M(k,q,E) = \frac{g(k)g(q)}{E-E_B}, \tag{3.101}$$

with some momentum dependence function $g(q)$. Employing this expression, the homogenus Faddeev equation can be written as

$$g(p) = \frac{4}{\pi}\int_0^\Lambda dk\, k^2 Z(p,k,E)\tau_i(k^*)g(k). \tag{3.102}$$

This can be solved by discretization of p and k along the same lines as in equation (3.86) and (3.92). Doing so results in a matix equation

$$\vec{g} = K(E)\vec{g}, \tag{3.103}$$

with a quadratic $n\times n$ kernel matrix $K(E)$, where n is the number of discretization steps. The components are

$$K_{ij}(E) = \frac{4\omega_j}{\pi}k_j^2 Z(k_i,k_j,E)\tau_i\left(\sqrt{\frac{3}{4}k_j^2 - mE}\right). \tag{3.104}$$

Equation (3.103) has a solution exactly if

$$\det\left(I_n - K(E)\right) = 0, \tag{3.105}$$

with the $n\times n$ identity matrix I_n. In figure 3.11 such a determinant is shown exemplary as a function of the energy E for $\tau_1(k^*)$ at NLO. We choose $n = 250$ steps for the discretization and $\Lambda = 250$ MeV. The number of roots gives the number of bound states and their positions the energies E_B of the states. Note that this is only true for energies below the two-body threshold. Above this a continuum of scattering states is expected. Due to the discretization this continuum collapses to an infinite amount of roots. For the Yamaguchi model instead of equation (3.100) the homogenus version of equation (3.68) is used, which results in a kernel matrix $K_Y(E)$ with components

$$K_{Y,ij}(E) = \frac{4\omega_j}{\pi}k_j^2 Z_Y(k_i,k_j,E)\tau_Y\left(k_j,E\right). \tag{3.106}$$

For the propagator $\tau_Y(q,E)$ see equation (3.69) and for the potential $Z(p,k,E)$ see equation (3.70). In the case of the Yamaguchi model we find two bound states: one shallow bound state at $E_B^{shallow} =$

-2.356 MeV and an additional deep bound state at $E_B^{deep} = -24.797$ MeV. The name $shallow$ refers to the relatively small difference between the three-body bound state and the binding energy of the dimer $E_D = k_1^2/M \approx 2.2$ MeV. In table 3.3.5 the results for these two bound states are compared to the corresponding predictions of the EFT in our different expansions. It can be seen that the $shallow$ bound state can be predicted very accurately at all orders. An improvement from LO to NLO is visible. However, the values do barely change from NLO to N^{2}LO. This fulfills the expectations, the corrections of the EFT due to a naive power counting are of the order of $|E_B|(\sqrt{M|E_B|}/\Lambda)^1 \approx 0.4$ MeV at LO, $|E_B|(\sqrt{M|E_B|}/\Lambda)^2 \approx 0.09$ MeV at NLO and $|E_B|(\sqrt{M|E_B|}/\Lambda)^2 \approx 0.01$ MeV for N^{2}LO. Within these error bars all results agree perfectly with the model. For the $deep$ bound state this is technically also the case. However, the error bars are very large, since in the model $\sqrt{M|E_B^{deep}|}/\Lambda \approx 61\%$. The predictions are not very repayable for states with such high binding momenta. However, they all qualitatively agree with the model. Note that this is not the case at LO, there $|E_B|(\sqrt{M|E_B|}/\Lambda)^1 \approx 147$ MeV $> |E_B|$. So the error bar is larger than the result. We have repeated the LO calculation for a higher cutoff $\Lambda = 600$ MeV and obtain $E_B^{deep} = -34.10$ MeV, which is of the correct order.
Finally we note that the results for the $shallow$ bound state do not change much with the number of subtractions i in the propagator $\tau_i(k^*)$.In contrast to that, for the $deep$ bound state the results depend on i more heavily. The results that lie the closest to the model are the EFT that uses $\tau_1(k^*)$ at NLO and the EFT that uses $\tau_2(k^*)$ at N^{2}LO. This strengthens the conclusions for the optimal subtraction given in section 3.3.5 further.

Table 3.6: Three-body bound states calculated for the Yamaguchi model and the EFT at different orders and different numbers of subtractions. All in units of MeV and for the ultraviolet cutoff $\Lambda = 250$ MeV. The calculations are done with $n = 250$ steps. For the $deep$ bound state at LO (highlighted by $*$) the error bar is larger than the result and thereby the value can not be trusted.

bound state	Yamaguchi	LO	NLO τ_1	NLO τ_2	NLO τ_3	N^{2}LO τ_1	N^{2}LO τ_2	N^{2}LO τ_3
$E_B^{shallow}$	-2.36	-2.29	-2.39	-2.39	-2.39	-2.39	-2.39	-2.34
E_B^{deep}	-24.80	-113.03*	-23.96	-29.11	-40.22	-21.88	-22.07	-18.62

We close the section about bound states with a comment on the Efimov effect. As described in [**?**], an EFT contains an infinite number of bound states in the unitary limit $1/a \to 0$. In this limit these obey a discrete scaling $E_B^n/E_B^{n+1} = \#$ for all states n. By increasing the cutoff Λ more and more of those bound states can be found. For a finite scattering length the discrete scaling is not true anymore, while by increasing the cutoff additional states should become visible. In table 3.3.5 this can be seen, for increasing cutoffs we found additional bound states. Note that here only a qualitative argument can be made, since those additional states lie below the energy regions the EFT can access due to the limitation by the break-down scale Λ_b.

Table 3.7: Number of three-body bound states found by using the EFT at N^{2}LO and $\tau_2(k^*)$ for different cutoffs Λ.

cutoff Λ/MeV	250	600	850	1000	1700
number of bound states	2	3	4	4	5

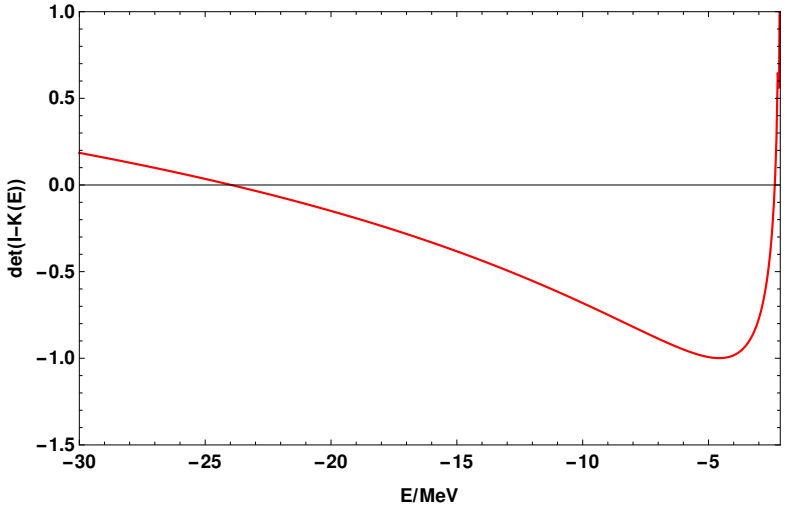

Figure 3.11: Determinant of the identity matrix minus the kernel. The roots of the determinant give the energy of the bound states E_B. The result for NLO and $\tau_1(k^*)$ is shown as an example.

3.3.6 Different choice of the effective range

To further test the non-perturbative method, we investigate a slightly different model than before. In this section we use the same Yamaguchi model as introduced before but with a different set of parameters λ and β. We aim to see if the conclusions taken before also hold for this variation. Also remember that for the parameters used before we found a zero for the particle-dimer phaseshift $\delta_Y = 0$ at approximately 80 MeV. This resulted in a spike in the Lepage plots and in the consistency assessment. Therefore we were limited to a rather small upper border of the 'window of opportunity' (compare to the discussion below equation (3.99).) The position of the zero is mostly determined by the effective range. In this section we choose for the EFT $r' = 0.8768$ fm and $a = 5.4164$ fm, so the same scattering length a and the half of the effective range used before. According to equation (3.66) this results in the following Yamaguchi parameters.

$$\lambda = -0.000049 \text{ MeV}^{-2}, \qquad \beta = 622.5 \text{ MeV}. \tag{3.107}$$

Note that the corresponding set of a and r also implies a spurious pole, compare to equation (3.15). The spurious pole is positioned at $k_2 = 410.1$ MeV, while the physical pole is at $k_1 = 40.0$ MeV. The values of the three-body forces are obtained as described in the second part of section 3.3.2. The results for the different orders of the EFT and different numbers of subtractions in the modified propagator $\tau_i(k^*)$ are given in table 3.8. The results for the quantity $p \cot \delta$, with the particle-dimer phaseshift δ, can be seen in figure 3.12. They are calculated using a cutoff of $\Lambda = 250$ MeV. The results for same quantity $p \cot \delta$ but a cutoff $\Lambda = 600$ MeV can be seen in figure 6.2 in the appendix. It can be seen that all observations for the previous choice of r also hold here. The description of the model at LO is only accurate for small momenta, while at NLO this improves for higher momenta and it further improves at N^{2}LO. To investigate the improvement order by order the Lepage plots and the consistency assessment are done (according to section 3.3.4). In the upper part of figure 3.13 the Lepage plot is shown, while the lower panel contains the consistency assessment. Since a peak is not present, the "window of opportunity" can be chosen to be larger than before. We choose a range from $p = 75$ MeV to $p = 125$ MeV. The plotted quantity is

Table 3.8: The three-body couplings H_0 and H_2 for the effective range $r' = 0.8768$ fm. Shown are the results for the different values of the cutoff Λ, and different numbers of subtractions in the propagator $\tau(k)$ (no subtraction is needed at LO). All quantities are given in MeV units. The values of H_0 are the same at NLO and N^{2}LO, whereas $H_2 = 0$ at NLO.

	τ_i	$H_0(\Lambda = 250)$	$H_2(\Lambda = 250)$	$H_0(\Lambda = 600)$	$H_2(\Lambda = 600)$
LO		-7.16		0.73	
NLO & N^{2}LO	τ_1	1.90	5.56	-0.57	-0.21
	τ_2	1.52	5.01	-0.78	0.38
	τ_3	1.45	4.96	-0.86	0.76

Table 3.9: Results for the slopes of the quantity $p \cot \delta$ fitted in the "window of opportunity" for the Yamaguchi model with $r' = 0.8768$. Left for the Lepage plot, right for the consistency assessment.

slope fit	LO	NLO	N^{2}LO
no sub.	0.8		
τ_1		3.2	4.6
τ_2		3.0	4.4
τ_2		3.1	4.4

slope fit	LO	NLO	N^{2}LO
no sub.	2.2		
τ_1		3.0	4.4
τ_2		3.1	4.3
τ_2		3.1	4.3

linear in this whole region for all orders of the EFT and all numbers i of subtractions in the propagator $\tau_i(k^*)$. In the inlays of the two plots the fitted slopes are shown for the optimal choice of i according to the discussion in section 3.3.5. The slopes for all $i < 4$ are given in table 3.9. Again all important previous observations hold. The value of the slopes increase order by order of the EFT. The increase from NLO to N^{2}LO in the Lepage plot is close to one. In the consistency assessment the increase from LO to NLO and the increase from NLO to N^{2}LO are both close to one. The step from LO to NLO in the Lepage plot is slightly larger than expected. Finally we note that there is no significant difference in the slopes at a given order of the EFT for the different number of subtractions i. This strengthens the assumption that in the case of the previous choice of r the deviating value for the slope in the consistency assessment for N^{2}LO and $\tau_2(k^*)$ was caused by a accidental zero and therefore has no physical implication (compare to table 3.3).

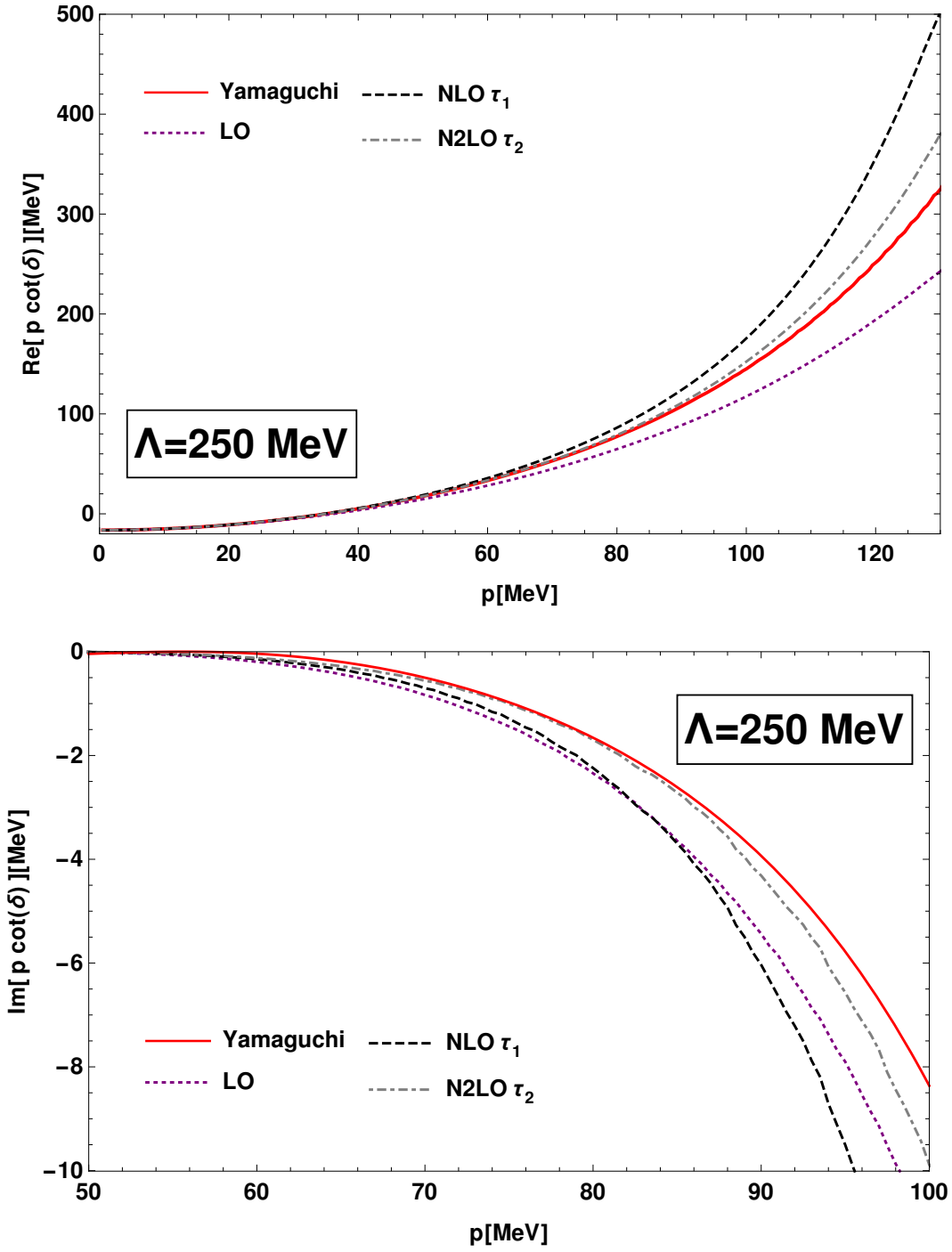

Figure 3.12: Numerical results for real (above) and imaginary (below) part of the quantity $p \cot \delta$ with the particle-dimer phase shift δ for the Yamaguchi model and the corresponding EFT with the effective range $r' = 0.8768$ fm. Red line: the result obtained in the Yamaguchi model; in purple dotted: the LO result; in black dashed: the NLO result for τ_1; in gray dot-dashed: the N^{2}LO result for τ_2.

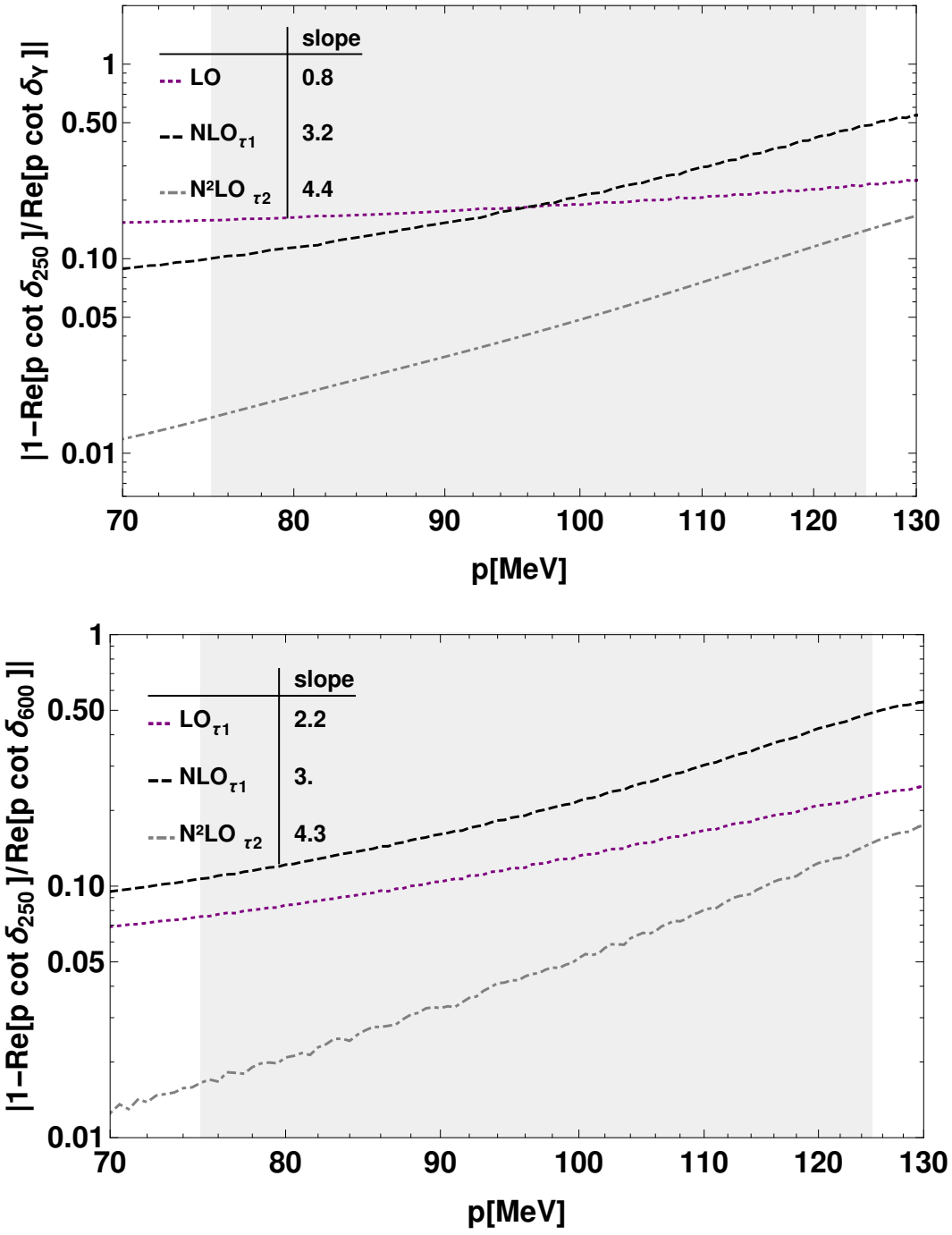

Figure 3.13: The Lepage plot (above) and the consistency assessment (below) for of the quantity $p \cot \delta$, with the particle-dimer phase shift δ in the Yamaguchi model with the effective range $r' = 0.8768$ fm. In purple dotted: the LO result; in black dashed: the NLO result for τ_1; in gray dot-dashed: the N^{2}LO result for τ_2. The cutoff was set to the value $\Lambda = 250$ MeV in the Lepage plot and to $\Lambda_1 = 250$ MeV and $\Lambda_2 = 600$ MeV in the consistency assessment. The inlays show the slopes for the ideal choice of the propagator $\tau_i(k^*)$ according to section 3.3.5. The increase of the slopes order by order fits the expected increase, which is one, very accurate. In contrast to this, the increase in the Lepage plot from LO to NLO is twice as large as expected.

3.3.7 Gauss model

We close the chapter and the analysis of the non-perturbative method in infinite volume by showing that the method can not only be used for the Yamaguchi model. For this purpose we investigate a model with a different interaction. In this section we choose a model interacting via a separable Gauss potential. The separable potential is treated along the lines of [79]. For this separable potential equation (3.62) holds with the exception that the regulator is given by a Gaussian function.

$$V_G(p,q) = \lambda \chi_G(p)\chi_G(q), \quad \chi_G(p) = e^{-p^2/\lambda_G^2}. \tag{3.108}$$

Using this potential the calculation of the two-body scattering amplitude yields

$$t_G(p,q,z) = \chi_G(p) d_G(z) \chi_G(q), \tag{3.109}$$

where $d_G(z)$ can be calculated using equation (3.64), for $E < 0$ this results in

$$\begin{aligned} d_G(E)^{-1} &= 2\pi^2 \left[\sqrt{mE_d} \exp\left(\frac{2mE_d}{\lambda_G^2}\right) \operatorname{erfc}\left(\frac{\sqrt{2mE_d}}{\lambda_G}\right) - \sqrt{-E} \exp\left(\frac{-2E}{\lambda_G^2}\right) \operatorname{erfc}\left(\frac{\sqrt{-2E}}{\lambda_G}\right) \right] \\ &= 2\pi^2 \sqrt{mE_d} \exp\left(\frac{2mE_d}{\lambda_G^2}\right) \operatorname{erfc}\left(\frac{\sqrt{2mE_d}}{\lambda_G}\right) + 2\pi^2 ip - \frac{4\sqrt{2}\pi^{3/2}}{\lambda_G} p^2 + O\left(p^3\right), \end{aligned} \tag{3.110}$$

which can be found in [82]. erfc means the error-function. Note that we have exchanged the parameter λ in the separable potential by the parameter E_d. Similar to the Yamaguchi model the terms of equation (3.110) can be compared to an ERE order by order. This results in conditions that connect the Gaussian parameters λ_G and E_d to the scattering length a and the effective range r.

$$\frac{1}{a} = \sqrt{mE_d} \exp\left(\frac{2mE_d}{\lambda_G^2}\right) \operatorname{erfc}\left(\frac{\sqrt{2mE_d}}{\lambda_G}\right), \quad \frac{r}{2} = \frac{4\sqrt{2}\pi^{3/2}}{\lambda_G 2\pi^2}. \tag{3.111}$$

We use the same scattering length $a = 5.4194$ fm and effective range $r = 1.7536$ fm as in section 3.3.1. For the Gauss model this results in $\lambda_G = 359.134$ MeV. The parameter E_d is equivalent to the position of the root of $d_G^{-1}(E)$ and therefore is the value of a two-body bound state (the dimer). For the values above this is given by $E_d \approx 2.22$ MeV, and corresponds to the deuteron (if fermions would be considered). The dimer-propagator $\tau_G(q,E)$ is given by

$$\tau_G(q,E) = d_G(z)\big|_{z=3q^2/(4m)-E-i\epsilon}. \tag{3.112}$$

The potential $Z_G(p,q,E)$ is discussed in the next subsection. In the numerical calculations we use the non-expanded equation for $d_G(z)$ (first line of equation (3.110)).
To test our non-perturbative method the EFT is used to describe this model. The three-body forces are fine-tuned to reproduce the Gauss results at $p = 0.001$ MeV for H_0 and at $p = 10$ MeV for H_2. The prescription is described in section 3.3.2. The resulting values for the different orders of the EFT and the different choices of the propagator $\tau_i(k^*)$ can be seen in Table 3.10.

Numerical treatment of the one particle exchange in the Gauss model

We investigate only a one particle exchange and no further three-body interactions. According to [79] the potential $Z_G(p,q,E)$ in S-wave is given by (compare to equation (3.70) for the Yamaguchi potential)

Table 3.10: The three-body couplings H_0 and H_2 for the Gauss model and different values of the cutoff Λ. All quantities are given in MeV units. The values of H_0 are the same at NLO and N^{2}LO, whereas $H_2 = 0$ at NLO.

	τ_i	$H_0(\Lambda = 250)$	$H_2(\Lambda = 250)$	$H_0(\Lambda = 600)$	$H_2(\Lambda = 600)$
LO		2.18		0.15	
NLO & N^{2}LO	τ_1	-0.45	1.00	0.29	18.94
	τ_2	-0.62	1.04	-0.57	3.62
	τ_3	-0.69	1.13	1.08	284.1

$$Z_G(p,q,E) = \frac{1}{2}\int_{-1}^{1} d\cos\theta_{p,q} \frac{\exp\left[-\left(\mathbf{p}/2+\mathbf{q}\right)^2/\beta^2\right]\exp\left[-\left(\mathbf{q}/2+\mathbf{p}\right)^2/\beta^2\right]}{E-\mathbf{p}^2/(2m)-\mathbf{q}^2/(2m)-(\mathbf{p}+\mathbf{q})^2/(2m)}. \tag{3.113}$$

This has a pole for

$$\left(\mathbf{q}+\frac{\mathbf{p}}{2}\right)^2 = \frac{3}{4}\mathbf{p}^2 - mE\,, \quad \text{or} \quad \left(\frac{\mathbf{q}}{2}+\mathbf{p}\right)^2 = \frac{3}{4}\mathbf{q}^2 - mE. \tag{3.114}$$

If unmodified, this pole can create difficulties if the angular integral is evaluated numerically. To circumvent this, we subtract and add the contribution at the pole position, which enables a specific treatment of this term.

$$\begin{aligned} Z_G(p,q,E) = {} & \frac{m}{2}\int_{-1}^{1} du \frac{1}{mE-p^2-q^2-pq\,u}\exp\left[-\frac{q^2+p^2/4+pq\,u}{\beta^2}\right]\exp\left[-\frac{q^2/4+p^2+pq\,u}{\beta^2}\right] \\ & - \frac{m}{2}\int_{-1}^{1} du \frac{1}{mE-p^2-q^2-pq\,u}\exp\left[-\frac{3p^2/4-mE}{\beta^2}\right]\exp\left[-\frac{3q^2/4-mE}{\beta^2}\right] \\ & + \frac{m}{2}\int_{-1}^{1} du \frac{1}{mE-p^2-q^2-pq\,u}\exp\left[-\frac{3p^2/4-mE}{\beta^2}\right]\exp\left[-\frac{3q^2/4-mE}{\beta^2}\right]. \end{aligned} \tag{3.115}$$

The original kernel together with the subtracted term is regular at the pole position, the nominator approaches zero faster than the denominator. The added term has no angular dependency and the integral can be calculated analytically.

$$\begin{aligned} Z_G(p,q,E) = {} & \frac{m}{2}\int_{-1}^{1} du \frac{1}{mE-p^2-q^2-pq\,u}\left(\exp\left[-\frac{q^2+p^2/4+pq\,u}{\beta^2}\right]\exp\left[-\frac{q^2/4+p^2+pq\,u}{\beta^2}\right]\right. \\ & \left. - \exp\left[-\frac{3p^2/4-mE}{\beta^2}\right]\exp\left[-\frac{3q^2/4-mE}{\beta^2}\right]\right) \\ & - \frac{m}{2}\frac{1}{pq}\exp\left[-\frac{3p^2/4-mE}{\beta^2}\right]\exp\left[-\frac{3q^2/4-mE}{\beta^2}\right]\ln\left[\frac{mE-p^2-q^2-pq}{mE-p^2-q^2+pq}\right]. \end{aligned} \tag{3.116}$$

The remaining integral can be calculated by the standard Gaussian method, similar to section 3.3.2.

In this section we analyse the numerical results for the Gauss potential as introduced in the last section. The results for the quantity $p \cot \delta$, with the particle-dimer phase shift δ can be seen in figure 3.14, above for the real part and below for the imaginary part. Since the parameters of the Gauss potential are chosen to produce the same scattering length and effective range as the Yamaguchi potential in section 3.3.1, the results for the models look similar. The LO EFT result for the real part can describe the model accurately only for small relative momenta p, at NLO using our non-perturbative method with the propagator $\tau_1(k^*)$ the description is improved significantly. Using N^{2}LO and $\tau_2(k^*)$ improves the situation further. For the imaginary part this is also true, but the improvement from NLO to N^{2}LO is only very small. Besides this, all results are in perfect agreement with our expectations.

In figure 3.15 (above) the Lepage plot is shown. We zoomed into the "window of opportunity", the window is chosen to reach from 42 MeV to 55 MeV. It can be seen that the results, indeed, can be described very accurately by linear functions. The resulting slopes are given in table 3.11 (left). The slope increases from LO to NLO by one for $\tau_1(k^*)$, as expected. For $\tau_2(k^*)$ and $\tau_3(k^*)$ the increase is slightly larger, even in the context of the estimated error of 10%. This indicates that $\tau_1(k^*)$ is the correct choice as discussed in section 3.3.5. The increase from NLO to N^{2}LO is larger than expected, it is around three instead of one. This can be explained by an accidental zero around 30 MeV (see figure 6.3 in the appendix for the whole momentum region). The zero appears for all choices of $\tau_i(k^*)$, therefore this results can not be trusted.
The consistency assessment is given in figure 3.15 (below), while the corresponding slopes are shown in table 3.11 (right). Within the window the results can be described by linear functions, the slopes for LO and NLO are in perfect agreement with the expectations. The increase from NLO to N^{2}LO also satisfies the expectations for $\tau_1(k^*)$ and $\tau_3(k^*)$. For $\tau_2(k^*)$ the increase is larger than the expected increase of one. The result seems to be better than expected. This might indicate a very small value of the shape parameter, meaning that there is only a small difference between N^{2}LO and N^{3}LO.
Besides this last comment, all results agree with the expectations. Therefore the EFT using our non-perturbative method, passes the Lepage and the consistency test also for the Gauss model.

Table 3.11: Results of the slopes for the real part of the quantity $k \cot \delta$ for the Gauss model fitted in the "window of opportunity". Left for the Lepage plot, right for the consistency assessment. All results for the Lepage plot for N^{2}LO, marked by an asterisk, exhibit a accidental zero and are therefore unexpected large.

slope fit	LO	NLO	N^{2}LO
no sub.	1.1		
τ_1		2.0	5.6*
τ_2		2.3	5.5*
τ_3		2.5	5.3*

slope fit	LO	NLO	N^{2}LO
no sub.	2.0		
τ_1		3.1	4.4
τ_2		3.3	5.3
τ_3		3.2	3.8

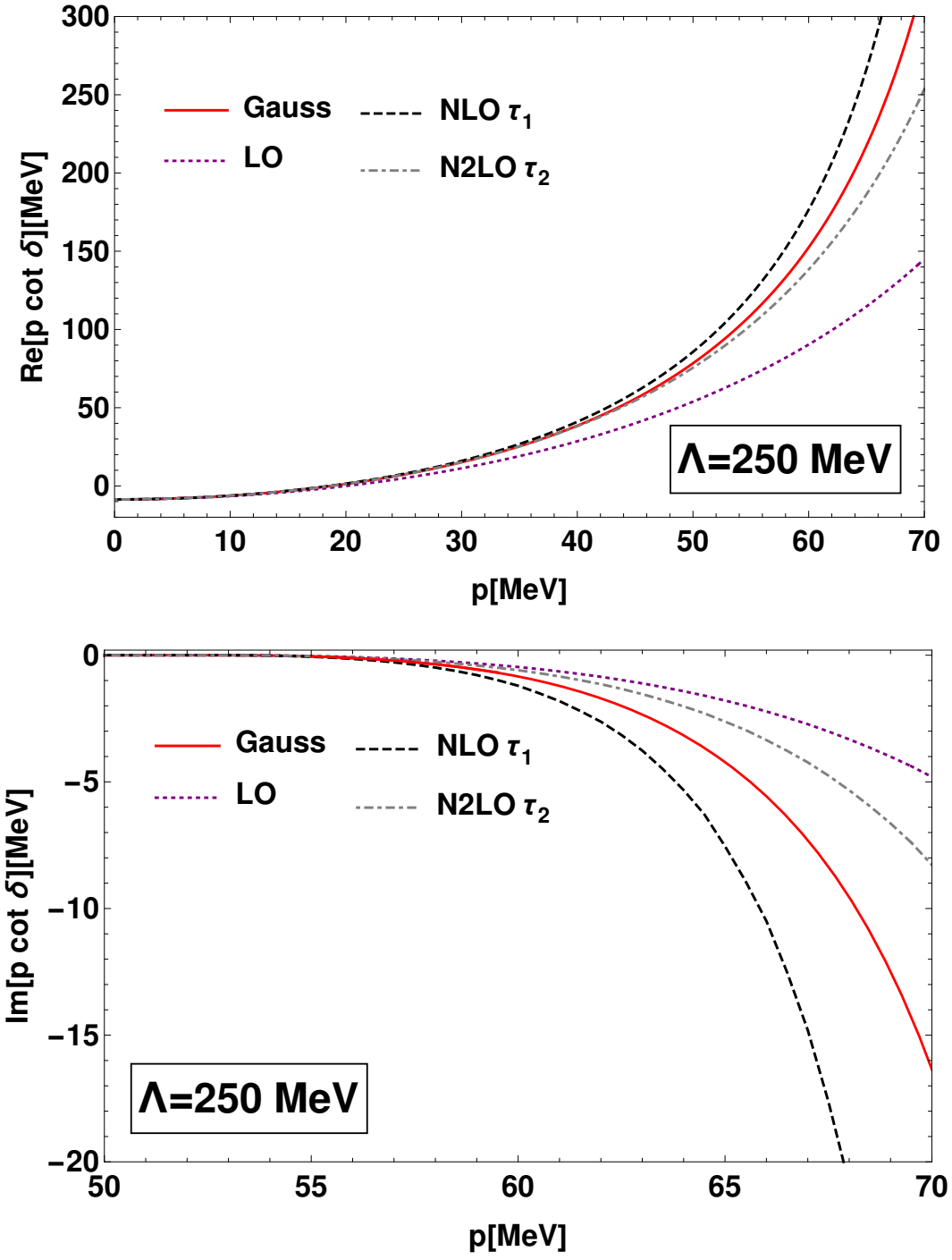

Figure 3.14: Numerical results for real (above) and imaginary (below) part of the quantity $p \cot \delta$ with the particle-dimer phase shift δ for the Gauss model. The scattering length is $a = 5.42$ fm and the effective range $r = 1.75$ fm (the same values as for the Yamaguchi model in figure 3.5). Red line: the result obtained in the Gauss model; in purple dotted: the LO result; in black dashed: the NLO result for τ_1; in gray dot-dashed: the N^{2}LO result for τ_2. The description of the model by the EFT increases order by order.

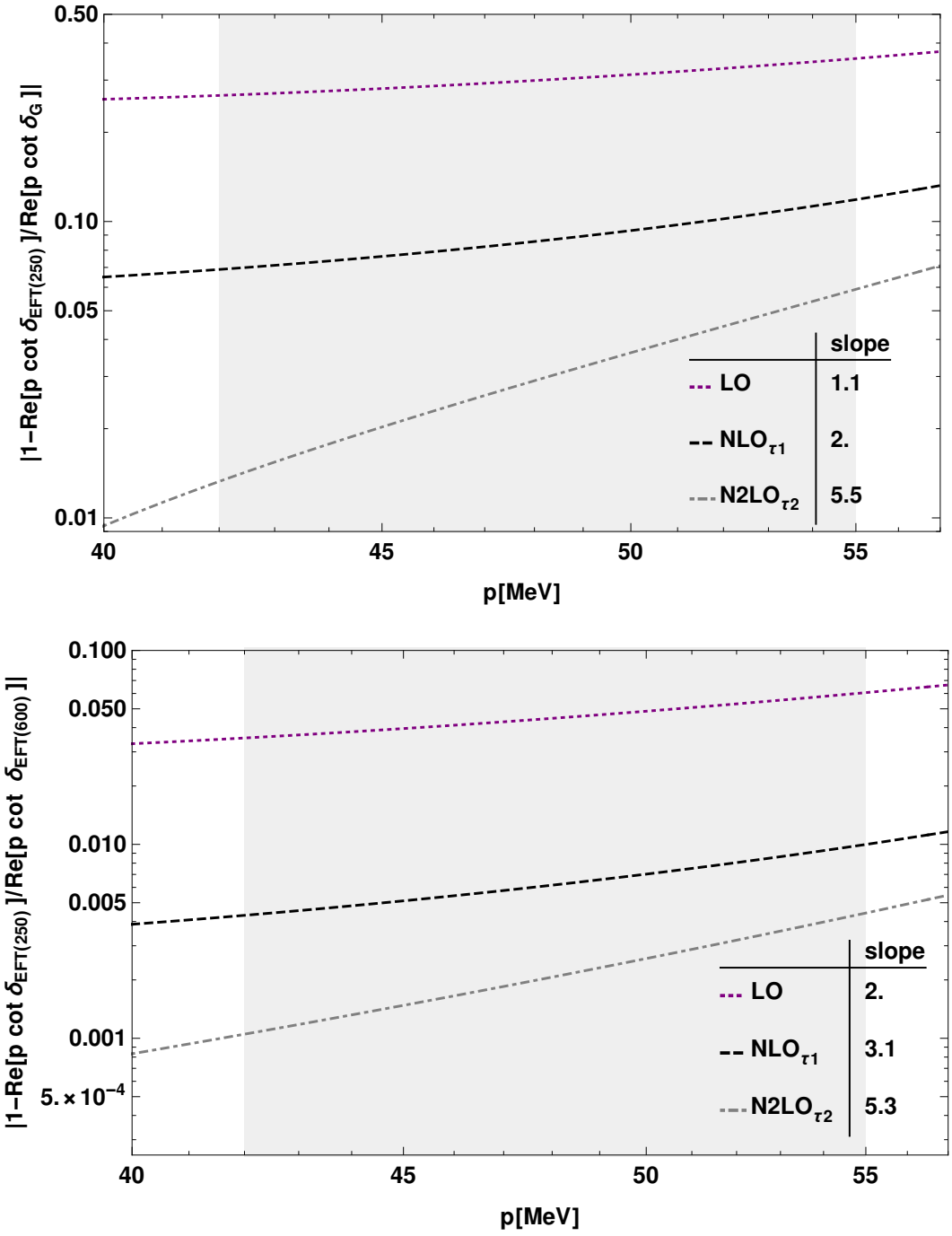

Figure 3.15: The Lepage plot (above) and the consistency assessment (below) for of the quantity $p \cot \delta$, with the particle-dimer phase shift δ in the Gauss model. In purple dotted: the LO result; in black dashed: the NLO result for τ_1; in gray dot-dashed: the N^{2}LO result for τ_2. The cutoff was set to the value $\Lambda = 250$ MeV in the Lepage plot and to $\Lambda_1 = 250$ MeV and $\Lambda_2 = 600$ MeV in the assessment. The inlays show the slopes of the ideal choice of the propagator $\tau_i(k^*)$ according to section 3.3.5. The "window of opportunity" is chosen between 42 MeV and 55 MeV. As expected, the slopes increase from LO to NLO by approximately one, for the Lepage plot as well as for the consistency assessment. The increase from NLO to N^{2}LO is slightly larger than expected, this can be explained by accidental zeros around $p \approx 30$ MeV, compare to figure 6.3 in the appendix.

3.4 Conclusion for the infinite-volume case

In this section we make conclusions based on the results of our investigations in infinite volume. Effective range corrections can be included in the three-body system in the particle-dimer picture by using the ERE for the two-body phase shift (equation (3.4)). The range corrections appear at NLO in the power-counting of the EFT. However by doing so one creates a spurious pole. In section 3.1 we showed, that this pole violates unitarity and leads to negative probabilities. Additionally, we obtained a condition for the pole to create numerical problems. This is given by

$$0 < r < \frac{a}{2}, \tag{3.117}$$

with the scattering length a and the effective range r. In this region special methods must be used to circumvent the problems. In section 3.1.4 we summarized existing methods to do so. We stated that they either lead to a loss of accuracy or create additional problems with diverging expressions when adopted to a finite volume. Therefore we motivated the need for a new non-perturbative method. In section 3.2 we developed such a method. The method can be summarized as follows. Exchange the dimer propagator $\tau(k^*)$ by

$$\tau(k^*) \to \tau_i(k^*), \tag{3.118}$$

with a modified propagator $\tau_i(k^*)$ given by equation 3.25. We expand the contribution of the spurious pole in $(k^*)^2$ and keep the first i terms. The contribution of the physical pole is not modified, thus the label non-perturbative. Therefore we prevent the convergence issues in finite volume. Then the difference between the new and original propagator is included in the three-body forces. The real part of this is absorbed in the renormalization prescription. The imaginary part, which causes the unphysical behaviour, is dropped. In section 3.2.1 we showed that this is allowed by carefully proving that the difference causes only an additional low-energy polynomial in an effective potential.
We tested the new non-perturbative method in infinite volume by using it to describe both, a Yamaguchi model and a Gauss model. By employing numerical calculations for the particle-dimer phase shift and three-body bound states, we showed that the method can describe the models very accurately. An improvement compared to LO calculations (where the spurious pole does not appear) can be realised. We used Lepage plots to show that this improvement of the description of the models follows the general expectations for EFTs. Additionally we used a consistency assessment to test the internal pattern of the EFT using our method. The method passes the test for all considered cases.
Finally, we give a prediction for the optimal choice of terms to keep in $\tau_i(k^*)$. In section 3.2.2 we estimated this to be $i = 2$ for NLO and $i = 3$ for N^{2}LO. This is based on perturbative power-counting arguments, for a non-perturbative problem. Therefore we revisited this question in section 3.3.5 by investigating the numerical results. We come to the final conclusion that the ideal choice is $i = 1$ for NLO and $i = 2$ for N^{2}LO. The remaining part of this thesis will be focused on adapting the non-perturbative method to a finite volume.

4 Spurious poles in finite volume

The methods, results and discussions presented in this chapter have been published in parts in [62]. They are the result of a cooperation with the other authors of this article. We especially highlight that the numerical calculations in finite volume have been performed by using the computer program developed and provided by J. Y. Pang [81]. Additionally, some of the calculations have been directly performed by J. Y. Pang, which it is marked on the corresponding figures. The code is based on [33, 34] and [21], a summary of the concepts is given in section 2.5.3.

4.1 Yamaguchi model in finite volume

Before we address the problem of spurious poles and our non-perturbative solution to it, we show what the EFT should reproduce if working correctly. We are interested in the finite volume energy spectra of bound and scattering states. This observable is very important in finite volume. It was investigated in multiple publications over the last two decades, for example [45, 47, 29, 30, 14]. We choose a model to produce such a spectrum. The model we investigate is the same separable Yamaguchi model introduced in section 3.3.1. We choose the same Yamaguchi parameters $\lambda = -0.00013$ MeV^{-2}, $\beta = 278.796$ MeV. According to equation (3.66) they correspond to the ERE parameters $a = 5.4164$ fm and $r = 1.7536$ fm and a dimer at $E_d = 2.22$ MeV. As discussed in section 3.3.5, in infinite volume these values result in a shallow three-body bound state at $E_B^{shallow} = -2.36$ MeV and a deep three-body bound state at $E_B^{deep} = -24.80$ MeV. In the limit $L \to \infty$ the energy spectra have to converge to these values.
Using the code by [81] to solve equation (2.74) with the Yamaguchi propagator (equation (3.69)) and the potential given by equation (3.70) creates the finite volume spectrum for the model. We use a cutoff $\Lambda = 1500$ MeV. Note that this value is large enough such that the numerical problems of the difference between the cutoff and the highest shell are negligible, compare to section 4.4.1. The spectrum can be seen in figure 4.1. The points are the roots of equation (2.74). The roots can be divided into two types. On the one hand, the results below the the energy of the dimer E_d. These are three-body bound states of the system. And one the other hand, results above the energy of the dimer. They correspond to scattering states. In the following, we will discuss the cases separately.
Due to the similar systems we investigate, the resulting spectrum looks very similar to the results of [33, 34] and [21].

Bound states

We find two bound states, one converges to $E_B^{shallow}$ for large volume L and a second one converging to E_B^{deep}. This is in perfect agreement with the infinite volume results. The finite volume corrections (the difference between E_∞^i and E_L^i) to both states can be seen in figures 4.2 and 4.3. The first for the deep

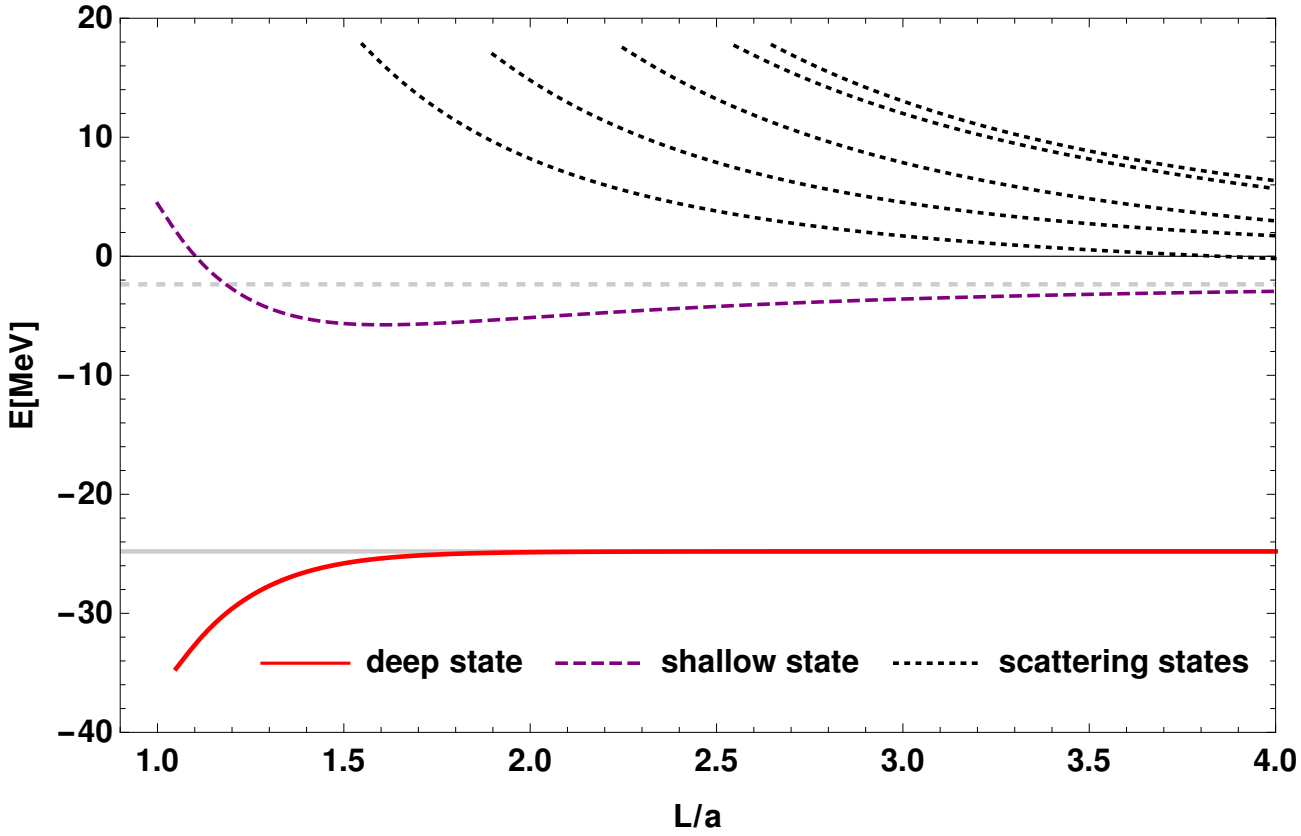

Figure 4.1: The finite volume spectrum for the Yamaguchi model. Plotted are the roots of equation (2.74). Below the break up they correspond to bound states. The deep bound state E^{deep} is given by the red line, the shallow bound state $E^{shallow}$ in purple dashed. Above the break up the roots correspond to scattering states, the first four are shown in black dotted. Also shown are the infinite volume results for the bound states (gray line for the deep state and gray dashed for the shallow state). For large volume L the finite volume results converge to the infinite volume counterparts. Data provided by [81].

state and second for the shallow state. Due to the similar systems and results the following analysis is heavily inspired by [21].
According to [60] or [37] the correction for a three-particle bound state is given by

$$E_{B,L} - E_{B,\infty} = \frac{c}{L^{3/2}} \exp\left(-\frac{2}{\sqrt{3}}\kappa L\right), \tag{4.1}$$

with a volume independent constant c. The binding momentum is given by $\kappa = \sqrt{|mE_B|}$. In a theory that supports a bound two-body state, meaning the dimer in our case, an additional possibility is a bound state of this dimer and the third particle. For a bound state of a dimer and a particle (an effective two-body system) the finite volume correction is given by the well known result of Lüscher [53] (for a more resent derivation see for example [50])

$$E_{B,L} - E_{B,\infty} = \frac{c'}{L} \exp\left(-\frac{2}{\sqrt{3}}\sqrt{\kappa^2 - a^{-2}}L\right), \tag{4.2}$$

with a volume independent constant c'. In reality the actual bound states can be superpositions of both cases. For the shallow state one expects it to be more like a dimer and a single particle, since the binding energy is close to the energy of the dimer. For the deep state no such argument can be made. In figures 4.2 and 4.3 a superposition of both cases is fitted to the results. Note that the volume region calculated is to narrow to resolve the polynomial suppression of L, only the exponential part can be obtained. Therefore, we fit the following equation to the numerical results:

$$E_{B,L} - E_{B,\infty} = c \exp\left(-\frac{2}{\sqrt{3}}\kappa L\right) + c' \exp\left(-\frac{2}{\sqrt{3}}\sqrt{\kappa^2 - a^{-2}} L\right). \tag{4.3}$$

For the shallow bound state we obtain $c/c' \approx 0.1$. So, the state can be described very accurately by the binding of the dimer and a single state. For the deep state we find $c/c' \approx 2.1$. This state contains both, the bound state of a dimer and a single particle as well as a three particle bound state. A more detailed discussion of the bound states as superposition of three-body and particle-dimer bound states can be found in [21].

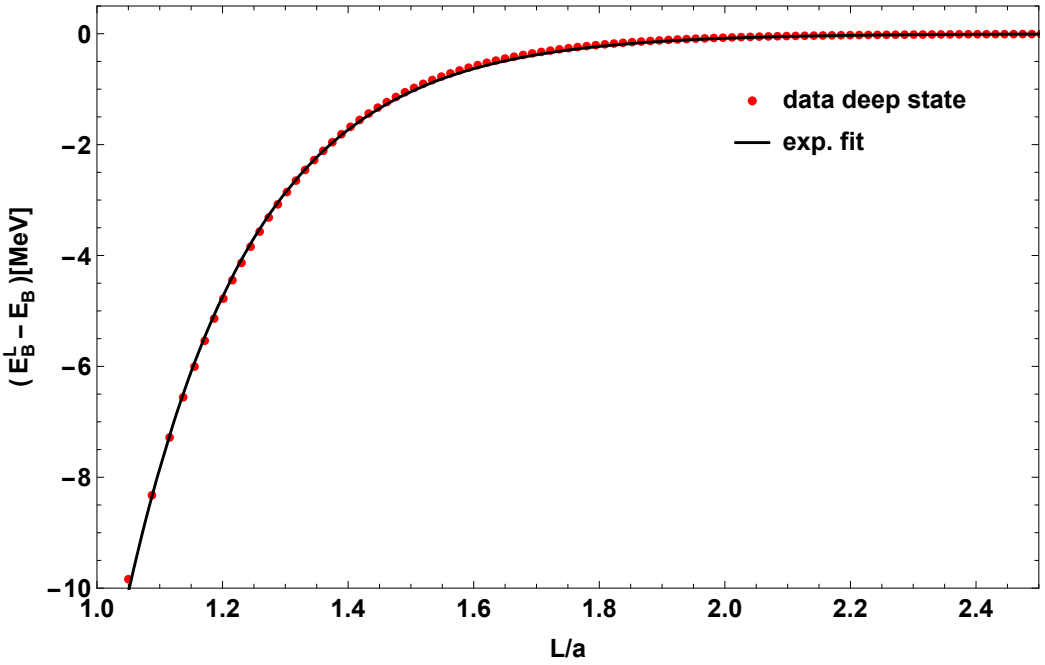

Figure 4.2: The finite volume corrections to the deep bound state. Also shown is a fit of the superposition of the possible finite volume corrections. We obtain that both corrections, meaning the correction due to a bound state of a dimer and a single particle as well as the correction due to a bound state off three particles, are needed. Data of the Yamaguchi model (red dots) provided by [81].

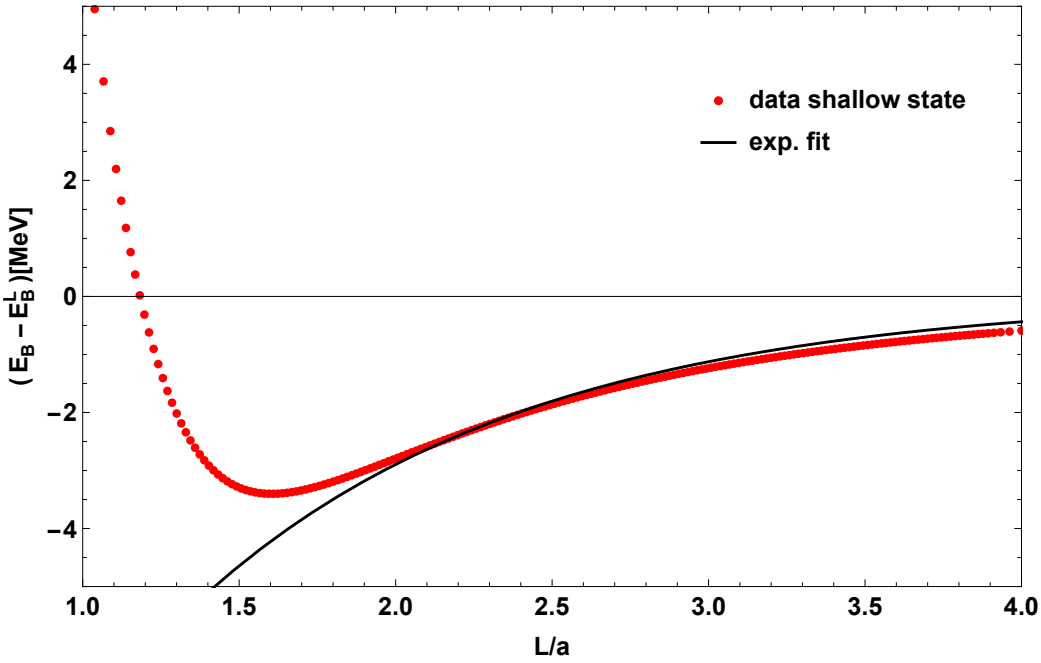

Figure 4.3: The finite volume corrections to the shallow bound state. Also shown is a fit of the superposition of the possible finite volume corrections. We obtain that the shallow state can be described as a bound state of a particle and a dimer. The contribution of the three-particle bound state can be neglected. Data of the Yamaguchi model (red dots) provided by [81].

Scattering states

For the scattering states there are again two possible cases, the scattering of three single particles and the scattering of the dimer and a particle. For the particles to scatter, they need some relative momentum to each other. Therefore, there must be energy in the system. For three-particles in infinite volume this is the case for $E > 0$, obviously. However, in finite volume the momenta are discrete. Hence the scattering is discrete and the minimal energy is determined by the lowest possible discrete momentum $p = 2\pi/L$. So, we expect a series of discrete states that converge to $E = 0$ for $L \to \infty$. Since there are an infinite number of such states the continuous scattering is restored in this limit.
The other possibility is the scattering of a particle and the dimer. Similar to above, a discrete spectrum of scattering states is expected, that converges to a continuous spectrum for infinite volume. In contrast to above, it starts not at $E = 0$, but $E = -E_d$. The dimer has a positive binding energy, the system gains energy by forming a dimer. This energy allows relative momenta between the dimer and the particle even at $E < 0$. Consequently, we expect a discrete spectrum of scattering states that converge to $-E_d$ for $L \to \infty$.
In figure 4.1 this behaviour is hinted. For the lowest lying scattering states this can be verified. By fitting a polynomial in $1/L$ the infinite volume behaviour of the states can be approximated. The fit results in $E_{L\to\infty} = -2.28$ MeV $\approx -E_d$ for the lowest lying state. For the second and third state we obtain $E_{L\to\infty} = 0$. For the fourth state we obtain $E_{L\to\infty} = -2.91$ MeV, which is smaller than expected. However, for this state the calculated volume range seems to be to small to obtain the correct convergence pattern. For the last shown state we get $E_{L\to\infty} = 0$. We conclude, that the scattering states converge to

zero or $-E_d$, as expected. A more detailed analysis of the two kinds of scattering states can be found in [1, 66].

4.2 Spurious poles and spurious scattering states

The problems with the spurious pole k_2, caused by using the ERE outside its range of applicability, manifest themselves in finite volume different than in infinite volume. We are interested in the finite volume energy spectrum, as introduced in the last section at the example of the Yamaguchi model. While the physical problems (negative residue, negative spectral density and violation of unitarity) stay, the numerical problem (results does not converge in the number of steps of discretization) does not appear. Compare this to section 3.1. However, a different problem appears. To see this we calculate the spectrum for the unmodified EFT at NLO (section 2.3), where the unmodified finite volume propagator $\tau^L(k^*)$ (equation (2.56)) is used. This means using the ERE (equation (3.4)) up to NLO. The propagator exhibits the spurious pole. We consider the same values of scattering length $a = 5.4164$ fm and effective range $r = 1.7536$ fm as resulting from the Yamaguchi model in the last section. These values result in a physical pole of the dimer propagator at $k_1 = 45.69$ MeV and a spurious pole at $k_2 = 179.37$ MeV. The interaction $Z(p, q, E)$ is given by equation (2.44), where we choose an arbitrary[1] value for the three-body force H_0. In figure 4.4 the resulting spectrum can be seen. The spectrum exhibits two clear differences to the spectrum of the Yamaguchi model (figure 4.1):

(a) There is a new series of states, behaving like scattering states. Additional to the states converging to zero and the physical pole, as discussed above, we find states that converge to a lower energy for large volume L. An exponential fit shows that they converge to $k_2^2/m = 34.2$ MeV. So, these states are connected to the scattering of one particle and the spurious state. The system gains energy by forming this spurious bound state. The energy can be transformed into relative momentum and scattering states appear. However, as stated multiple times in this thesis, the spurious pole is an artefact of the ERE and has no physical meaning. There is no deep two-body state in the real system. Therefore, this additional scattering is an artefact. Consequently, in the Yamaguchi model it can not be seen. This is exactly where the problems regarding the spurious pole as an additional bound state manifest themselves. The method developed in the next sections must not have this spurious scattering states.

(b) By recalculating the spectrum in higher resolution (figure 4.5) an even more critical difference to the Yamaguchi model (or any meaningful physical theory) can be seen. The spurious scattering states seem to merge with the other states of the spectrum. For example at $L = 1.33a$ the lowest spurious scattering state merges directly into (what seems to be) the shallow bound state. At $L = 1.47a$ this state than merges into the second spurious scattering state. This behaviour is clearly non-physical. First, the same state has different energies for the same volume size L. For example the merged state described above has an energy of $E = -0.78$ MeV, $E = -0.27$ MeV, $E = -0.08$ MeV or $E = 0.41$ MeV at $L = 1.45\,a$. This is not meaningful. Second, there is a theoretical argument that forbids this in a physical theory, the so called avoided-level-crossing, for example [8]. Assume we have a theory with two volume-dependent states $E_1(L)$ and $E_2(L)$.

[1] At this moment the aim is to show the problem, not to accurately reproduce the model. Since the EFT with the spurious pole is unphysical, we do not focus on fine-tuning the three-body forces. When we introduce and test our non-perturbative method this will be done for the modified EFT. The problems discussed here are not related to the choice of H_0. This would only change the infinite volume limit of the bound states.

Further assume that the Lagrangian of the theory contains a term such that this states can interact with each other. Let the interaction strength of it be g. Consider now a particular value of $L = L'$, for which $E_1(L') = E_2(L')$, if $g = 0$. In the vicinity of this L', the energy is determined from the secular equation:

$$\det \begin{pmatrix} E - E_1 & g\, H_{12} \\ g\, H_{12} & E - E_2 \end{pmatrix} = 0\,, \tag{4.4}$$

here, H_{12} stands for the matrix element of the Hamiltonian that describes the transition between the two states and g for the strength of this transition. This equation has solutions for

$$E_\pm = \frac{1}{2}(E_1 - E_2) \pm \sqrt{\frac{1}{4}(E_1 - E_2)^2 + g^2 H_{12}^2}\,. \tag{4.5}$$

For $g = 0$ the two solutions coincide for $L = L'$ as expected. But for $g \neq 0$ they can never be the same. If g is small they come close to each other, but can never touch each other. By this mechanism a level crossing is avoided. In contrast to these arguments for a physical theory, in the theory with the spurious pole it can be: $g^2 < 0$, due to the negative residue of the propagator at the position of the spurious pole. This causes the non-physical level crossing seen in figure 4.5.

To summarize, using the unmodified dimer propagator $\tau(k^*)$ creates additional spurious scattering states. The wrong sign of the residue of the corresponding pole causes non-physical merging of states. In the context of this thesis the correct spectra and the structure of the poles of the dimer propagator are always known. However, in general applications the amount of two-body bound states, and therefore the amount of scattering thresholds, might be unknown. So, in this case the findings of (a) are not a clear indicator of spurious behavior. Taking a look at figure 4.4 without knowledge of the model results (figure 4.1) might lead to the conclusion, that there are two bound two-body subsystems at k_1^2/m and k_2^2/m. But a closer look and the findings described in (b) are clear indicators that this is not the case. The merging of the different levels will not happen in a meaningful theory. Something like this should be forbidden by the avoided-level-crossing. This is non-physical and can be used to identify spurious scattering states and the incorrect implementation of the dimer propagator.

4.3 Adaption of the non-perturbative method to finite volume

In the last section, we demonstrated the devastating effects of the spurious pole to the finite volume spectrum. In this section, we will adapt the non-perturbative method, developed above in the infinite volume, to the finite volume and thereby solve the problems caused by the pole.
We follow the same idea as before and define a new propagator similar to equation (3.25) by

$$\tau_i^L(k^*) = \tau^L(k^*) - f_i^L(k^*), \tag{4.6}$$

with the unmodified dimer propagator in finite volume $\tau^L(k^*)$ given by equation (2.56). The function $f_i^L(k^*)$ is chosen, such that $\tau_i^L(k^*)$ does not exhibit the spurious pole and the change of the finite volume counterpart of the effective potential $W^L(p, q, E)$ is a low energy polynomial, than the change can be absorbed in a change of the renormalization prescription similar to the infinite volume case. We follow

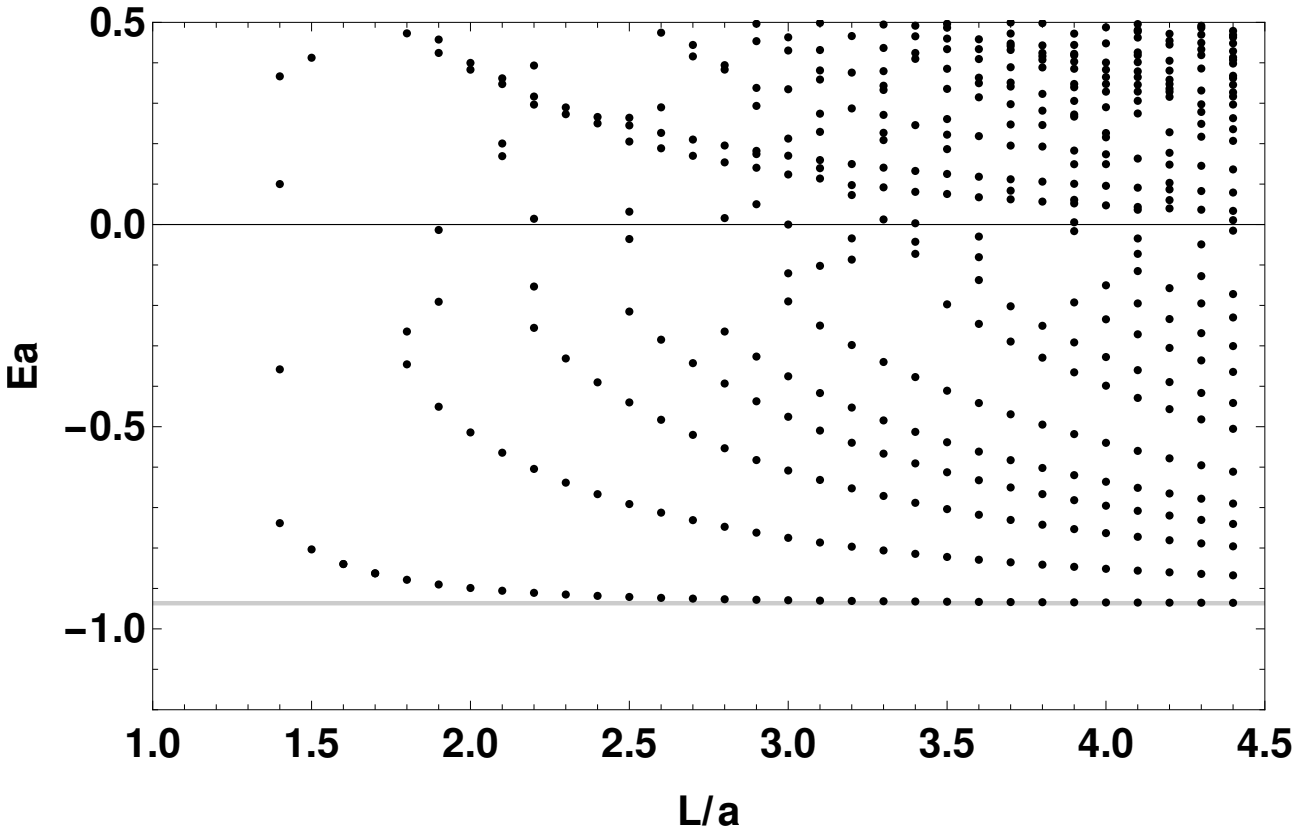

Figure 4.4: The spurious finite volume spectrum. Here the unmodified dimer propagator $\tau(k^*)$ which exhibits a spurious pole at $k_2 = 179.37$ MeV is used. This corresponds to an additional (spurious) bound state at $k_2^2/m = 34.24$ MeV $\approx 0.94\,a$ in infinite volume (gray line). Compared to the Yamaguchi spectrum, shown in figure 4.1, additional scattering states are found. They converge to the spurious bound state.

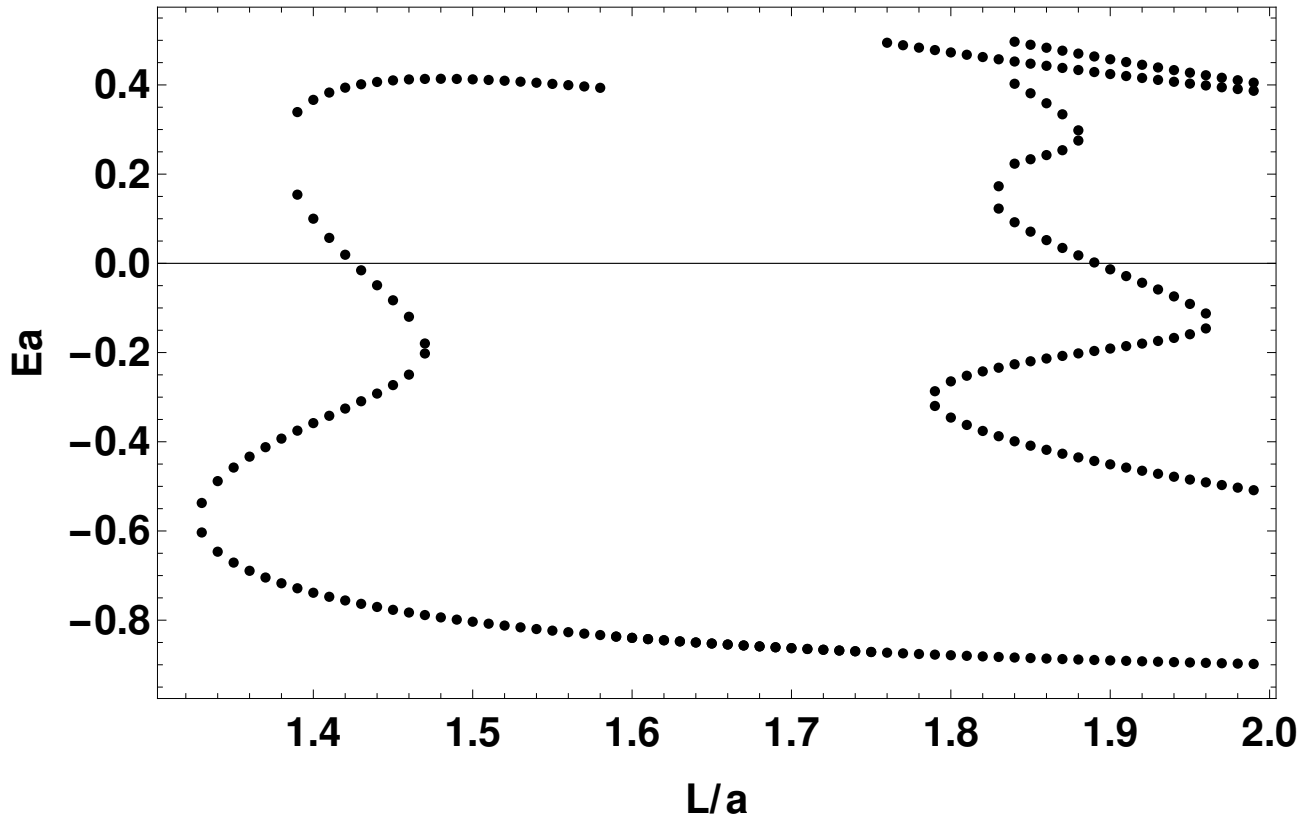

Figure 4.5: The spurious finite volume spectrum in higher resolution. It can be seen, that the additional scattering states in figure 4.4 merge with the shallow bound state and other scattering states. The expected avoided level-crossing is not present. The states can be transformed in to each other by changing the volume size L. This is clearly non-physical and a consequence of the negative residue of the spurious pole.

this by the same steps, done in infinite volume. With this new propagator the Faddeev equation in finite volume (equation (2.55)) can be re-written as

$$M^L(\mathbf{p},\mathbf{q};E) = W^L(\mathbf{p},\mathbf{q};E) + \frac{1}{L^3}\sum_{\mathbf{k}}^{\Lambda} W^L(\mathbf{p},\mathbf{k};E)\tau_i^L(k^*)M^L(\mathbf{k},\mathbf{q};E)\,,$$

$$W^L(\mathbf{p},\mathbf{q};E) = Z(\mathbf{p},\mathbf{q};E) + \frac{1}{L^3}\sum_{\mathbf{k}}^{\Lambda} Z(\mathbf{p},\mathbf{k};E)f_i^L(k^*)W^L(\mathbf{k},\mathbf{q};E)\,. \tag{4.7}$$

The aim is to choose $f_i^L(k^*)$ such, that $W^L = Z+$ polynomial, as we have done in the infinite volume case. An obvious first choice is $f_i^L(k^*) = f_i(k^*)$, meaning choosing the same function $f_i(k^*)$ as in infinite volume. But the situation in finite volume is slightly different than in infinite volume. The analysis in section 3.2.1 is based on a perturbation of the effective potential $W(p,q,E)$. In infinite volume, this does not create a problem. However, in finite volume the singularities of the one-particle exchange in the potential $Z(p,q,E)$ above the three-particle threshold hinders this perturbative arguments. In infinite volume, these singularities condense to a branch cut, and are removable. In finite volume the effective potential should be calculated non-perturbatively. While the perturbative calculation in infinite volume can not change the pole positions, and therefore does not change the energy levels, the non-perturbatively calculation in finite volume can change the structure of the energy levels. This is what happens. It can be shown [81], that the singularity structure of $W(p,q,E)$ and $Z(p,q,E)$ is different above the threshold. This can be understood by comparing the quantity $Z(p,k,E)\tau_L(k^*)$ in the Faddeev equation to $Z(p,k,E)f_i(k^*)$ in the definition of the effective potential. $\tau_L(k^*)$ becomes zero exactly at those energies where $Z(p,q,E)$ is singular (i.e., at the free three-particle energies). This is a direct result of the replacement of the branch-cut $k^* \to S(k^*)$. $S(k^*)$ is singular at the free three-particle energies, so $\tau_L(k^*)$ is zero. Therefore, the product $Z(p,k,E)\tau_L(k^*)$ is regular. A detailed analysis of this can be found in [56]. On the other hand, $f_i(k^*)$ is a continuous function above threshold. So the product $Z(p,k,E)f_i(k^*)$ is singular at these energies. By writing down explicitly the matrix equation that relates $W(p,q,E)$ and $Z(p,q,E)$ in a finite volume, one can verify that the poles in $Z(p,q,E)$, corresponding to the excited levels, are spitted into several levels in $W(p,q,E)$. Although this splitting is small, as $f_i(k^*)$ is small at small momenta, the singularity structure of $W(p,q,E)$ and $Z(p,q,E)$ is indeed different and replacing $W(p,q,E)$ by $Z(p,q,E)$ in the quantization condition cannot be justified. Compare this discussion to [62].
Note that this issues only appear above the three-particle threshold. Therefore, a simple solution for the problem is to choose

$$f_i^L(k^*) = \begin{cases} f_i(k^*) & (k^*)^2 \geq 0\,, \\ 0 & \text{else}\,. \end{cases} \tag{4.8}$$

This ensures, that the quantity $Z(p,k,E)f_i(k^*)$ is regular above threshold and that the spurious pole disappears in $\tau_i^L(k^*)$. Doing so, allows to repeat the perturbative calculations for the effective potential $W(p,q,E)$. With this calculations one can prove that the effective potential in finite volume can be written as

$$W^L(\mathbf{p},\mathbf{q};E) = Z(\mathbf{p},\mathbf{q};E) + \text{polynomial}\,. \tag{4.9}$$

Therefore, the change can be absorbed in the three-body forces as in the infinite volume case. The calculations can be found in [62]. Here we sketch the general idea of the prove. A very useful tool in

finite volume calculations is Poisson's summation formula:

$$\sum_{n\in\mathbb{Z}} f(n) = \sum_{m\in\mathbb{Z}} \int_{-\infty}^{\infty} dt f(t) e^{-2\pi i m t} \,. \tag{4.10}$$

A sum of a function $f(n)$ over an integer n can be replaced by the sum over the Fourier transform of that function over an other integer m. After separating the factor $2\pi/L$ from k, this can be used to re-write a perturbative expansion of equation (4.7). Now the $m = 0$ terms in this new sum are exactly the infinite volume parts discussed in section 3.2.1. This results in polynomial corrections as shown above. The other parts are suppressed with at least $\exp[-Lk]$ and also result in a polynomial.
To summarize, the problem caused by the spurious pole can be avoided by changing the propagator by $\tau_i^L(k^*)$. The particular choice of $f_i^L(k^*)$ given by equation 4.8 ensures that all consequences[2] of this can be absorbed in a change of the renormalization prescription. We close this section by noting, that the choice of $f_i^L(k^*)$ is not unique. Other choices are possible as long as they fit these two criteria. An example of a different choice can be found in [62]. In the following, we show that the specific choice of equation (4.8) is working. This will be done by comparing numerical results using this to the spectrum of the Yamaguchi model.

4.4 Numerical test

In this section, the EFT using the finite volume version of our non-perturbative method is compared to the finite volume spectrum of the Yamaguchi model. The model, the corresponding spectrum and a physical interpretation of the results are given in section 4.1. The non-perturbative method is introduced in section 4.3. The scattering length is $a = 5.4164$ fm and the scattering length is $r = 1.7536$ fm for NLO and N^{2}LO. At LO the scattering length is $a = 4.3193$ fm and the effective range is $r = 0$. According to our findings[3] in infinite volume we choose for the number of subtractions in the modified propagator $\tau_i^L(k^*)$ (equation (4.6) and equation (4.8)) $i = 2$ at NLO and $i = 2$ at N^{2}LO. For the S-wave potential (equation (2.44)), the quantization condition takes the simple form of equation (2.74).
Because of the finite volume cutoff effects described below, we use a very large cutoff compared to our infinite volume calculations. We use a cutoff $\Lambda = 1700$ MeV for NLO and N^{2}LO. For LO those effects are larger, we use a cutoff $\Lambda = 2200$ MeV for the LO calculations. The three-body forces are determined in infinite volume in the same way as described in section 3.3.2. They are fine-tuned to reproduce the quantity $p \cot \delta_Y$ of the model at $p = 0.001$ MeV for H_0 and at $p = 50$ MeV for H_2. In table 4.1 the results for the three-body forces can be seen.

Table 4.1: The three-body forces H_0 and H_2. They are determined in infinite volume as described in section 3.3.2. The results are given in units of MeV.

	$H_0(\Lambda = 2200)$		$H_0(\Lambda = 1700)$	$H_2(\Lambda = 1700)$
LO	-2.01	NLO & N^{2}LO	0.414	3.401

[2] Except the removing of the spurious pole.
[3] In section 3.3.5 we found as a optimal choice $i = 1$ at NLO. However, as also shown in this section, the choice $i = 2$ is not significantly worse. By choosing $i = 2$ at NLO and N^{2}LO (here it is the optimal choice) one can use the same value of the three-body force H_0 for both orders, and saves the determination of one three-body force.

4.4.1 Cutoff effects

If a sharp cutoff Λ is used to regularize the loop integrals, or more precise, the loop sums in finite volume calculation one has to be careful. Since the momentum is discrete in finite volume such a cutoff should be understood as follows:

$$\Lambda \geq |\mathbf{p}| = \frac{2\pi}{L}|\mathbf{n}|; \quad \mathbf{n} \in \mathbb{Z}^3. \tag{4.11}$$

No momentum can be larger than the cutoff. But, in general, there there will be a non-zero distance between Λ and the maximal value of the momentum $|\mathbf{p}_{max}|$. This maximal value $|\mathbf{p}_{max}|$ is the actual cutoff, meaning the highest possible momentum, of the theory. For this value the three-body forces have to be fine-tuned. Also note, the value of $|\mathbf{p}_{max}|$ depends on the volume size L. If one uses Λ instead of $|\mathbf{p}_{max}|$ to determine the three-body forces, this creates a systematic error. It will manifest itself in an oscillation of the results. Say, we start at some volume size L with a value of $|\mathbf{p}_{max}|$ that is very close to Λ. Now we increase the volume, due to equation (4.11) the value of $|\mathbf{p}_{max}|$ decreases and the distance to Λ grows. Therefore, the systematic error in the results also grows. Eventually the distance becomes large enough, so an additional value of $|\mathbf{p}|$ becomes possible. This will be the new $|\mathbf{p}_{max}|$ and the distance between this and Λ is small again. The systematic error also is small again. Increasing L even more repeats this process and the systematic error oscillates.
There are two ways of solving this problem. The first method is to calculate all possible values of $|\mathbf{p}_{max}|$ for all considered values of L. Than determine the three-body forces for all values and use them as a input to the quantization condition. Obviously, this is time consuming, it is done for example in [62]. The second method is to choose a very large value of the cutoff Λ. Because of the three-dimensionality of $\mathbf{p}$ the distance between to different neighbouring values of $|\mathbf{p}|$ increases with increasing value of $|\mathbf{p}|$. This is visualized in figure 4.6 in a 2D simplification. Therefore the maximal difference between Λ and $|\mathbf{p}_{max}|$ also decreases with increasing Λ. This leads to the effect being negligible for cutoffs large enough. For the results shown below, we choose this method and a cutoff $\Lambda = 1700$ MeV.

4.4.2 The energy spectrum for the non-perturbative method

In figure 4.7 the results for the energy spectrum are shown. Shown are the numerical results for the EFT at LO, NLO and N^{2}LO. For the calculation of the NLO and N^{2}LO results the non-perturbative method is used. All results are compared to the spectrum of the Yamaguchi model. The Yamaguchi model and a physical interpretation of the results are discussed in section 4.1. It can be seen, that the LO results can describe the model only qualitatively. The EFT at LO finds scattering states, but their calculated values deviate from the model significantly. The infinite volume behaviour of the shallow bound state is obtained correctly, however, the finite volume correction for small values of L can not be predicted by the EFT at LO precisely. The description of both, the scattering states and the shallow bound state improves drastically if one uses the NLO calculations. The scattering states are predicted correctly, and the finite volume correction to the shallow bound state is close to the model even for small values of the volume size L. The situation further improves at N^{2}LO. The shallow bound state is described especially well by the N^{2}LO results. Note that the deep bound state can not be described by the EFT at all orders very well. This is due to the large value of the corresponding binding momentum κ.

$$\kappa = \sqrt{mE_B^{deep}} \approx 150 \text{ MeV}\,. \tag{4.12}$$

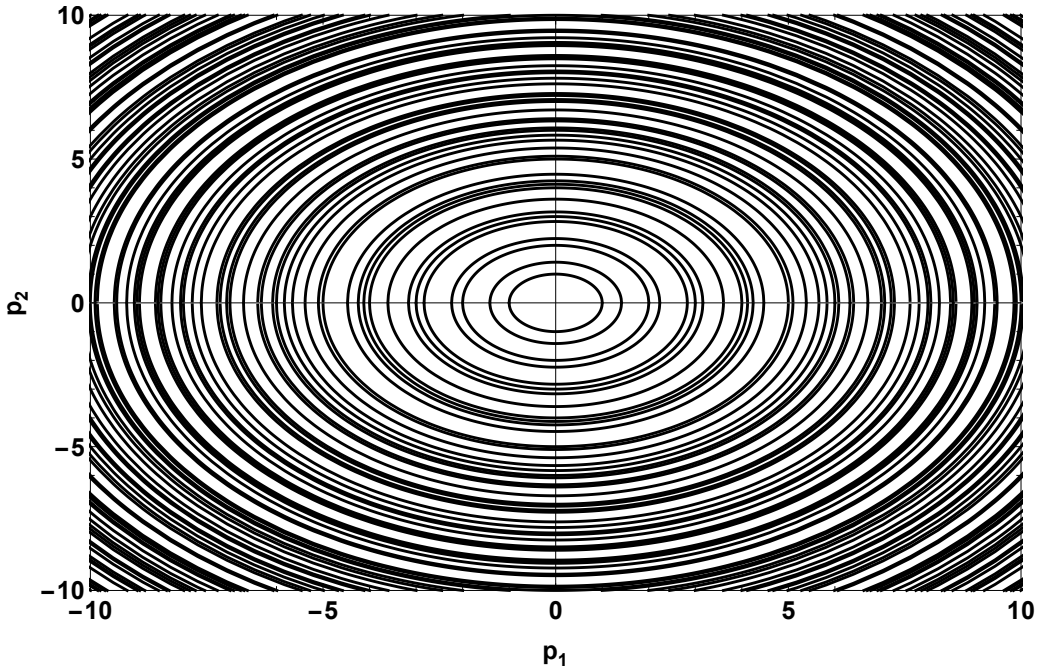

Figure 4.6: Visualization of the decrease of the distance between neighbouring values of $|\mathbf{p}|$ in 2D. Plotted are possible values of $|\mathbf{p}|$ in units of $2\pi/L$. It can be seen, that the density of the circles increases with increasing values of $|\mathbf{p}|$. Note that the increasing of the density also can be understand as a restoration of the spherical symmetry for $L \to \infty$.

This is larger than the break down scale Λ_b of the pionless EFT, which is given by the mass of the pion $m_\pi \approx 140$ MeV. Therefore the results of the EFT can not be trusted for such large momenta and it is of no surprise, that the deep bound state can not be obtained precisely. We conclude, the EFT using the non-perturbative method can describe the energy spectrum very precise as long as we are inside the range of applicability of the EFT. Additional, the description increases order by order of the EFT as expected. The non-perturbative method in finite volume fulfills all expectations.

4.5 Conclusion for the finite-volume case

We summarize our investigation of the spurious poles in finite volume. We have calculated the energy spectrum of a Yamaguchi model in finite volume using the quantization condition given by equation (2.74). We found two three-body bound states, namely a shallow and a deep bound state. We were able to reproduce results of [21] and showed, the shallow bound state is mostly a bound state of the dimer and a single particle. The deep bound state is a superposition of such particle-dimer state and a bound state of three single particles. The spectrum also contains a series of scattering states. For the lowest lying states we found that they converge either to zero or the binding energy of the dimer. They describe the scattering of three single particles or the scattering of a particle and the dimer, respectively.
In the EFT with range corrections, meaning using the ERE at NLO in the dimer propagator, we have two poles. The first pole k_1 corresponds to the dimer in the model, while the second pole k_2 is a spurious pole. In the previous chapter we have discussed this in detail. In this chapter, we have investigated the influence of the spurious pole to the finite volume energy spectrum. Using the unmodified propagator

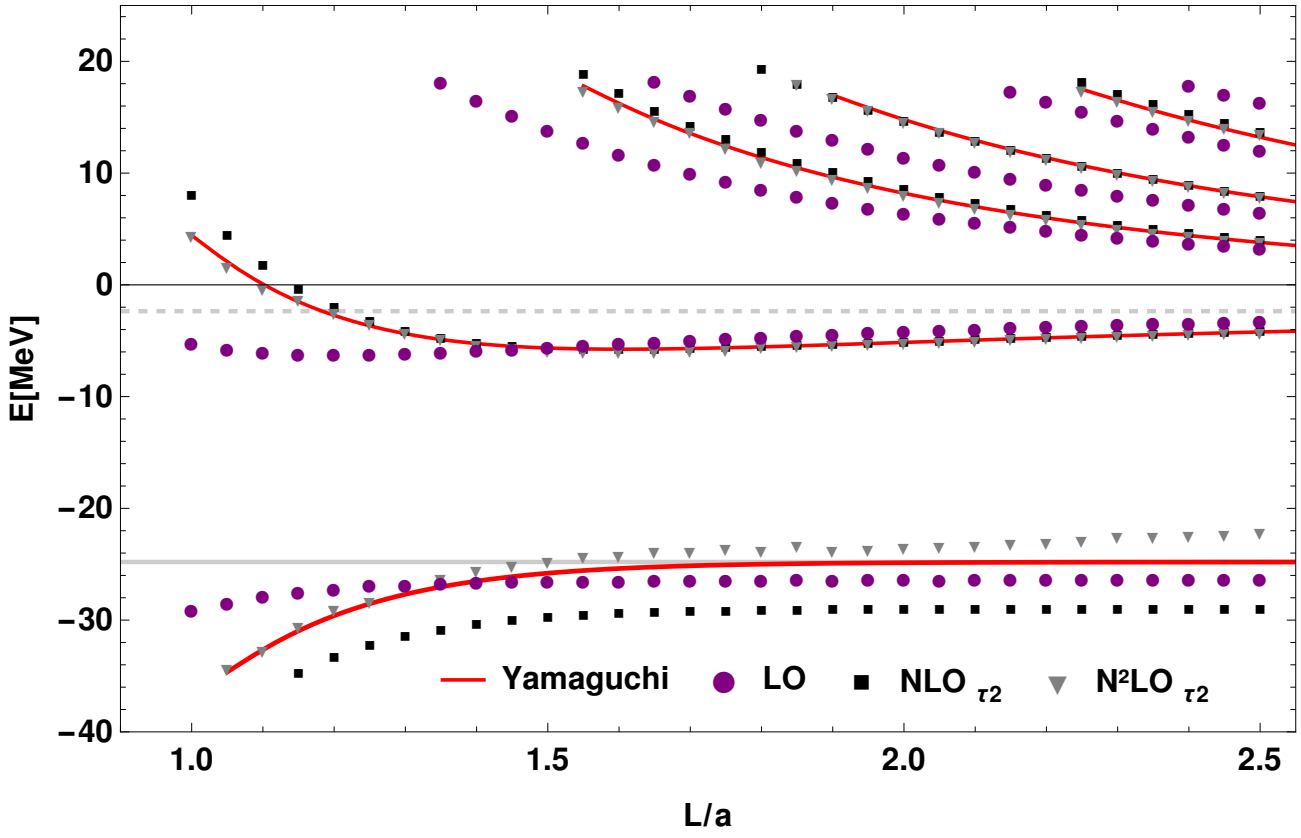

Figure 4.7: The energy spectrum in finite volume. Shown are the bound and scattering states dependent on the volume size L. The red lines are the results of the Yamaguchi model, the purple dots are the EFT results in LO, the black squares are the EFT result at NLO, and the gray triangles are the results for the EFT at N^{2}LO. The calculations at NLO and N^{2}LO are performed by using the non-perturbative method. We use two subtractions at NLO and N^{2}LO. The improvement of the description of the model is clearly seen order by order. Data provided by [81].

with the spurious pole results is a spurious spectrum. Besides the scattering states that converge either to zero or the energy of the dimer k_1^2/m, the spurious spectrum contains a series of scattering states that converge to the two-body binding energy that is connected to the spurious pole k_2^2/m. This incorrectly predicts the scattering between a single particle and the spurious state. Even worse we obtained an un-physical merging of different states. For the same volume size L the same state can have different energies. In a meaningful theory this should be forbidden by avoided-level-crossings. Due to the negative residue of the propagator at the position of the spurious pole, this mechanism is not present here. To summarize, the unmodified propagator can not be used to calculate the energy spectrum and a special method is needed.

Therefore, we have adopted the non-perturbative method, developed in infinite volume, to the case of finite volume. This could be done by using a modified propagator $\tau^L(k^*) \to \tau_i^L(k^*) = \tau^L(k^*) - f_i^L(k^*)$, where the function $f_i^L(k^*)$ is the same as in infinite volume $f_i^L(k^*) = f_i(k^*)$ below the three-particle threshold and $f_i^L(k^*) = 0$ above the threshold. This separation is needed, since the poles of $\tau_L(k^*)$ above threshold, that are connected to the three-particle scattering states, would lead to a non-polynomial change in the effective potential and could therefore not be absorbed in the three-body forces. Equipped with the modified non-perturbative method, we were able to calculate the energy spectrum in finite volume. The spectrum obtained by the EFT at LO, NLO and N^{2}LO describes the Yamaguchi model very accurate and the description is improving order by order of the EFT as expected. We conclude, the modified non-perturbative method is working in finite volume.

5 Conclusion and outlook

In this chapter, we give a summary of our main results, namely the non-perturbative method for spurious poles in infinite and finite volume. We discuss possible further projects and a few selected natural extension routes of our non-perturbative method.

5.1 Conclusion

In this thesis, we have investigated bosonic three-particle systems, using pionless effective field theory ($\not\pi$EFT) in the particle dimer picture. The considered systems we have an unnaturally large two-body scattering length $1/a \sim m_{low}$ and a naturally sized two-body effective range $1/r \sim m_{high}$, where m_{low} (m_{high}) is the low (high) momentum scale of the EFT.
Range corrections can be included in the dimer propagator and enter at NLO of the power-counting of the EFT. In the widely used non-perturbative or re-summarized method they lead to the following dimer propagator in infinite volume

$$\tau(k^*) = \frac{1}{-1/a - r/2\,(k^*)^2 + k^*}\,,$$

where k^* is the magnitude of the relative momentum of the two particles of the dimer in their center-of-mass frame. We have shown in section 3.15 that for $0 < r < a$ this propagator exhibits a spurious pole at $k_2 \approx r/2$. The propagator has a negative residue at the pole position. We have shown that this negative residue is directly connected to negative imaginary part of the particle-dimer phase shift (section 3.1.1). This leads to a violation of the unitarity relation of the S-matrix. The negative residue also causes negative spectral densities, spectral densities are a positive definite quantity. Besides these un-physical predictions, numerical calculations are not possible if the spurious pole is not treated specially. We have discussed that the existing methods either lead to a loss of accuracy or have convergence issues in a finite volume. Therefore we concluded that a new non-perturbative method, to deal with the spurious pole, is needed.
In section 3.2, we have developed such a method, which can be described as follows. Exchange the dimer propagator by

$$\tau(k^*) \to \tau_i(k^*) = \tau(k^*) - f_i(k^*)\,,$$

where the function $f_i(k^*)$ is the contribution of the spurious pole to the propagator, subtracted by an expansion of $\tau(k^*)$ for small momenta compared to k_2. This is given by

$$f_i(k^*) = -\frac{4k_2/r}{(k_2-k_1)((k^*)^2-k_2^2)} - \frac{4k_2/r}{(k_2-k_1)k_2^2}\left[1 + \frac{(k^*)^2}{k_2^2} + \frac{(k^*)^4}{k_2^4} + \cdots\right].$$

The index i counts the number of terms in the expansion. By doing so, we were able to ensure two objectives. First, the new propagator is regular at the position of the spurious pole. Therefore the negative residue does not appear. Second, we have not changed the contribution of the physical pole k_1 at all. This motivates the label non-perturbative and avoids the convergence issues expected in finite volume for perturbative methods. We have demonstrated in section 3.2.1, that this change of the propagator can be justified by a change in the re-normalization prescription of the three-body forces of the EFT. This was done by proving analytically that the subtraction of $f_i(k^*)$ only leads to an additional low-energy polynomial in an effective potential. Since the three-body forces are also a low-energy polynomial, the additional terms can be absorbed in the corresponding coupling constants.
In the remaining part of the investigations in infinite volume, in section 3.3 we have calculated observables using $\not\pi$EFT at LO, NLO, and N^{2}LO numerically. At NLO and N^{2}LO we have used our non-perturbative method. We have investigated the particle-dimer phase shift δ, the quantity $p \cot \delta$, and binding energy of three-body bound states. All these observables were compared to model calculations. The models we considered were the Yamaguchi model and the Gauss model. The predictions of the EFT at the different orders agreed within their corresponding error bands with the models. We also obtained that the accuracy of the description increases order by order. To further investigate this increase we performed an analysis based on Lepage plots [51]. All results of this fulfill the expectations. Additionally, we have shown that our method conserves the power-counting of the EFT. This was done by doing a consistency assessment [27].
In the last part of the investigations in infinite volume, in section 3.3.5, we have obtained the optimal choice of subtractions i in the function $f_i(k^*)$ for a given order of the EFT. The results are $i = 1$ at NLO and $i = 2$ at N^{2}LO.

In the second part of the thesis, we have investigated the spurious pole in a finite cubic volume with periodic boundary conditions. The motivation for such a volume are calculations on the lattice, for example lattice QCD. We have used the quantization condition in finite volume [33, 34] to obtain the volume-dependent energy spectrum. By using the unmodified re-summarized dimer propagator, including the spurious pole, we showed in section 4.2 that the spurious pole leads to an un-physical series of scattering states. The formalism treats the spurious pole as a physical two-body bound state. Additionally, we obtained that some of the energy levels merged into each other. This is un-physical and we connected this to the negative residue. By showing this un-physical behavior we have motivated the need for a non-perturbative method also in finite volume. In the remaining part of the thesis, we adapted the non-perturbative method developed in infinite volume to finite volume. This was done in section 4.3 by changing the dimer propagator in finite volume $\tau^L(k^*)$ by

$$\tau^L(k^*) \to \tau_i^L(k^*) = \tau^L(k^*) - f_i^L(k^*)\,,$$

with the, compared to the infinite volume case, slightly different function $f_i^L(k^*)$. It is given by

$$f_i^L(k^*) = \begin{cases} f_i(k^*) & (k^*)^2 \geq 0\,, \\ 0 & \text{else}\,. \end{cases}$$

This choice of $f_i^L(k^*)$ was necessary, since otherwise the additional poles of $\tau^L(k^*)$, compared to $\tau(k^*)$, would result in a non-polynomial change in an effective potential above the three-body threshold $(k^*)^2 < 0$. Therefore it could not be absorbed in the three-body forces. This would lead to incorrect predictions of the physical scattering states. However, by using $f_i^L(k^*)$, and our non-perturbative method in the quantization condition, we were able to calculate the energy spectrum in section 4.4.2. The obtained spectrum did not exhibit the un-physical scattering states. The spectrum of the EFT described the

spectrum of a Yamaguchi model precisely. Additionally, the description improves order by order of the EFT.

To conclude, we were able to develop a non-perturbative method to solve the issues caused by the spurious pole in the re-summarized dimer propagator in infinite volume. We have shown, that this method can accurately describe different models. The accuracy of the description improves order by order of the EFT, and the method conserves the internal consistency of an EFT. In the second part, we could extend this method to the finite volume and calculate the energy spectrum correctly.

5.2 Outlook

We finish the thesis by discussing possible further projects and extensions of our non-perturbative method. In this thesis, we have considered range corrections. A natural next step is to include higher orders in the ERE. The next order is proportional to the shape parameter P. Corrections due to the shape parameter enter at N^{3}LO of the EFT. By performing a similar re-summation, as for the range corrections, the dimer propagator can be extended to higher-order easily, it reads

$$\tau(k^*) = \frac{1}{-1/a - r/2\,(k^*)^2 + P(k^*)^4 + k^*}\,.$$

This comes with the same downside as the range correction. The denominator of the propagator is a polynomial of order four. The propagator can exhibit up to three spurious poles, k_2, k_3 and k_4. It might be interesting to investigate if the non-perturbative method, developed in this thesis, can be expanded to higher orders. A possible approach could be to exchange the propagator by

$$\tau(k^*) \to \tau_i(k^*) = \tau(k^*) - f_i^2(k^*) - f_i^3(k^*) - f_i^4(k^*)\,,$$

with functions $f_i^{2,3,4}(k^*)$ similar to $f_i(k^*)$ for each spurious pole. To investigate whether this can be done, the analytical and numerical calculations performed in this thesis have to be repeated for this situation. It is not a priory clear if the change due to the different $f_i^{2,3,4}(k^*)$ will also lead to a low-energy polynomial for the potential.

In the Faddeev equation, we have exchanged the momentum dependent three-body force at N^{2}LO by a energy dependent three-body force. At this order it was shown in [5] that this leads to the same physics up to higher orders of the EFT. In [25] it was assumed, that this exchange can also be done for higher-order three-body forces. However, a strict prove of this is still missing and is an interesting further project.

So far, we have only considered bosons. An additional interesting extension of the method is to use it for fermionic systems, especially for nucleons. To do so, the quantization condition in finite volume [33, 34] and their projection on the irreducible representations of the cubic group [21] has to be re-derived for nucleons at LO. In a second step, this could be extended to NLO by using the non-perturbative propagator.

Of further interest is the extension to larger momenta. For momenta $p \sim m_\pi$ $\not\pi$EFT can not be used any longer. In the region of this momenta pions have to be included explicitly. This means using chiral EFT

instead of $\not\pi$EFT. An intriguing question is if and how the spurious poles manifest in such systems and if our method can be applied there.

Finally, we have analyzed our method by comparing it to different models. However it would be beneficial to apply the non-perturbative method to investigate real lattice data.

6 Appendix

6.1 Details of calculations for the effective potential

In this part of the appendix we show additional details of the calculation for the effective potential. The calculation in the last step of equation (3.44) is shown. The integral can be modified by adding and subtracting the following term:

$$\begin{aligned} I_{e0}^{pole,\infty} &= \frac{-1}{3\pi i p} \ln\left[(x-x_0) + i\sqrt{\frac{4A^2}{p^2} - (x-x_0)^2 - i\epsilon}\right]\Bigg|_0^1 \\ &= \frac{-1}{6\pi i p} \ln\left[\frac{(x-x_0) + i\sqrt{\frac{4A^2}{p^2} - (x-x_0)^2 - i\epsilon}}{(x-x_0) - i\sqrt{\frac{4A^2}{p^2} - (x-x_0)^2 - i\epsilon}}\right]\Bigg|_0^1 + \frac{1}{6\pi i p} \ln\left[(x-x_0)^2 + \frac{4A^2}{p^2} - (x-x_0)^2 - i\epsilon\right]\Bigg|_0^1, \end{aligned} \tag{6.1}$$

whereby the subtracted term was included in the logarithm of the first part and the third binomial formula was used for the second term. The second term can be expanded in the energy as a polynomial and therefore we drop it.

$$\begin{aligned} I_{e0}^{pole,\infty} &= \frac{-1}{6\pi i p} \ln\left[\frac{(x-x_0) + i\sqrt{\frac{4A^2}{p^2} - (x-x_0)^2 - i\epsilon}}{(x-x_0) - i\sqrt{\frac{4A^2}{p^2} - (x-x_0)^2 - i\epsilon}}\right]\Bigg|_0^1 + \text{polynomial} \\ &= \frac{-1}{6\pi i p}\left(\ln\left[\frac{\frac{p}{2}(1-x_0) + i\sqrt{-mE + \frac{3}{4}p^2 - i\epsilon}}{\frac{p}{2}(1-x_0) - i\sqrt{-mE + \frac{3}{4}p^2 - i\epsilon}}\right] - \ln\left[\frac{-\frac{p}{2}x_0 - \rho}{-\frac{p}{2}x_0 + \rho}\right]\right) + \cdots \\ &= \frac{-1}{6\pi i p} \ln\left[\frac{\frac{p}{2}(1 - \frac{2(p^2 - mE + \rho^2)}{p^2}) + i\sqrt{-mE + \frac{3}{4}p^2 - i\epsilon}}{\frac{p}{2}(1 - \frac{2(p^2 - mE + \rho^2)}{p^2}) - i\sqrt{-mE + \frac{3}{4}p^2 - i\epsilon}}\right] + \text{polynomial} \\ &= \frac{-1}{6\pi i p} \ln\left[\frac{1 - \frac{5}{4}\frac{p^2}{\rho^2} + i\frac{p}{\rho^2}\sqrt{-mE + \frac{3}{4}p^2 - i\epsilon} - \frac{\rho^2}{p^2}\left(i\frac{p}{\rho^2}\sqrt{-mE + \frac{3}{4}p^2 - i\epsilon}\right)^2}{1 - \frac{5}{4}\frac{p^2}{\rho^2} - i\frac{p}{\rho^2}\sqrt{-mE + \frac{3}{4}p^2 - i\epsilon} - \frac{\rho^2}{p^2}\left(i\frac{p}{\rho^2}\sqrt{-mE + \frac{3}{4}p^2 - i\epsilon}\right)^2}\right] + \cdots \\ &= \frac{-1}{6\pi i p} \frac{-2i\frac{p}{\rho^2}\sqrt{-mE + \frac{3}{4}p^2 - i\epsilon}}{1 + \frac{5}{4}\frac{4}{3}mE} + \cdots \\ &= \frac{1}{4\pi}\frac{1}{k_2^2}\sqrt{-mE + \frac{3}{4}p^2 - i\epsilon} + \cdots + \text{polynomial}\,. \end{aligned} \tag{6.2}$$

In the second to last step the logarithm was expanded in the root term.

6.2 The normalization for the scattering amplitude

In this appendix we discuss the normalization of the scattering amplitudes. After a review of the K-matrix formalism we derive the normalization for the various amplitudes used in this thesis.

6.2.1 The K-matrix formalism

In this part of the appendix we introduce briefly, how the normalization of the scattering amplitudes can be calculated. Therefore we use the so called 'K-matrix formalism' [6]. By normalization we mean the quantity N in the phase-shift parameterization of the scattering amplitude:

$$M(p,p,E_p) = N\frac{1}{p\cot\delta - ip}. \tag{6.3}$$

Let a general form of a Faddeev equation in S-wave be

$$M(p,q,E) = Z(p,q,E) + \int_0^\Lambda dk \frac{f(p,k,E)}{k-q-i\epsilon} Z(p,k,E)M(k,q,E), \tag{6.4}$$

with some 'propagator' $f(p,k,E)$. To simplify the notation we drop the energy-dependence for the rest of this section. By using the Sokhotski-Plemelj theorem (equation (3.31)) the contribution of the pole can be separated:

$$\begin{aligned} M(p,q) =& Z(p,q) + \mathcal{P}\int_0^\Lambda dk \frac{f(p,k)}{k-q} Z(p,k)M(k,q) \\ &+ i\pi f(p,q)Z(p,q)M(q,q), \end{aligned} \tag{6.5}$$

with the principal value integral $\mathcal{P}$. Subsequently, we introduce a matrix $K(p,q)$ by

$$K(p,q) = Z(p,q) + \mathcal{P}\int_0^\Lambda dk \frac{f(p,k)}{k-q} Z(p,k)K(p,k), \tag{6.6}$$

This can be written as

$$\begin{aligned} Z(p,q) &= \int_0^\Lambda dk \left(\delta(q-k) - f(p,k)\frac{\mathcal{P}}{k-q}Z(p,k)\right) K(p,k) \\ &= \mathcal{O}K(p,q), \end{aligned} \tag{6.7}$$

Here $\mathcal{O}$ is an operator acting on the matrix $K(p,q)$. This operator includes the integral above. Consequently, the last equation can be written as

$$\mathcal{O}^{-1}Z(p,q) = K(p,q), \tag{6.8}$$

with the inverse $\mathcal{O}^{-1}$ of this operator. Modifying the Faddeev equation (6.5) in a similar pattern yields

$$\int_0^\Lambda dk \left(\delta(q-k) - f(p,k)\frac{\mathcal{P}}{k-q}Z(p,k)\right) M(p,k) = Z(p,q)\left(1 + i\pi f(p,q)M(q,q)\right). \tag{6.9}$$

The first part on the left-hand side is exactly the operator $\mathcal{O}$. Applying $\mathcal{O}^{-1}$ from the left on both sides, leads to

$$M(p,q) = K(p,q)\left(1 + i\pi f(p,q) M(q,q)\right). \tag{6.10}$$

Finally, setting $q = p$ and solving for the scattering amplitude gives

$$M(p,p) = \frac{1}{K^{-1}(p,p) - i\pi f(p,p)} = \frac{\frac{p}{\pi f(p,p)}}{\frac{p}{\pi f(p,p)} K^{-1}(p,p) - ip}. \tag{6.11}$$

This can be compared part by part to equation (6.3). $p/(\pi f(k,k))K^{-1}(p,p)$ is just a different parameterization of the phase shift δ. And the normalization N is finally given by

$$N = \frac{p}{\pi f(p,p)}. \tag{6.12}$$

So, to obtain the normalization of the Yamaguchi (Gauss) model and the EFT for the different orders, all that has to be done is to reshape the corresponding Faddeev equation into the from of equation (6.5) and calculate $p/(\pi f(p,p))$.

6.2.2 The normalizations for the EFT at different orders and for the different models

The EFT at LO

The propagator at LO is given by

$$\tau(k, E_q) = \frac{1}{-1/a + \sqrt{3/4(k^2 - q^2) + 1/a^2}} = \frac{1/a + \sqrt{3/4(k^2 - q^2) + 1/a^2}}{3/4(q+k)(q-k)}. \tag{6.13}$$

Therefore

$$f(q,k) = \frac{4}{\pi} k^2 \tau(k, E_q)(k - q). \tag{6.14}$$

And for $p = k = q$

$$\begin{aligned} f(p,p) &= \frac{4}{\pi} k^2 \tau(k, E_q)(k-q) = \frac{k_1}{p} \frac{1}{k_1 - k_2} \approx \frac{16}{3\pi} \frac{p}{a} \\ \Rightarrow N &= \frac{3}{16} a. \end{aligned} \tag{6.15}$$

The EFT at NLO and N^{2}LO

Since the function $f(p,k,E)$ does not depend on $Z(p,q,E)$ the normalizations at NLO and N^{2}LO are the same. We use the unmodified propagator (equation (3.2)) to determine the normalization N. The modified differs only for large values of the momentum (compare to figure 3.3). Therefore for $p_{typ} \sim M_{low}$ they lead to the same N. The propagator can be written as

$$\tau(k, E_q) = \frac{-2/r}{(k^* - k_1)(k^* - k_2)} = \frac{-2/r(\sqrt{3/4(k^2 - q^2) + k_1^2} + k_1)}{3/4(k+q)(k-q)(\sqrt{3/4(k^2 - q^2) + k_1^2} - k_2)}. \tag{6.16}$$

With $E_q = 3q^2/4 - mE_D$. And therefore

$$f(q,k) = \frac{4}{\pi} k^2 \tau(k, E_q)(k-q). \tag{6.17}$$

For $p = q = k$ this yields

$$f(p,p) = \frac{16}{3\pi} \frac{p}{r} \frac{k_1}{k_2 - k_1}. \tag{6.18}$$

Consequently the normalization is given by

$$N = \frac{3}{32} \frac{r}{k_1} (k_2 - k_1). \tag{6.19}$$

In the limit of $r/a \to 0$ (and therefore $k_1 \to 1/a$) this results in

$$N = \frac{3}{32} \frac{r}{k_1} \left(2 \frac{\sqrt{1 - 2r/a}}{r} \right) \to \frac{3}{16} a. \tag{6.20}$$

So the LO result is reproduced, as expected.

The Yamaguchi model

For the normalization of the scattering amplitude in the Yamaguchi model one can use the remaining propagator $\tau_Y^{rest}(k^*)$ at $k = q$ as defined in equation (3.84). Using this leads to

$$f(p,p) = \frac{1}{2\pi^2} k^2 \tau_Y^{rest}(k, E_q) = \frac{8\pi}{3m} \frac{\gamma}{\beta^3} (\beta + \gamma)^3. \tag{6.21}$$

Here the additional factor of $1/2\pi^2$ originates from the normalization of the potential $Z_Y(p,q,E)$ and the missing $(2\pi)^3$ in the normalization of the integral. Therefore, the normalization of the scattering amplitude is given by

$$N = \frac{3}{8} \frac{m\beta^3}{\gamma(\beta + \gamma)^3}. \tag{6.22}$$

The Gauss model

For the Gauss model it appears to be difficult to calculate the reduced propagator $\tau_G^{rest}(k^*) = \tau_G(k^*)(k-q)$ analytically. This is due to the error-functions in the propagator. A numerical approach seems to be more appealing. By using the first term of a Laurent series the propagator can be calculated numerically.

$$\tau_G^{rest}(k^*) = \left(\frac{d}{dq} \tau_G^{-1}(q^*) \right)^{-1} \Bigg|_{q \to k}. \tag{6.23}$$

On this basis the function $f(q,k)$ is given by

$$f(q,k) = \frac{4}{\pi} k^2 \tau_G^{rest}(k, E_q). \tag{6.24}$$

For given parameters λ_G and E_d of the Gauss model, this gives a numerical expression for the normalization N.

6.3 Additional numerical results for the different models

The purpose of this appendix is to provide plots of the additional results. In figure 6.1 we show the Lepage plots and consistency assessment for the remaining choices of the propagator $\tau_i(k^*)$ for the Yamaguchi model. In figure 6.2 the results for the phase-shift for the Yamaguchi model with a higher cutoff Λ are shown. In figure 6.3 we show the Lepage plot and the consistency assessment for the Gauss model for a larger momentum region.

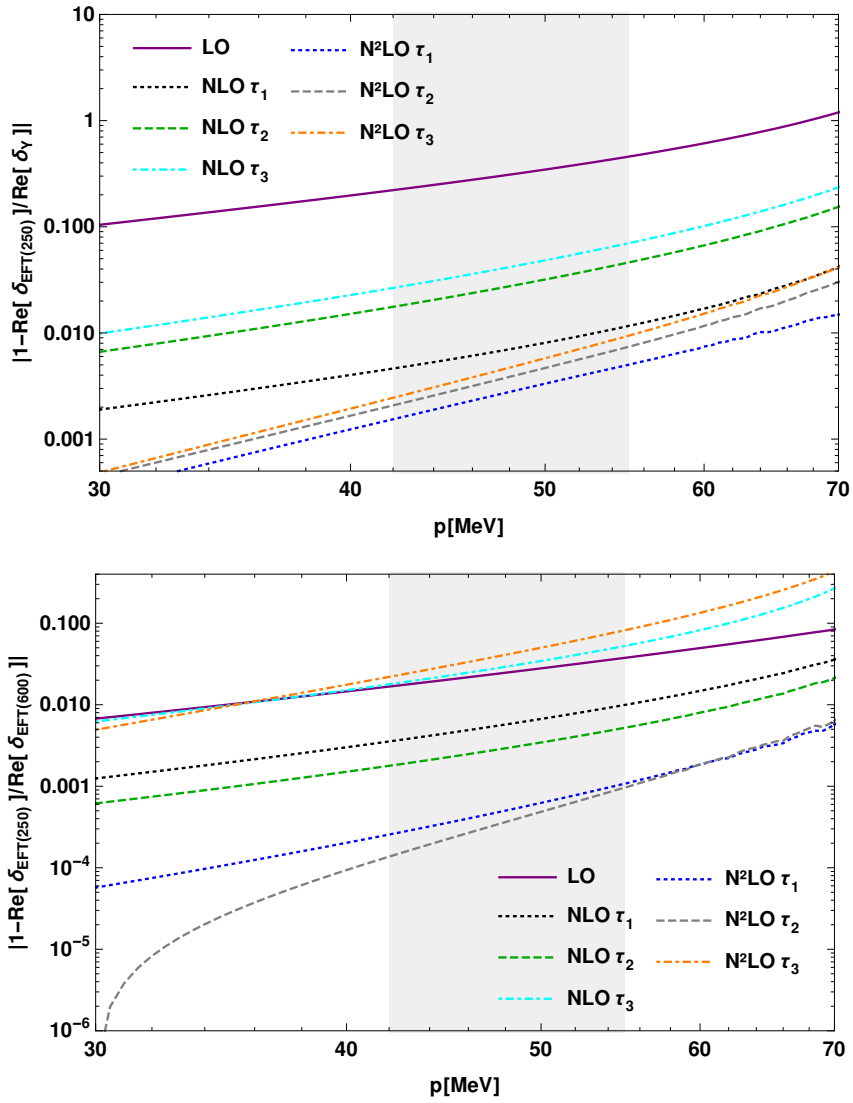

Figure 6.1: Lepage plot (above) and consistency assessment (below) for the particle-dimer phase shift in the Yamaguchi model. Shown are the first three choices of the number of terms i in the expansion of the modified dimer propagator $\tau_i(k^*)$. In the 'window of opportunity' (gray shaded) the slope of the different choices is very similar for the same order of the EFT expansion. The slopes can be seen in table 3.3.

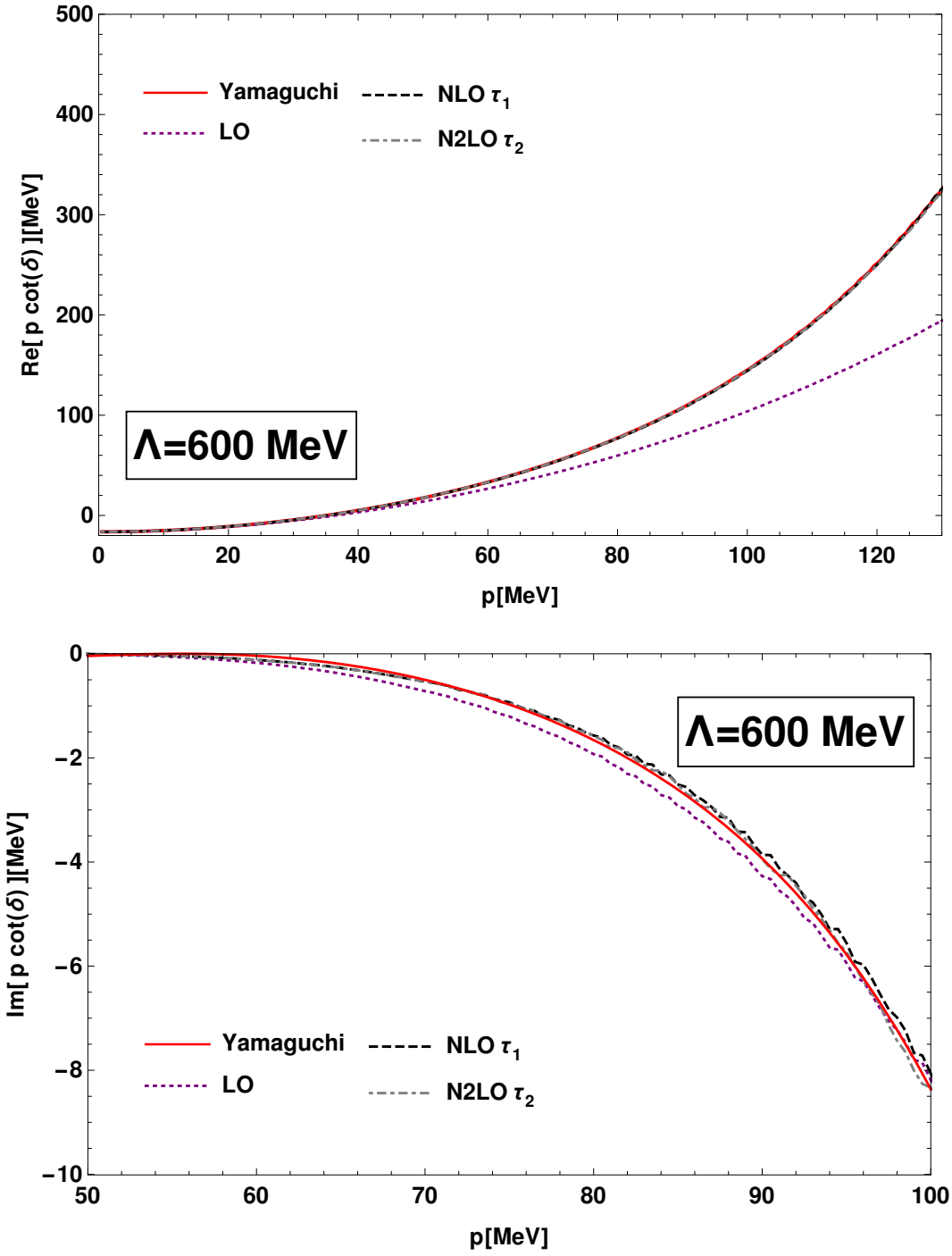

Figure 6.2: Numerical results for real (above) and imaginary (below) part of the quantity $p \cot \delta$ with the particle-dimer phase shift δ for the Yamaguchi model with the effective range $r' = 0.8768$ fm. Red line: the result obtained in the Yamaguchi model; in purple dotted: the LO result; in black dashed: the NLO result for τ_1; in gray dot-dashed: the N^{2}LO result for τ_2. For the real part the NLO and N^{2}LO results are on top of the Yamaguchi model. All for a cutoff $\Lambda = 600$ MeV. The results for NLO, N^{2}LO and the model are on top of each other.

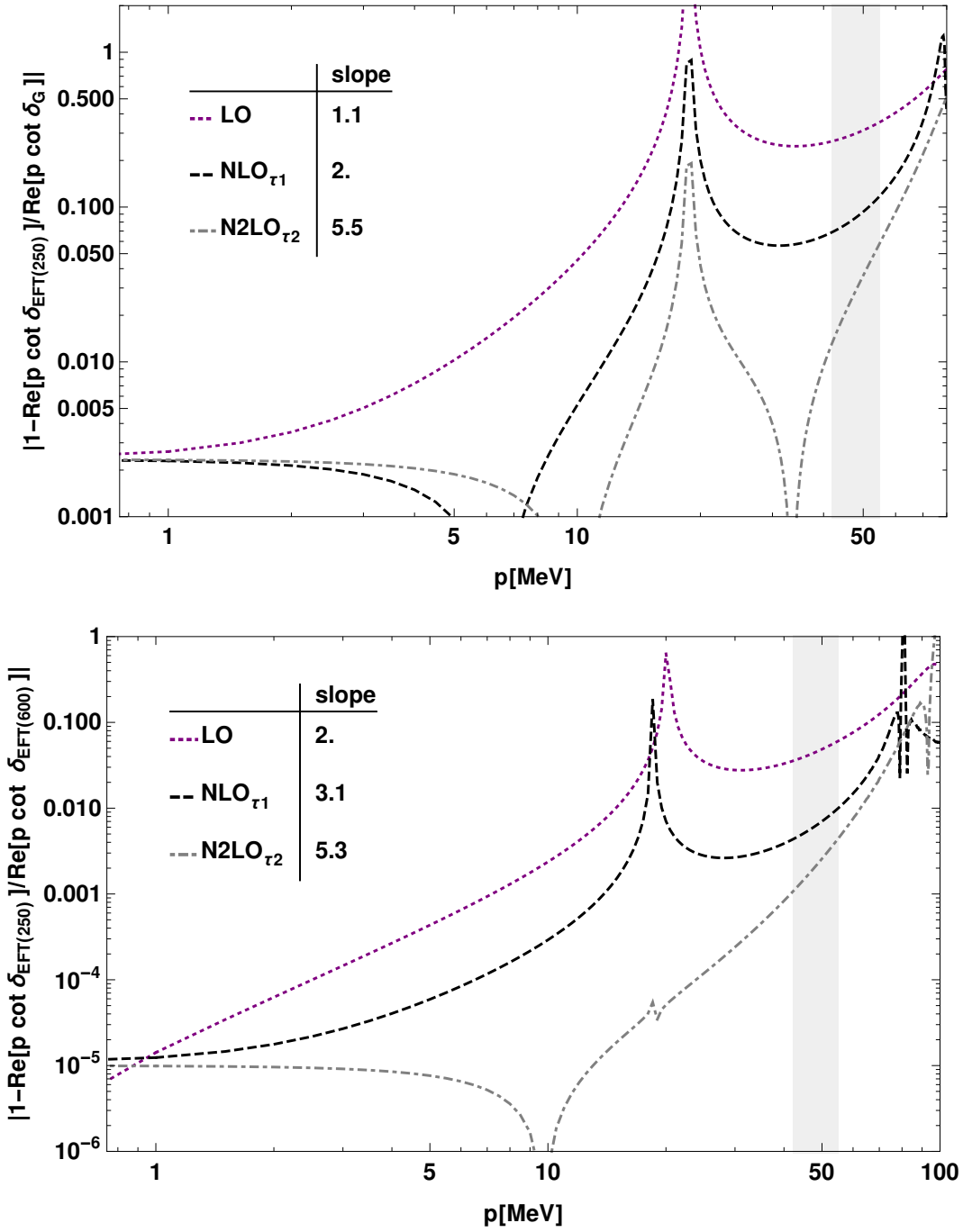

Figure 6.3: The Lepage plot (above) and the consistency assessment (below) for the Gauss potential. This plot is the same as in figure 3.15 but with a larger momentum regime plotted. The spike (accidental zero) for the N^{2}LO result in the Lepage plot can be seen clearly around 30 MeV. This is the reason why the corresponding slope (table 3.11) in the 'window of opportunity' (gray shaded) is to large. The consistency assessment does not exhibit such a spike.

7 References

7.1 References from articles

[1] S. R. Beane, W. Detmold, and M. J. Savage. n-boson energies at finite volume and three-boson interactions. *Physical Review D*, 76(7), 2007.

[2] S. R. Beane and M. J. Savage. Rearranging pionless effective field theory. *Nuclear Physics A*, 694(3-4):511–524, 2001.

[3] P. F. Bedaque and H. W. Grießhammer. Quartet s wave neutron deuteron scattering in effective field theory. *Nuclear Physics A*, 671(1-4):357–379, 2000.

[4] P. F. Bedaque, H.-W. Hammer, and U. van Kolck. The three-boson system with short-range interactions. *Nuclear Physics A*, 646(4):444–466, 1999.

[5] P. F. Bedaque, G. Rupak, H. W. Grießhammer, and H.-W. Hammer. Low energy expansion in the three body system to all orders and the triton channel. *Nuclear Physics A*, 714(3-4):589–610, 2003.

[6] P. F. Bedaque and U. van Kolck. Nucleon-deuteron scattering from an effective field theory. *Physics Letters B*, 428(3-4):221–226, 1998.

[7] P. F. Bedaque and U. van Kolck. Effective field theory for few-nucleon systems. *Annual Review of Nuclear and Particle Science*, 52(1):339–396, 2002.

[8] V. Bernard, M. Lage, U.-G. Meißner, and A. Rusetsky. Resonance properties from the finite-volume energy spectrum. *Journal of High Energy Physics*, 2008(08):024–024, 2008.

[9] H. A. Bethe. Theory of the effective range in nuclear scattering. *Phys. Rev.*, 76:38–50, 1949.

[10] S. Bour, S. König, D. Lee, H.-W. Hammer, and U.-G. Meißner. Topological phases for bound states moving in a finite volume. *Physical Review D*, 84(9), 2011.

[11] E. Braaten and H.-W. Hammer. Three-body recombination into deep bound states in a bose gas with large scattering length. *Phys. Rev. Lett.*, 87:160407, 2001.

[12] E. Braaten and H.-W. Hammer. Universality in few-body systems with large scattering length. *Physics Reports*, 428(5-6):259–390, 2006.

[13] E. Braaten and H.-W. Hammer. Efimov physics in cold atoms. *Annals of Physics*, 322(1):120–163, 2007.

[14] R. A. Briceño, M. T. Hansen, and S. R. Sharpe. Relating the finite-volume spectrum and the two-and-three-particle s matrix for relativistic systems of identical scalar particles. *Physical Review D*, 95(7), 2017.

[15] J.-W. Chen, G. Rupak, and M. J. Savage. Nucleon-nucleon effective field theory without pions. *Nuclear Physics A*, 653(4):386–412, 1999.

[16] C. Chin, R. Grimm, P. Julienne, and E. Tiesinga. Feshbach resonances in ultracold gases. *Reviews of Modern Physics*, 82(2):1225–1286, 2010.

[17] F. Dalfovo, S. Giorgini, L. P. Pitaevskii, and S. Stringari. Theory of bose-einstein condensation in trapped gases. *Reviews of Modern Physics*, 71(3):463–512, 1999.

[18] G. S. Danilov. On the three-body problem with short-range forces. *Sov. Phys. JETP*, 13(249):498, 1961.

[19] J. J. de Swart, C. P. F. Terheggen, and V. G. J. Stoks. The low-energy neutron-proton scattering parameters and the deuteron, 1995.

[20] S. Durr, Z. Fodor, J. Frison, C. Hoelbling, R. Hoffmann, S. D. Katz, S. Krieg, T. Kurth, L. Lellouch, T. Lippert, K. K. Szabo, and G. Vulvert. Ab initio determination of light hadron masses. *Science*, 322(5905):1224–1227, 2008.

[21] M. Döring, H.-W. Hammer, M. Mai, J.-Y. Pang, A. Rusetsky, and J. Wu. Three-body spectrum in a finite volume: The role of cubic symmetry. *Physical Review D*, 97(11), 2018.

[22] M. Ebert, H.-W. Hammer, and A. Rusetsky. An alternative scheme for effective range corrections in pionless EFT. *The European Physical Journal A*, 57(12), 2021.

[23] V. Efimov. Energy levels arising from resonant two-body forces in a three-body system. *Physics Letters B*, 33(8):563–564, 1970.

[24] E. Epelbaum, H.-W. Hammer, and U.-G. Meißner. Modern theory of nuclear forces. *Reviews of Modern Physics*, 81(4):1773–1825, 2009.

[25] H. W. Grießhammer. Improved convergence in the three-nucleon system at very low energies. *Nuclear Physics A*, 744:192–226, 2004.

[26] H. W. Griesshammer. Assessing theory uncertainties in eft power countings from residual cutoff dependence. *Proceedings of Science*, CD 15(104), 2016.

[27] H. W. Grießhammer. A consistency test of EFT power countings from residual cutoff dependence. *The European Physical Journal A*, 56(4), 2020.

[28] H. W. Grießhammer. What can possibly go wrong? *Few-Body Systems*, 63(2), 2022.

[29] P. Guo and V. Gasparian. A solvable three-body model in finite volume. *Physics Letters B*, 774:441–445, 2017.

[30] P. Guo and V. Gasparian. Numerical approach for finite volume three-body interaction. *Physical Review D*, 97(1), 2018.

[31] H.-W. Hammer, S. König, and U. van Kolck. Nuclear effective field theory: Status and perspectives. *Reviews of Modern Physics*, 92(2), 2020.

[32] H.-W. Hammer and T. Mehen. Range corrections to doublet s-wave neutron–deuteron scattering. *Physics Letters B*, 516(3-4):353–361, 2001.

[33] H.-W. Hammer, J.-Y. Pang, and A. Rusetsky. Three-particle quantization condition in a finite volume: 1. the role of the three-particle force. *Journal of High Energy Physics*, 2017(9), 2017.

[34] H.-W. Hammer, J.-Y. Pang, and A. Rusetsky. Three-particle quantization condition in a finite volume: 2. general formalism and the analysis of data. *Journal of High Energy Physics*, 2017(10), 2017.

[35] M. T. Hansen and S. R. Sharpe. Relativistic, model-independent, three-particle quantization condition. *Physical Review D*, 90(11), 2014.

[36] M. T. Hansen and S. R. Sharpe. Expressing the three-particle finite-volume spectrum in terms of the three-to-three scattering amplitude. *Physical Review D*, 92(11), 2015.

[37] M. T. Hansen and S. R. Sharpe. Applying the relativistic quantization condition to a three-particle bound state in a periodic box. *Physical Review D*, 95(3), 2017.

[38] M. T. Hansen and S. R. Sharpe. Lattice qcd and three-particle decays of resonances. *Annual Review of Nuclear and Particle Science*, 69(1):65–107, 2019.

[39] C. Ji and D. R. Phillips. Effective field theory analysis of three-boson systems at next-to-next-to-leading order. *Few-Body Systems*, 54(12):2317–2355, 2013.

[40] C. Ji, D. R. Phillips, and L. Platter. The three-boson system at next-to-leading order in an effective field theory for systems with a large scattering length. *Annals of Physics*, 327(7):1803–1824, 2012.

[41] R. C. Johnson. Angular momentum on a lattice. *Physics Letters B*, 114(2-3):147–151, 1982.

[42] D. B. Kaplan. More effective field theory for non-relativistic scattering. *Nuclear Physics B*, 494(1-2):471–483, 1997.

[43] D. B. Kaplan, M. J. Savage, and M. B. Wise. A new expansion for nucleon-nucleon interactions. *Physics Letters B*, 424(3-4):390–396, 1998.

[44] D. B. Kaplan, M. J. Savage, and M. B. Wise. Two-nucleon systems from effective field theory. *Nuclear Physics B*, 534(1-2):329–355, 1998.

[45] S. Kreuzer and H. W. Grießhammer. Three particles in a finite volume: The breakdown of spherical symmetry. *The European Physical Journal A*, 48(7), 2012.

[46] S. Kreuzer and H.-W. Hammer. Efimov physics in a finite volume. *Physics Letters B*, 673(4-5):260–263, 2009.

[47] S. Kreuzer and H.-W. Hammer. On the modification of the efimov spectrum in a finite cubic box. *The European Physical Journal A*, 43(2):229–240, 2010.

[48] S. Kreuzer and H.-W. Hammer. The triton in a finite volume. *Physics Letters B*, 694(4-5):424–429, 2011.

[49] S. König and H.-W. Hammer. Low-energy p-d scattering and he-3 in pionless eft. *Physical Review C*, 83(6), 2011.

[50] S. König and D. Lee. Volume dependence of n-body bound states. *Physics Letters B*, 779:9–15, 2018.

[51] G. P. Lepage. How to renormalize the schrodinger equation. *Lectures at the VIII Jorge Andr e Swieca Summer School, Brazil*, 1997.

[52] P. Lowdon. Spectral density constraints in quantum field theory. *Physical Review D*, 92(4), 2015.

[53] M. Lüscher. Volume dependence of the energy spectrum in massive quantum field theories. *Commun. Math. Phys.*, 105:153–188, 1986.

[54] M. Lüscher. Two-particle states on a torus and their relation to the scattering matrix. *Nuclear Physics*, 354:531–578, 1991.

[55] M. Lüscher. Two-particle states on a torus and their relation to the scattering matrix. *Nuclear Physics B*, 354(2):531–578, 1991.

[56] M. Mai and M. Döring. Three-body unitarity in the finite volume. *The European Physical Journal A*, 53(12), 2017.

[57] M. Mai, M. Döring, and A. Rusetsky. Multi-particle systems on the lattice and chiral extrapolations: a brief review. *The European Physical Journal Special Topics*, 230(6):1623–1643, 2021.

[58] J. E. Mandula, G. Zweig, and J. Govaerts. Representations of the rotation reflection symmetry group of the four-dimensional cubic lattice. *Nuclear Physics B*, 228(1):91–108, 1983.

[59] U.-G. Meißner, K. Polejaeva, and A. Rusetsky. Extraction of the resonance parameters at finite times. *Nuclear Physics B*, 846(1):1–20, 2011.

[60] U.-G. Meißner, G. Rí os, and Akaki Rusetsky. Spectrum of three-body bound states in a finite volume. *Physical Review Letters*, 114(9), 2015.

[61] F. Müller, J.-Y. Pang, A. Rusetsky, and J.-J. Wu. Relativistic-invariant formulation of the NREFT three-particle quantization condition. *Journal of High Energy Physics*, 2022(2), 2022.

[62] J.-Y. Pang, M. Ebert, H.-W. Hammer, F. Müller, A. Rusetsky, and J.-J. Wu. Spurious poles in a finite volume. *JHEP, accepted*, 2022.

[63] L. Platter and D. R. Phillips. The three-boson system at next-to-next-to-leading order. *Few-Body Systems*, 40(1-2):35–55, 2006.

[64] E. Ryberg, C. Forssén, and L. Platter. Three-body halo states in effective field theory: Renormalization and three-body interactions in the helium-6 system. *Few-Body Systems*, 58:1–12, 2017.

[65] J. Schwinger. A variational principle for scattering problems. *Phys. Rev*, 72(8):742–742, 1947.

[66] S. R. Sharpe. Testing the threshold expansion for three-particle energies at fourth order in ϕ^4 theory. *Physical Review D*, 96(5), 2017.

[67] G. V. Skorniakov and K. A. Ter-Martirosian. Three body problem for short range forces. 1. scattering of low energy neutrons by deuterons. *Sov. Phys. JETP*, 4(648), 1957.

[68] U. van Kolck. Nucleon-nucleon interaction and isospin violation. In *Chiral Dynamics: Theory and Experiment*, pages 62–77. Springer Berlin Heidelberg, 1998.

[69] J. Vanasse. Fully perturbative calculation of nd scattering to next-to-next-to-leading-order. *Physical Review C*, 88(4), 2013.

[70] S. Weinberg. Phenomenological lagrangians. *Physica A: Statistical Mechanics and its Applications*, 96(1):327–340, 1979.

[71] S. Weinberg. Nuclear forces from chiral lagrangians. *Physics Letters B*, 251(2):288–292, 1990.

[72] S. Weinberg. Effective chiral lagrangians for nucleon-pion interactions and nuclear forces. *Nuclear Physics B*, 363(1):3–18, 1991.

[73] K. G. Wilson. Confinement of quarks. *Physical Review D*, 10(8):2445–2459, 1974.

[74] Y. Yamaguchi. Two-nucleon problem when the potential is nonlocal but separable. i. *Phys. Rev.*, 95:1628–1634, 1954.

7.2 References from books

[75] T. Fliessbach. *Quantenmechanik, Lehrbuch zur Theoretischen Physik III*, volume 5. Springer Spektrum Berlin, Heidelberg, 2008.

[76] M. E. Peskin and D. V. Schroeder. *An introduction to quantum field theory*. Westview, Boulder, CO, 1995.

[77] J. J. Sakurai and J. Napolitano. *Modern Quantum Mechanics*. Cambridge University Press, 2 edition, 2017.

[78] S. Scherer. *Symmetrien und Gruppen in der Teilchenphsik*, volume 1. Springer Spektrum Berlin, Heidelberg, 2016.

[79] E. W. Schmid and H. Ziegelmann. *The Quantum Mechanical Three-Body Problem*. Pergamon Press, 1974.

7.3 Other references

[80] W. Elkamhawy. Electroweak properties of halo nuclei in effective field theory. *Dissertation*, 2021.

[81] J.-Y. Pang. *Private Communication*. College of Science, University of Shanghai for Science and Technology, Shanghai 200093, China, 2022.

[82] L. Platter. From cold atoms to light nuclei: The four-body problem in an effective theory with contact interactions. *Dissertation*, 2005.

8 Acknowledgements

An erster Stelle möchte ich meinem Doktorvater Hans-Werner Hammer danken. Er hat mich früh in seiner Arbeitsgruppe aufgenommen und mich durch die verschiedenen Stufen meines Studiums begleitet. Vielen Dank für die Hilfe, das Vertrauen, die Ratschläge und das Zeitgeben, wenn Ich sie gebraucht habe.

Vielen Dank an Jens Braun für die Zustimmung diese Arbeit zu Bewerten und die hilfreichen Fragen und Anmerkungen zu meiner Forschung im Rahmen der HGS-HIRe PhD-Committee Treffen.

Ich möchte meinen Kooperationspartnern danken: Akaki Rusetsky, Jin-Yi Pang, Jia-Jun Wu und Fabian Müller. Besonderer Dank gilt hierbei Jin-Yi Pang für das Bereitstellen seines Finite-Volume-Codes und der Daten für die Energiespektren.

Ich bedanke mich herzlich bei meinen aktuellen und ehemaligen Kollegen in der Arbeitsgruppe. Insbesondere möchte ich mich bei Fabian Hildenbrand und Sebastian Dietz für die Hilfe bei meinen numerischen Rechnungen bedanken, bei Wael Elkamhawy für die hilfreichen physikalischen und, wahrscheinlich noch mehr, sonstigen Gespräche, bei Matthias Göbel für die Hilfe mit allerlei Computerdingen und bei Fabian Brauneis für mindestens einen Ohrwurm. Außerdem möchte ich den genannten für ihre Anmerkungen und Korrekturvorschläge zu dieser Dissertation danken.
Ich bedanke mich bei Artem Volosniev für die hervorragende Betreuung meiner Bachelor-Thesis und darüber hinaus.

Abschließend bedanke ich mich bei meinen Eltern Edeltraud und Raimund und meinem Bruder Roland für, nun ja, eigentlich für alles.

Danke.